Order Number 9304751

New optical methods for signal processing

Zhang, Yan, Ph.D.

City University of New York, 1992

U·M·I
300 N. Zeeb Rd.
Ann Arbor, MI 48106

NEW OPTICAL METHODS FOR SIGNAL PROCESSING

by

Yan Zhang

A dissertation submitted to the Graduate Faculty in Engineering in partial fulfillment of the requirements for the degree of Doctor of Philosophy, The City University of New York.

1992

This manuscript has been read and accepted for the Graduate Faculty in Engineering in satisfaction of the dissertation requirement for the degree of Doctor of Philosophy.

5/28/92
Date

Chair of Examining Committee

5/29/92
Date

Executive Officer

Prof. Samir Ahmed

Prof. Joseph Barba

Prof. Roger Dorsinville

Prof. Sanghamitra Basu

Dr. Emmanuel G. Kenterakis

Dr. Ming H. Wu

Supervisory Committee

The City University of New York

ABSTRACT

NEW OPTICAL METHODS FOR SIGNAL PROCESSING

by

Yan Zhang

Advisor: Dr. Yao Li, Associate Professor of Electrical Engineering

This doctoral thesis studies the optical implementations of various new algorithms and methods for large bandwidth signal and image processing. Among the schemes to be studied are the long data stream convolution/correlation, the Gabor and the wavelet transforms, and their applications to system failure prediction, dense target signal processing and image coding.

Based on the Chinese remainder theorem, optically implementable algorithms are described, which convert the convolution/correlation of long data streams to relatively small scale linear operations such as a group of short-term vector-matrix multiplications

or short-term convolutions/correlations. The proposed algorithms can be realized by using the existing optical analog data processors. Simulations were performed to prove their validity. Technical problems and fundamental limitations of the above schemes are studied.

Following the consideration of the above time domain operations, signal's representations in joint time-frequency (scale) domain are then considered. An opto-electronic Gabor coefficient processor is designed to perform the Gabor transform on short one-dimensional (1-D) signals in real-time. Some experimental results are presented to confirm the operational principle of the system. As an application of this processor, Gabor transform based transient signal detection is studied. Other schemes for implementing Gabor transform of long 1-D signals based on the long data stream convolver, and 2-D signals are also investigated. Following the study of the Gabor transform, the newly suggested wavelet transform is considered for its optical implementation. Using commercially available opto-electronic components, an optical wavelet processor is designed and built to perform the wavelet transforms on short 1-D signals in real-time. As an extension, architectures for 2-D optical wavelet transform are also described and computer simulated with the consideration of their technical problems of optical implementation. Applications of the wavelet transforms to system failure prediction, dense target signal processing and image coding are briefly explained. Schemes for optical wavelet transform of long 1-D signals are also studied.

The goal of this thesis is to further our knowledge and understanding on how the free-space optical processing methods could help developing efficient signal and image processing tools and what the potential applications and limitations of these optical methods are.

ACKNOWLEDGEMENT

This research was performed with the guidance and support of Dr. Yao Li, Associate Professor of Electrical Engineering at The City College and at The Graduate School of The City University of New York.

I would like to acknowledge the financial support from Defense Advanced Research Program Agency through the Air Force Office of Scientific Research AFOSR-90-0346, Naval SBIR grant N60921-91-C-0002, and the NEC Research Institute.

To my wife Bo

and my daughter Stephanie

Table of Contents

List of Figures

List of Tables

1 INTRODUCTION

1.1 Optical Signal processing

Natural signals, no matter what forms they are taking (optical, mechanical, acoustic, electromagnetic, etc.), can be detected and converted into electrical signals by appropriate sensors. The obtained signals can thus be used to analyze their characteristics by available signal processing facilities.

Digital signal processing, with its wide applications almost everywhere, has been enjoying an explosive growth. A large number of VLSI[1] processor chips and their supporting algorithms have been developed [1.1],[1.2],[1.3]. Most of them are designed for conventional digital electronic computer realization. However, because of the sequential processing nature of a conventional computer, when the number of data points to be processed becomes very large, the processing speed becomes unacceptably slow in some applications. Parallel processing schemes to enhance the speed performance must be employed to solve the problem.

An optical system with its inherently parallel processing property is a suitable candidate for handling such a parallel processing task. Based on coherent and incoherent optical methods, an optical system may perform various key signal processing operations such as the two-dimensional (2-D) Fourier transform [1.4] and the vector-matrix multiplication in real-time [1.5].

---

1 See Appendix for the abbreviations.

As an example, a coherent optical system illustrated in Fig.1.1.1, where a spherical lens is used, can be shown (see Section 2.1 for details) to perform 2-D Fourier transform on an input image in real-time. Also, by substituting the spherical lens in Fig.1.1.1 by a set of anamorphic optical components (combination of cylindrical and spherical lenses), a one-dimensional (1-D) Fourier transform can be performed optically. Therefore, different kinds of signal processing may be carried out by using the system of Fig.1.1.1 as a basic function unit. Examples of available optical information processing systems based on optical Fourier transform are an optical matched filter, a joint transform correlator, etc [1.4],[1.6]-[1.9].

Not only the Fourier analysis, but some also algebraic operations may be performed by an optical system [1.5],[1.10]-[1.13]. In algebraic operations, the vector-matrix multiplication is considered as a basic operation. Different schemes using Bragg cell devices and charge coupled devices (CCD) were described. The hybrid system shown in Fig.1.1.2, which was suggested by E. P. Mosca, et al, is a typical example. Another example is an acousto-optic convolver for 1-D signals by W. Rhodes [1.10],[1.11].

It seems that an optical processor is perfect for linear signal processing because of its ultra-fast speed and inherent parallel processing. However, the processing performed by an optical system is more qualitative than quantitative under current technical conditions, which means that accurate calculation results should not be expected from optical processing. Fortunately, in some applications, such as signal detection and pattern recognition, the purpose of operation is to classify and

allocate certain targets in signal and thus the optical processing for these applications is justified. Even in the cases where accurate calculation results are necessary, optical processing is still helpful to speed up part of entire process. Because, in a long sequence of signal, usually only small portions of data are useful, optical processing may first be used to locate these parts of signal and then conventional signal processing schemes are carried out (see Fig.1.1.3) to obtain the results, which are considered more accurate than optical processing.

1.2 Time-Frequency or Time-Scale Signal Representation[2]

To be analyzed or processed by any signal processing method, the signal must be first described or represented by an appropriately selected mathematical representation which is suitable for the analysis to be carried out. It is well known that conventional signal representations for both continuous and discrete cases are describable under two general categories: the time domain and the frequency domain representations. Many signal analysis techniques were developed based on these two signal representations, examples among them are convolution, correlation, Fourier transform, etc.

Although the above mentioned pure time or frequency signal representations successfully solved a lot of practical problems, they show a serious weakness in some applications, which is the bad time and frequency separability. Consider the

2 In this doctoral dissertation, *time* means time for electrical signals or space for optical signals while *frequency* means frequency for electrical signals or spatial-frequency for optical signals.

image shown in Fig.1.2.1, in which letter "A" and letter "B" are well separated in spatial domain. However, when 2-D Fourier transform is applied to the image, the spectra of the two letters are mixed up in frequency domain (also see Fig.1.2.1. Therefore, the algorithms designed to function in frequency domain can not work properly. Specifically, if a filter is made to pick up the spectrum of letter "A" for further processing, strong crosstalk between "A" and "B" exists. For another example, an important problem in pattern recognition and signal detection theory is the representational separability of time and frequency domains. Consider the detection of transient signals in an additive noise environment. Conventional detection schemes use either matched filter or likelihood ratio based methods to determine the presence of such signals. However, when both waveforms and arriving times of transient signals are unknown, it is difficult for these methods to succeed. Methods with improved representational separability relative to pure time and frequency will be useful in this kind of applications.

Time-frequency joint representations originated from the quantum mechanics have been used to solve the problem of representational separability since 1946 [1.14]. Typical time-frequency representations include the ambiguity function, the Wigner distribution, the spectrogram, the difference of Gaussian, the Gabor transform and wavelet transform [1.14]-[1.17]. With time-frequency representations, signals are transformed into a joint time and frequency domain. These joint time-frequency representations greatly enhance the separability of target signatures regardless of energy in these signatures being segregated only in the time or

frequency domain, or in the joint time and frequency domain. A better result is thus expected when correlation is carried out using the signal's time-frequency representation.

Using coherent optical systems, some system architectures were proposed and implemented for the realization of the ambiguity function and Wigner distribution [1.18]-[1.20]. In this thesis, based on the developed concepts of these optical implementations and the new understanding and appreciation of the Gabor and wavelet transforms, optical versions of them are proposed as powerful tools to analyze and synthesize signals.

1.3 Convolution/Correlation of Long Data Streams

The calculation of the digital convolution

$$y(i) = \sum_{k=0}^{N-1} h(i-k)x(k) \qquad (1.3.1)$$

$$i = 0, 1, \ldots, N-1$$

has important applications in communication, sensing and signal processing. It is used to compute auto and cross correlations, to design and implement finite impulse response (FIR) and infinite impulse response (IIR) digital filters, to solve difference equations, and to compute power spectrum. Since the introduction of Cooley-Turky FFT algorithm, many algorithms for digital convolution/correlation have been discussed in literatures[1.21]-[1.25]. Some of them were designed based on the Number

Theory Transform (NTT) to shuffle the 1-D sequences into multidimensional sequences and to express the original 1-D convolution as a multidimensional convolution problem.

Although these algorithms based on FFT and NTT were successfully used in electronic computers for relatively short sequences, due to the sequential processing nature of a conventional digital processor, convolution or correlation of long data streams at high speed is still difficult to perform. To resolve this problem, concepts of parallel and distributed processing are needed. Optical systems with their inherent parallel processing capabilities are potential candidates for processing long data streams. Optical correlation of two signals with large time-bandwidth product was designed by Rhodes [1.26], who proposed to use a non-interlaced raster scan scheme to convert one-dimensional (1-D) signals to their two-dimensional (2-D) formats subject to an optical correlation suggested by Weaver and Goodman [1.6]. Turpin [1.27] suggested a system which realizes an optical discrete Fourier transform of long sequence by first converting the original 1-D data sequence into a 2-D data array and then performing a 2-D optical Fourier transform on the 2-D pattern. A specially designed phase-correcting prism was placed super accurately in the system to cancel an extra phase term. Various other interesting schemes of converting a 1-D sequence to its 2-D format suitable for optical processing were suggested by Stoner [1.28].

1.4 Research Goal and Thesis Organization

The research goal of this doctoral thesis is to study new methods of optical long data stream convolution/correlation, optical Gabor and wavelet transform implementations and their applications to system failure prediction, radar and sonar signal processing and image coding.

The thesis has been divided into eight chapters. This introductory chapter provides background information regarding optical signal processing. In the second chapter, a brief review of the state-of-the-art optical signal processing techniques is included. Beginning at the third chapter, new methods of optical implementation of long data stream convolution/correlation, Gabor transform and wavelet transform are presented.

In Chapter Three, an optically implementable algorithm, which separates a long data stream into several shorter sequences based on the Chinese remainder theorem, is described. Using this algorithm, the convolution/correlation of long data streams are performed by relatively small scale vector-matrix multiplications, which can be realized using the state-of-the-art optical algebraic processing technologies. Computer simulation results of this algorithm are presented. A suitable optical processing architecture is also proposed. As an alternative to the above algorithm, the convolution/correlation of the two 1-D data sequences is converted into a convolution/correlation of the two corresponding 2-D arrays. An opto-electronic

scheme using the algorithm to solve the problem of real-time convolution/correlation of long data streams is thus described. Three video rate optical and opto-electronic data permutation schemes are presented. Computer simulations for the entire three-stage algorithm and their results are discussed. Technical problems and fundamental limitations of the described schemes are also studied.

In Chapter Four, an opto-electronic Gabor coefficient processor for short one-dimensional (1-D) signals is first designed. Using an acousto-optic modulator as an input device, a liquid crystal SLM as a reconfigurable window and a two-dimensional (2-D) CCD detector array as an output device, a real-time opto-electronic Gabor coefficient processing architecture is described. Some experimental results are presented. As an application of this processor, a Gabor transform based transient signal detection scheme is proposed. Schemes for implementing an Gabor coefficient processor for long 1-D signals and two-dimensional (2-D) signals are also investigated.

In the following chapter, a scheme for optical realization of wavelet transform of short 1-D signals is described. Using commercially available components, the constructed system can perform wavelet transform for short 1-D signals in real-time. Some experimental results are demonstrated. As an extension of this scheme, a 2-D optical wavelet transformer is proposed and computer simulated. Technical problems of optical implementation are studied. Applications of the wavelet transforms to system failure prediction, dense target signal processing and image

coding are studied. To perform wavelet transform on long 1-D signals, schemes based on long data stream convolution/correlation described in Chapter Three are proposed.

In Chapter Six, a novel system architecture is designed for detection of spatial and temporal target in motion pictures, which is based on 1-D Gabor and wavelet transform. Although this system does not perform processing in real-time, it is expected less sensitive to noise than conventional detectors because of its utilization of time-frequency representation.

Chapter Seven contains the thesis summary. In Appendix A, the abbreviations used in the thesis are explained. Following this, in Appendix B, Zak transform, as one of the basic tools used in Gabor transform, is briefly described. And finally, a list of thesis related publications and bibliography are given.

1.5 References

[1.1] A. V. Oppenheim and R. W. Schafer, *Digital Signal Processing*, Prentice-Hall, New Jersey, 1975.

[1.2] R. E. Blahut, *Fast Algorithm for Digital Signal Processing*, Addison-Wesley, Reading, 1985.

[1.3] Texas Instruments Incorporated, *First-Generation TMS320: User's Guide*, Houston, 1989

[1.4] J. W. Goodman, *Introduction to Fourier Optics*, McGraw-Hill, New York, 1968.

[1.5] E. P. Mosca, R. D. Griffin, F. P. Pursel and J. N. Lee, "Acoustooptical Matrix-Vector Product Processor: Implementation Issues," *Applied Optics*, vol.28, no.18, pp.3843-3851, 15 September 1989.

[1.6] C. S. Weaver and J. W. Goodman, "A Technique for Optically Convolving Two Function," *Appl. Opt.*, vol. 5, no. 7, pp. 1248-1249, July 1966

[1.7] S. Jutamulia, K. Company and D. A. Gregory, "Intensity-Invariant Joint Transform Correlator," *Optics & Photonics News*, p.13, December 1991.

[1.8] J. L. Horner and P. D. Gianino, "Phase-Only Matched Filtering," *Applied Optics*, vol.23, no.6, pp.812-816, 1984

[1.9] B. Javidi and C. J. Kuo, "Joint Transform Image Correlation Using a Binary Spatial Light Modulator at the Fourier Plane," *Applied Optics*, vol.27, no.4, pp.663-665, 1988

[1.10] W. T. Rhodes, "Acousto-Optic Signal Processing: Convolution and Correlation," *Proc. IEEE*, vol.69, no.1, pp.65-79, January 1981.

[1.11] W. T. Rhodes and P. S. Guilfoyle, "Acoustooptic Algebraic Processing Architectures," *Proc. IEEE*, vol.72, no.7, pp.820-830, July 1984.

[1.12] H. Nakano and K. Hotate, "Optical System for Real-Time Multiplication of the Multiple Matrix with a 2-D Light Source Array," *Applied Optics*, vol.26, no.5, pp.917-923, 1 March 1987.

[1.13] H. Nakano and K. Hotate, "Operational Error in the Optical Real-Time Multiple Matrix Multiplier and its Compensation," *Applied Optics*, vol.25, no.18, pp.3132-3136, 15 September 1986.

[1.14] D. Gabor, "Theory of Communication," *J.I.E.E.*, vol.93, pp.429-459, 1946.

[1.15] H. Wechsler, *Computational Vision*, Academic Press, San Diego, 1990.

[1.16] A. Grossman and J. Morlet, "Decomposition of Hardy Functions into Square Integrable Wavelets of Constant Shape," *SIAM J. MATH.*, vol.15, no.4, pp.723-736, July 1984.

[1.17] I. Daubechies, "The Wavelet Transform, Time-Frequency Localization and Signal Analysis," *IEEE Trans. Info. Theory*, vol.36, no.5, pp.961-1005, 1990.

[1.18] D. Casasent and B. V. K. V. Kumar, "Optical Image Plane Correlator for Ambiguity Surface Computation," *Applied Optics*, vol.18, no.10, pp.1673-1678, 15 May 1979.

[1.19] R. J. Marks II, J. F. Walkup and T. F. Krile, "Ambiguity Function Display: An Improved Coherent Processor," *Applied Optics*, vol.16, no.3, March 1977.

[1.20] B. Ha and Y. Li, "Real-Time Self-Pumped Optical Phase Conjugate Based Wigner Distribution Processor for Complex Signals," *Applied Optics*, vol.30, pp.174-176, 1991.

[1.21] R. Agarwal and J. W. Cooley, "New Algorithms for Digital Convolution," *IEEE Trans. on Acoust., Speech and Sig. Proc.*, vol.ASSP-25, no.5, pp.392-410, October 1977.

[1.22] R. C. Agarwal and C. S. Burrus, "Fast Convolution using Fermat Number Transforms with Applications to Digital Filtering," *IEEE Trans. on Acoust., Speech and Sig. Proc.*, vol.ASSP-22, pp.87-99, April 1974.

[1.23] R. C. Agarwal and C. S. Burrus, "Number Theoretic Transforms to Implement Fast Digital Convolution," *Proc. IEEE*, vol.63, pp.550-560, April 1975.

[1.24] C. M. Rader, "Discrete Convolution via Mersenne Transforms," *IEEE Trans. on Comput.*, vol.C-21, pp.1269-1273, December 1972.

[1.25] R. C. Agarwal and C. S. Burrus, "Fast One-Dimensional Digital Convolution by Multidimensional Techniques," *IEEE Trans. on Acoust., Speech and Sig. Proc.*, vol.ASSP-22, pp.1-10, February 1974.

[1.26] W. T. Rhodes, "One-Dimensional to Two-Dimensional and Two-Dimensional to One-Dimensional Mappings in Optical Signal Processing," *SPIE Proc.*, vol.128, pp.322-331, 1977.

[1.27] T. M. Turpin, "Spectrum Analysis Using Optical Processing," *IEEE Proc.*, vol.68, no.1, pp.79-92, January 1981.

[1.28] W. Stoner, "Review of 1-D Signal Processing Using the Optical Transfer Function," *SPIE Proc.*, vol.634, pp.64-79, 1986.

1.6 Figures

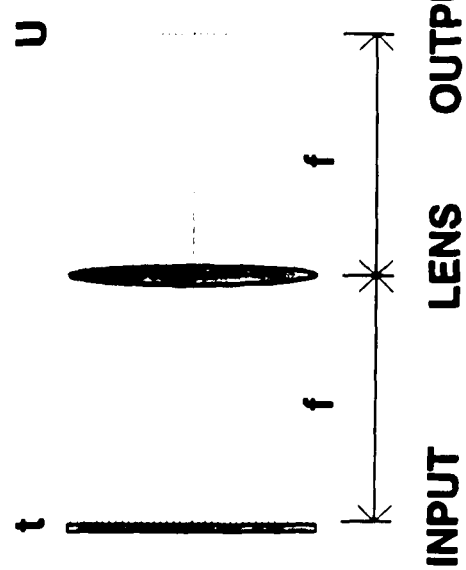

Fig.1.1.1. Optical implementation of Fourier transform.

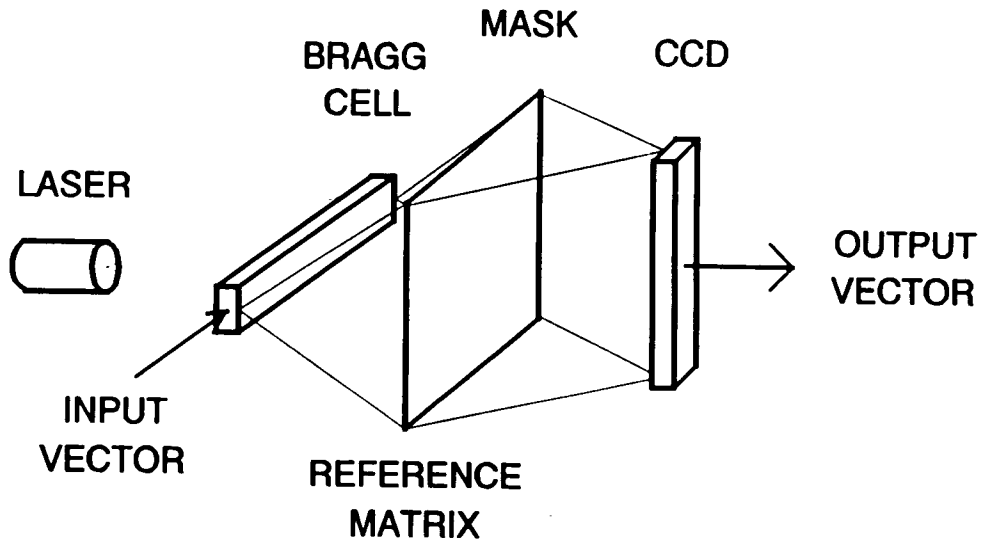

Fig.1.1.2. Optical implementation of vector-matrix multiplication.

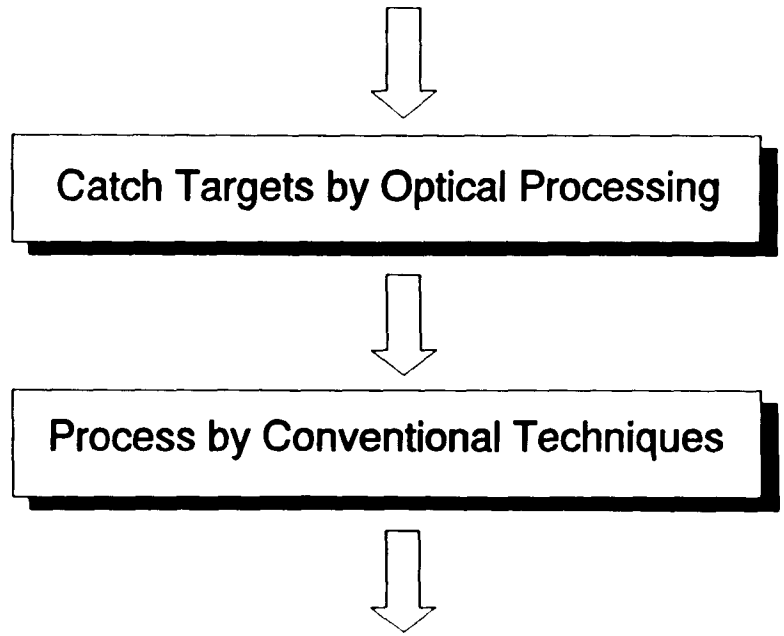

Fig.1.1.3. Optics aided signal processing.

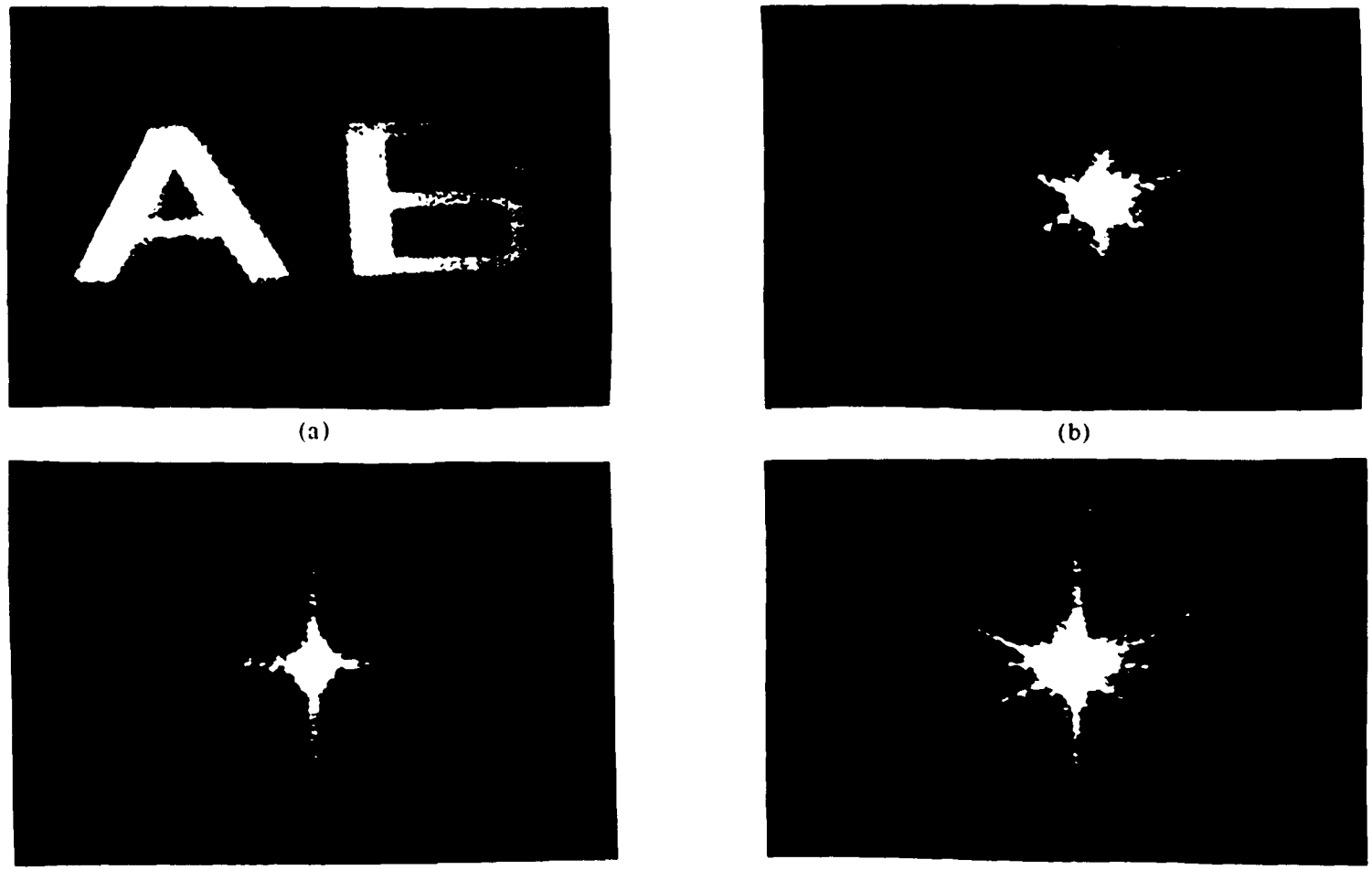

Fig.1.2.1. Weakness of Fourier transform. (a) Image with letters "A" and "B", (b) the Fourier transform of letter "A", (c) the Fourier transform of letter "B", and (d) the Fourier transform of the image in (a).

2 A BRIEF REVIEW OF OPTICAL SIGNAL PROCESSING TECHNIQUES

2.1 Optical Fourier Transform

As one of the basic signal processing operations, N-dimensional (N-D) Fourier transform and inverse Fourier transform are defined by

$$\mathbf{G}(f_1, f_2, \ldots, f_n) = \int_{-\infty}^{+\infty}\int_{-\infty}^{+\infty}\cdots\int_{-\infty}^{+\infty} \mathbf{g}(x_1, x_2, \ldots, x_n)\, e^{-j2\pi(f_1x_1+f_2x_2+\cdots+f_nx_n)}\, dx_1\, dx_2 \cdots dx_n \tag{2.1.1}$$

and

$$\mathbf{g}(x_1, x_2, \ldots, x_n) = \int_{-\infty}^{+\infty}\int_{-\infty}^{+\infty}\cdots\int_{-\infty}^{+\infty} \mathbf{G}(f_1, f_2, \ldots, f_n)\, e^{j2\pi(f_1x_1+f_2x_2+\cdots+f_nx_n)}\, df_1\, df_2 \cdots df_n \tag{2.1.2}$$

where $\mathbf{g}$ is a complex function of n independent variables $x_1, x_2, \ldots, x_n$ while its Fourier transform G is a complex function of n independent variables $f_1, f_2, \ldots, f_n$. Besides their analog realizations, many algorithms have been developed for electronic computer to carry out the above defined Fourier transform in discrete

form, the so called discrete Fourier transform (DFT). Examples are the Cooley-Turkey Fast Fourier Transform [2.1] and Winograd Fast Fourier Transform [2.2]. Although, they were originally designed to perform 1-D Discrete Fourier Transform (FFT), they could be used to calculate N-D DFT by transforming the N-D array in each dimension sequentially. A flowing chart for performing 2-D FFT by 1-D FFT is shown in Fig.2.1.1. Because of the inherent sequential processing property of electronic computer, these algorithms become unacceptably slow in some applications, such as in sonar and radar signal detection, especially when the data array is very large. Parallel processing schemes have thus to be employed to solve the problem.

The coherent optical system shown in Fig.2.1.2 is one of the candidates to solve the processing speed problem of Fourier transform. The kernel component in this system is a spherical lens. The coherent light beam which can be generated by a laser source is collimated and illuminates onto the input image which is located at the front focal plane of the spherical lens. The output pattern at the back focal plane of the lens is therefore the required Fourier transform of the input image.

To illustrate this principle mathematically, it is assumed that the coherent plane wave obtained from collimation is of amplitude A. The amplitude of optical field at the right side of the input image mask is described by

$$U_{in}(x_i, y_i) = A\,t(x_i, y_i) \qquad (2.1.3)$$

where $t(x_o, y_o)$ is the intensity transmittance of the input image. Based on the Fresnel diffraction theory, the optical field directly at the left side of the spherical lens is [3]

$$U_l(x_l, y_l) = \int_{-\infty}^{+\infty} \int_{-\infty}^{+\infty} U_{in}(x_i, y_i) e^{j\frac{k}{2f_l}[(x_l - x_i)^2 + (y_l - y_i)^2]} dx_i dy_i \qquad (2.1.4)$$

where f_l is the focal length of the employed lens, λ is the optical wavelength and $k = \frac{2\pi}{\lambda}$. The optical field on the right side of the spherical lens is thus described by [2.3]

$$U'_l(x_l, y_l) = e^{j\frac{k}{2f_l}(x_l^2 + y_l^2)} \int_{-\infty}^{+\infty} \int_{-\infty}^{+\infty} U_{in}(x_i, y_i) e^{j\frac{k}{2f_l}[(x_l - x_i)^2 + (y_l - y_i)^2]} dx_i dy_i \qquad (2.1.5)$$

Applying the Fresnel diffraction theory again and simplifying the resulted equation using the Fraunhoffer's approximation, the optical field at the back focal plane of the lens is obtained as

$$U_{out}(x_o, y_o) = \int_{-\infty}^{+\infty} \int_{-\infty}^{+\infty} t(x_i, y_i) e^{-j\frac{2\pi}{\lambda f_l}(x_o x_i + y_o y_i)} dx_i dy_i \qquad (2.1.6)$$

This result apparently is in the form of the 2-D Fourier transform of the input image.

---

3 Complex constants before the integral symbol of this and the following equations are omitted without sacrificing the analysis accuracy.

To perform 1-D Fourier transform optically, an anamorphic optics shown in Fig.2.1.3 is used. In this system, the focal length of the cylindrical lenses L1 and L3 is half of the focal length of cylindrical lens L2. In principle, it images the input pattern in one direction while performs Fourier transform in another direction. The 1-D Fourier transform of the input pattern is thus resulted. With the above discussed optical system available as a basic unit, various signal processing systems can be built.

2.2 Optical Correlators

An N-dimensional Correlation is mathematically defined by

$$y(t_1, t_2, \cdots, t_n) = \int_{-\infty}^{+\infty} \cdots \int_{-\infty}^{+\infty} h(\tau_1 - t_1, \tau_2 - t_2, \cdots, \tau_n - t_n) \cdot x(\tau_1, \tau_2, \cdots, \tau_n) d\tau_1 d\tau_2 \cdots d\tau_n \qquad (2.2.1)$$

where $x(\cdot)$ is the input signal, $h(\cdot)$ is the reference and $y(\cdot)$ is the correlation result. When the input signal is matched with the reference, a correlation peak is resulted which shows the existence of certain target. Based on this definition, a coherent optical system for correlating two 2-D signals as shown in Fig.2.2.1 was described by Goodman [2.3].

In this optical setup, the coherent light from laser source is first spatially filtered and collimated. The image to be processed (signal) is placed at the front

focal plane of the spherical lense L2. Based on the principle of optical Fourier transform discussed in the last section, the 2-D Fourier transform of the input image is obtained at the back focal plane of lense L2. On the other hand, since the correlation of Eq.(2.2.1) may also be described by its counterpart in frequency domain as

$$Y(\omega_1, \omega_2, \ldots, \omega n) = H^*(-\omega_1, -\omega_2, \ldots, -\omega_n) X(\omega_1, \omega_2, \ldots, \omega_n) \tag{2.2.2}$$

a filtering mask (transparency) with its transmittance proportional to $H^*(-\omega_1, -\omega_2)$ may be realized and placed it at the back focal plane of lens L2. A multiplication operation between the Fourier transform of the input image and the reversed version of the complex conjugate of the reference image is thus resulted. A second Fourier transform delivers the correlation result at the back focal plane of the lens L3 except a complex constant.

Generally, for a real image as the reference, its Fourier transform is a complex valued function. To directly make a complex valued filtering mask is obviously difficult. To bypass this obstacle, a clever method to synthesize the frequency-plane filtering mask was invented by Vander Lugt in 1963 (see Fig.2.2.2) [2.3],[2.4],[2.5]. It was proved that, using this setup, a pure "absorbing" mask with its transmittance

$$t \propto r_0^2 + \frac{1}{\lambda^2 f^2} |H|^2 + \frac{r_0}{\lambda f} H e^{j2\pi\alpha y_2} + \frac{r_0}{\lambda f} H^* e^{-j2\pi\alpha y_2} \tag{2.2.3}$$

was obtained. Once this filtering mask was obtained, it was inserted into the coherent processing system of Fig.2.2.1. An output pattern (see Fig.2.2.3) at the back focal plane of lens L3 contains the convolution and the correlation of the input image and the reference image at the same time. Placing the detector array at the location corresponding to the correlation pattern delivers the required results.

Although the above discussed optical correlator may deliver the mathematically defined correlation operation, in some of the applications such as pattern recognition, the correlation peaks are not sharp enough. To improve the performance of optical correlator, a number of techniques were developed specifically for applications such as signal detection and pattern recognition.

2.2.1 Joint Transform Correlator

Originally suggested by Weaver and Goodman [2.6] in 1966, the Joint Transform Correlator (JTC) has been used widely in applications such as pattern recognition. Fig.2.2.4 schematically shows a optical joint transform correlator. In this setup, the Fourier transforms of data and reference generate an interference pattern on CCD detector A which transfers the intensity of the pattern to a second SLM. The pattern on the SLM is then read by a coherent light beam and Fourier transformed. Targets can thus be located on the pattern detected by the CCD detector B. Although JTC does not deliver the exact mathematically defined correlation, it is very useful when applications are for finding the locations of certain targets rather than obtaining the mathematically accurate

correlation results. A correlation peak resulted by JTC is much sharper than that obtained by a conventional correlation. This makes JTC a better tool for pattern recognition. However, it also suffers a drawback. Since what is detected by the CCD are interference fringes, the nonuniform intensities of signal and reference images will result in a low contrast and therefore cause a low correlation efficiency. To overcome this problem, an intensity-invariant JTC was suggested recently by S. Jutamulia, et al [2.7]. In the scheme (see Fig.2.2.5), the images of signal and reference are illuminated by two coherent but orthogonally polarized beams. The pedestal terms existing in the conventional interference pattern are cancelled through a hybrid operational amplifier leading to a high correlation efficiency.

2.2.2 Optical Phase-Only Filter

Another scheme which is widely used to enhance the performance of optical correlator is the optical phase-only filter [2.8]. In principle, the phase only correlator shares the same system architecture with a conventional optical correlator (see Fig.2.2.1) except for the filtering mask located at the Fourier plane of lens L2. While the filter of the conventional correlator is the complex conjugate of the 2-D Fourier transform of the reference pattern as

$$F^*(u,v) = A(u,v)\exp(-j2\pi\phi(u,v)) \qquad (2.2.4)$$

with the amplitude and phase terms preserved, the phase only filter is defined to be

$$F_{\phi}^{*}(u,v) = \exp(-j2\pi\phi(u,v)) \qquad (2.2.5)$$

obtained by setting $A(u,v)$ equal to unity. Because the amplitude of a phase-only filter is one, a high optical throughput efficiency is obtainable in an optical phase-only filter. On the other hand, the definition of phase-only filter may be rewritten in another form of

$$F_{\phi}^{*}(u,v) = F^{*}(u,v) \cdot \frac{1}{A(u,v)} \qquad (2.2.6)$$

which indicates that a phase-only filter is, in fact, a cascade of a conventional matched filter and a followed filter of $\frac{1}{A(u,v)}$. Since the signal spectra usually approach zero for high frequencies, the additional filter acts as a high-pass filter which emphasizes high frequency components. Therefore, sharper and more localized correlation peaks are expected by phase-only filtering. The above two properties of phase-only filter were experimentally demonstrated [2.8],[2.9],[2.10]. The concept of binary phase-only filter was also suggested to decrease the large memory requirement of regular phase-only filter [2.11],[2.12]

2.3 Optical Algebraic Processor

Algebraic operations such as convolution / correlation and vector-matrix multiplication belong to another group of basic operations employed in signal processing, which are directly calculated without the aid of their descriptions in the transform domain. To carry out the above operations on very long data sequence, optical processing is also preferred for its parallel processing capability

and ultra-fast processing speed.

2.3.1 Optical Convolver and Correlator

To optically perform the convolution or correlation operation, many architectures were proposed [2.13],[2.14]. As an example, the system shown in Fig.2.3.1 originally investigated by Kellman [2.15] is briefly described here.

In the setup, the coherent source is modulated by a 1-D signal $s_1(t)$ while two acousto-optic modulators are employed as the input devices for 1-D signals $s_2(t)$ and $s_3(t)$. This leads to the intensity distribution at the output domain at one instant described by

$$I(x, y, t) = s_1(t)s_2(t - x/v)s_3(t - y/v) \quad (2.3.2)$$

where v is the acoustic speed. If a 2-D Charge Coupled Device (CCD) array is placed at the output plane, its time integration effect delivers the following 2-D intensity distribution of

$$E_T(x, y) = bias + \int_{\Delta T} s_1(t)s_2\left(t - \frac{x}{v}\right)s_3\left(t - \frac{y}{v}\right)dt \quad (2.3.2)$$

The system is thus called a triple product processor. Operations like cross-ambiguity functions and spectrum analysis with the appropriate selection of $s_1(t)$, $s_2(t)$ and $s_3(t)$. Slight modification to the system results in the operations of convolution and correlation. Specifically, the convolution of $s_2(t)$ and $s_3(t)$

is realized by setting a constant intensity laser source, feeding $t_2(t)$ in opposite direction and placing a horizontal 1-D CCD array at the output plane. Convolution may also be carried out by using intensity modulated (by $t_1(t)$) laser source, one of the two acousto-optic modulators and a horizontal or vertical 1-D CCD array [2.13].

2.3.2 Optical Vector-Matrix Multiplier

Schemes for optical implementation of vector-matrix multiplication were widely described in literatures [2.16]-[2.20] as alternatives to computer implementations.

The hybrid system shown in Fig.2.3.2, which was suggested by E. P. Mosca, et al [2.20], is an example. In this hybrid system, the beam from a diode laser is shaped by a spherical and cylindrical lens so that it illuminates the 1-D Bragg cell device along the horizontal direction (along the window). The longitudinal power distribution of the acoustic field is a representation of the elements of the input vectors. At the other side of Bragg cell device, the vector becomes encoded in the horizontal intensity distribution of the diffracted radiation. This diffracted radiation is then incident on the mask which carries the matrix. The radiation transmitted through the mask is directed onto a linear CCD detector so that the radiation from each row of mask is summed by a corresponding element of the detector array. The vector-matrix multiplication is thus performed.

2.4 State-of-the-Art Optical Components

Besides to conventional optical components such as lens, prism, beamsplitter and mirror, electro-optic components are also employed in optical signal processing system as input / output device and incoherent-to-coherent converter. Examples are acousto-optic modulator, SLM and CCD detector array.

Analog optical one-dimensional and two-dimensional Bragg cell devices are now commercially available [2.21]. Depending on a particular cell, their time windows are limited in the range from milli- to micro-seconds. For a one-dimensional Bragg cell, in general, the time-bandwidth product, which is equal to the number of resolvable data or signal points that the processor is able to accommodate, is in the range of 1000 to 2000. There also exist channelized two-dimensional Bragg cell structures. In terms of dynamic range, new device technologies are able to accommodate detectors with a dynamic range of 60 dB. This dynamic range is now sufficient for Bragg cell devices used in most convolution and correlation applications as input devices.

On the other hand, the development of two-dimensional spatial light modulators is also in progress [2.22]. A deformable mirror device (DMD) has already reached the resolution of 128 × 128 pixels and has demonstrated its potential for higher resolution and faster frame rate, say 1000 × 1000 pixels with 1KHz frame rate. 2-D SLM devices using magnetooptic modulation mechanism are currently available

in a 256 x 256 pixel format with line update rates of microseconds. Other commercially available SLM's are Electron Beam Addressed SLM, Liquid Crystal Light Valve (LCLV) and Microchannel Plate SLM. As an economic SLM, Liquid Crystal TV (LCTV) is also used in optical signal processing [2.23].

Since the first demonstration of Charge Coupled Device (CCD) at Bell Laboratories in 1970, CCD detector has experienced an unbelievable progress [2.24]. The advantages of a CCD device expected when it was first suggested twenty years ago benefit a wide range of applications. Among them are small size and weight, very high quantum efficiency, broad spectral response, geometric stability and fidelity, linear response, high resolution, low noise, low dark current, and very large dynamic range. 1-D and 2-D high resolution CCD detector arrays are now available. Typical high resolution for 2-D CCD array is 1024x1024. Arrays with their pixel numbers more than this is also available, such as TK2048 of Tektronix Inc. with resolution of 2048x2048 pixels.

2.5 References

[2.1] A. V. Oppenheim and R. W. Schafer, *Digital Signal Processing*, Prentice-Hall, New Jersey, 1975.

[2.2] S. Winograd, "On Computing of Discrete Fourier Transform," *Math. of Comp.*, vol.32, no.141, pp.175-199, January 1978.

[2.3] J. W. Goodman, *Introduction to Fourier Optics*, McGraw-Hill, New York, 1968.

[2.4] A. B. Vander Lugt, *Signal Detection by Complex Spatial Filtering*, Radar Lab., Rept. No. 4594-22-T, Institute of Science and Technology, The University of Michigan, Ann Arbor, 1963.

[2.5] A. B. Vander Lugt, "Signal Detection by Complex Spatial Filtering," *IEEE Trans. Infor. Theo.*, vol.IT-10, no.2, 1964.

[2.6] C. S. Weaver and J. W. Goodman, "A Technique for Optically Convolving Two Functions," *Applied Optics*, vol.5, no.7, pp.1248-1249, July 1966.

[2.7] S. Jutamulia, K. Comany and D. A. Gregory, "Intensity-Invariant Joint Transform Correlator," *Optics & Photonics News*, p.13, December 1991.

[2.8] J. L. Horner and P. D. Gianino, "Phase-Only Matched Filtering," *Appl. Opt.*, vol.23, no.6, pp.812-816, 15 March 1984.

[2.9] P. G. Gianino and J. L. Horner, "Additional Properties of the Phase-Only Correlation Filter," *Opt. Eng.*, vol.23, p.695, 1984.

[2.10] C. S. Anderson and R. C. Anderson, "Comparison of Phase-Only and Classical Matched Filter Scale Sensitivity," *Opt. Eng.*, vol.26, p.276, 1987.

[2.11] D. L. Flannery, J. S. Loomis and M. E. Milkovich, "Design Elements of Binary Phase-Only Filters," *Appl. Opt.*, vol.27, no.20, pp.4231-4235, 15 October 1988.

[2.12] D. M. Cottrell, R. A. Lilly, J. A. Davis and T. Day, "Optical Correlator Performance of Binary Phase-Only Filters Using Fourier and Hartley Transforms," *Appl. Opt.*, vol.26, no.18, pp.3755-3761, 15 September 1987.

[2.13] H. J. Caulfield, *Optical Computing*, Editor SPIE Milestones Series, vol.1142, 1989.

[2.14] W. T. Rhodes, "Acousto-Optic Signal Processing: Convolution and Correlation," *Proc. IEEE*, vol.67, no.1, pp.65-79, January 1981.

[2.15] P. Kellman, "Time Integration Optical Signal Processing," *Ph.D. Dissertation*, Stanford University, Stanford, CA, June 1979.

[2.16] W. T. Rhodes and P. S. Guifoyle, "Acoustooptic Algebraic Processing Architectures," *Proc. IEEE*, vol.72, no.7, pp.820-830, July 1984.

[2.17] N. Goto, Y. Yanayama and Y. Miyazaki, "Integrated Optic Matrix-Vector Multiplier using Multifrequency Acoustooptic Bragg Diffraction," *Appl. Opt.*, vol.30, no.5, pp.523-530, 1991.

[2.18] D. Psaltis and R. A. Athale, "High Accuracy Computation with Linear Analog Optical Systems: a Critical Study," *Appl. Opt.*, vol.25, no.18, pp.3071-3077, 15 September 1986.

[2.19] H. Nakano and K. Hotate, "Operational Error in the Optical Real-Time Multiple Matrix Multiplier and its Compensation," *Appl. Opt.*, vol.25, no.18, pp.3132-3136, 15 September 1986.

[2.20] E. P. Mosca, R. D. Griffin, F. P. Pursel and J. N. Lee, "Acoustooptical Matrix-Vector Product Processor: Implementation Issues," *Appl. Opt.*, vol.28, no.18, pp.3843-3851, 15 September 1989.

[2.21] N. J. Berg and J. N. Lee, *Acousto-Optic Signal Processing: Theory and Implementation*, Marcel Dekker, New York, 1983.

[2.22] J. A. Neff, R. A. Athale and S. H. Lee, "Two-Dimensional Spatial Light Modulator: A Tutorial," *Proc. IEEE*, vol.78, no.5, pp.826-855, 1990.

[2.23] A. Kostrzeswki, "Optical Arithmetic-Logic Processors Based on Location, Content Addressable and Associative Memories," *Ph.D Dissertation*, City University of New York, New York, 1990.

[2.24] M. M. Blouke, "Charge-Coupled Devices Reach Maturity," *Laser Focus World*, pp.A17-A19, March 1991.

2.6 Figures

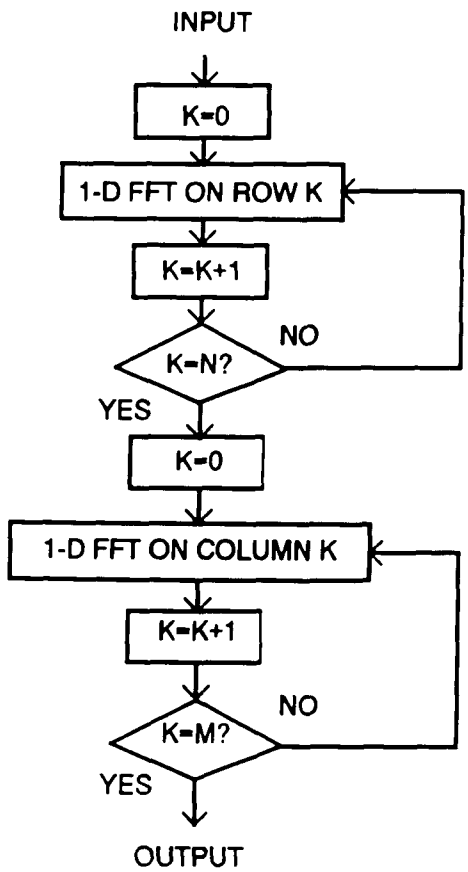

Fig.2.1.1. The flowing chart of performing 2-D FFT by 1-D FFT algorithms.

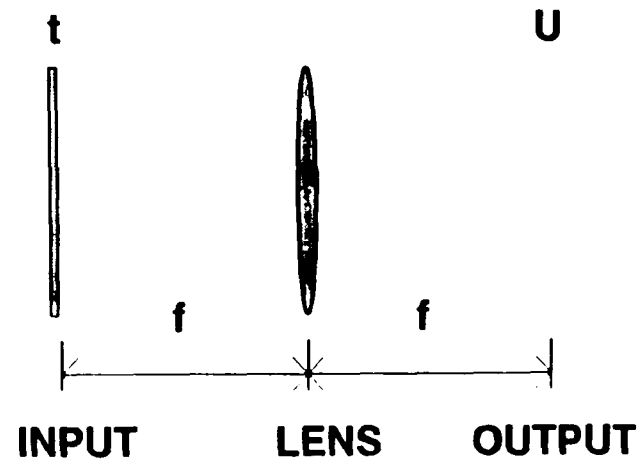

Fig.2.1.2. 2-D optical Fourier transform, where t is the image to be transformed, l is the transformation result, and L is a spherical lens with focal length of f_L.

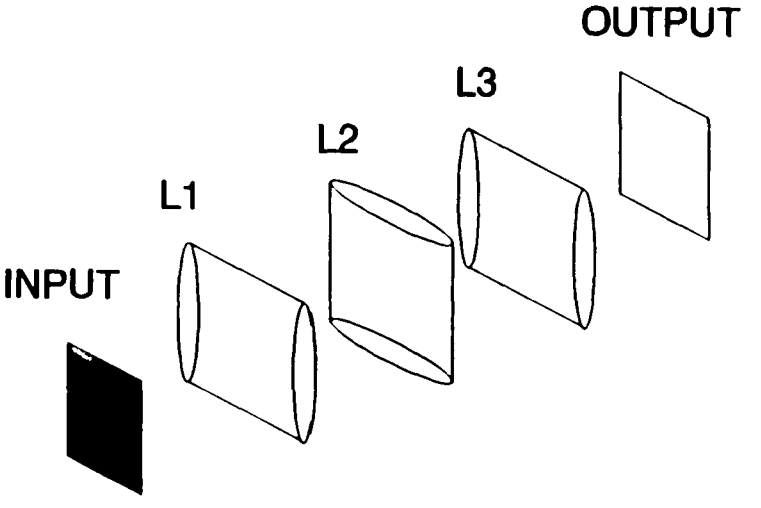

Fig.2.1.3. 1-D optical Fourier transform, where the focal length of the lens L2 is f, while that of the lenses L1 and L3 is $\frac{f}{2}$.

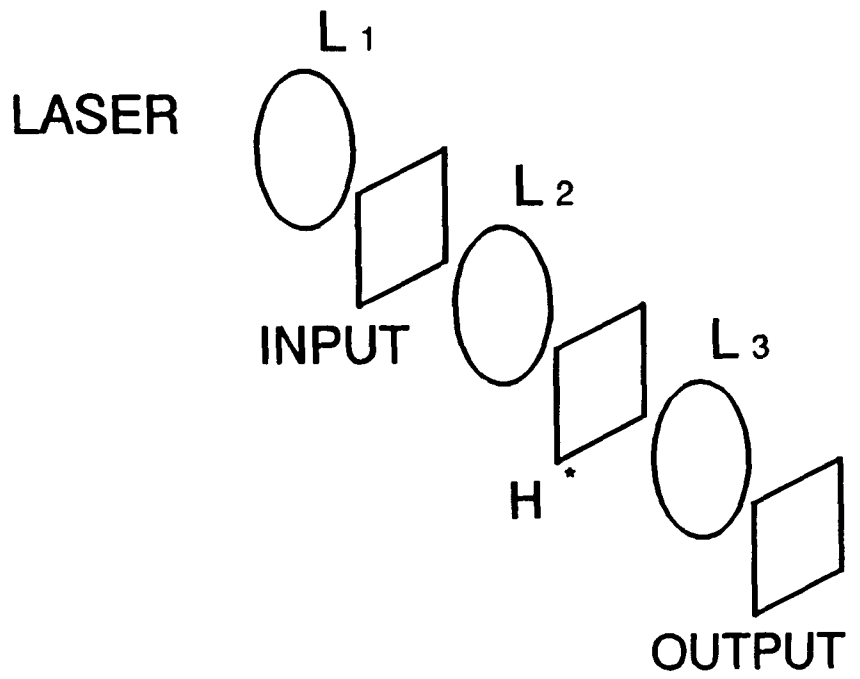

Fig.2.2.1. Conventional optical correlator, where H^* is the complex conjugate of the reference. The focal length of L2 and L3 is f_2.

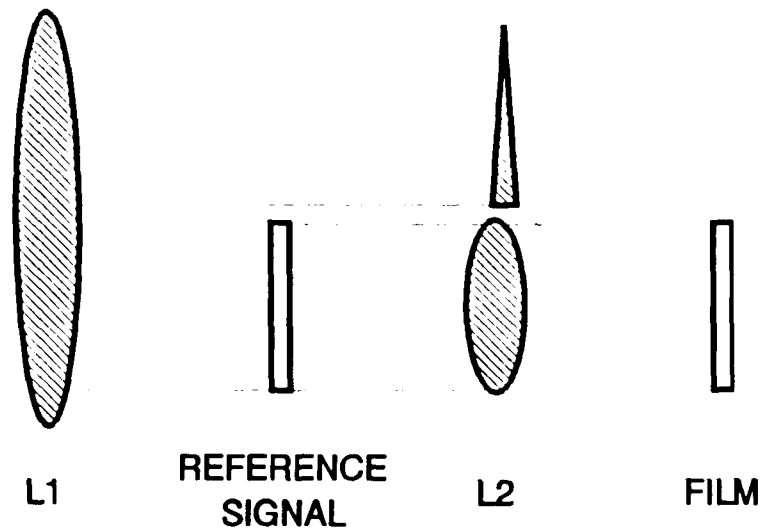

Fig.2.2.2. VanderLugt filter. The reference signal and the film are located at the front focal plane and back focal plane of the spherical lens L2, respectively.

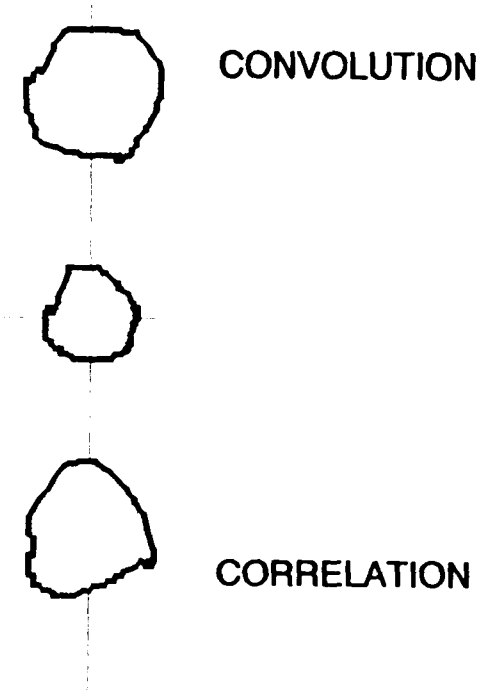

Fig.2.2.3. Output pattern of an optical correlator using VanderLugt filter.

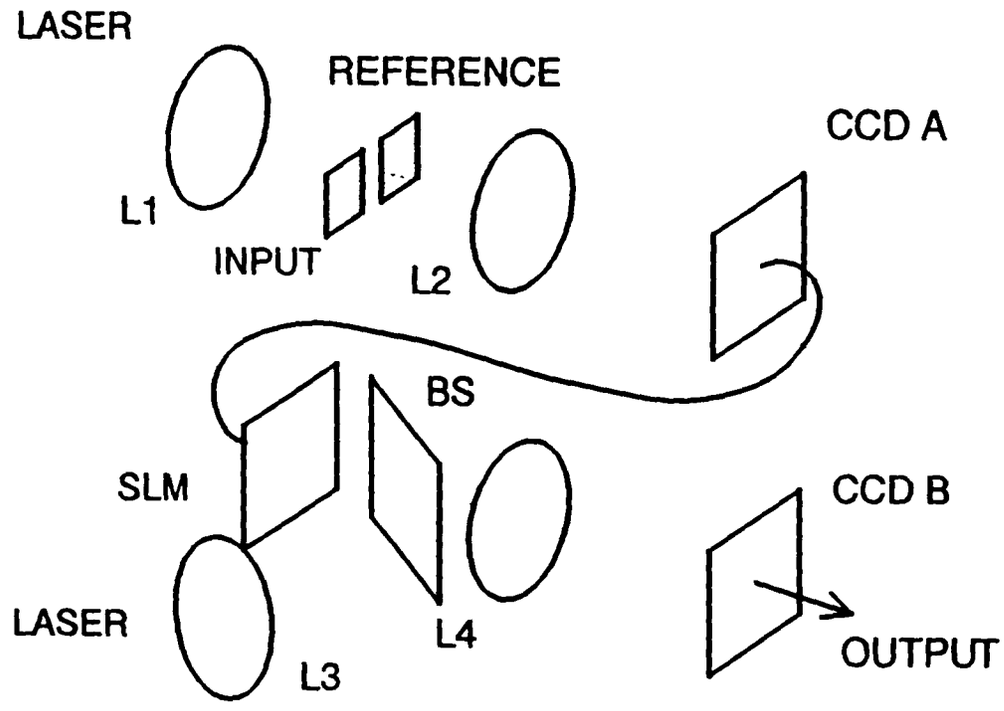

Fig.2.2.4. Optical joint correlator. The focal length of the lenses L2 and L4 is f, Reference, input, CCD A, SLM and CCD B are located at the focal planes of the lenses L2 and L4, respectively.

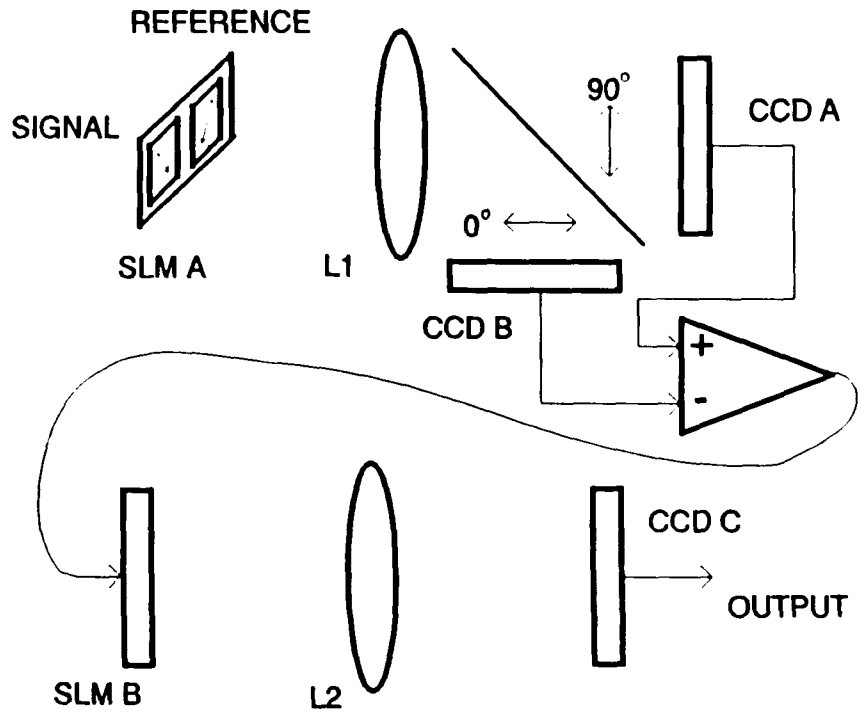

Fig.2.2.5. Jutamulia's modified joint transform correlator. The focal length of the lenses L1 and L2 is f, Reference, signal, CCD A, CCD B, SLM B and CCD C are on the focal plane of the lenses L1 and L2, respectively.

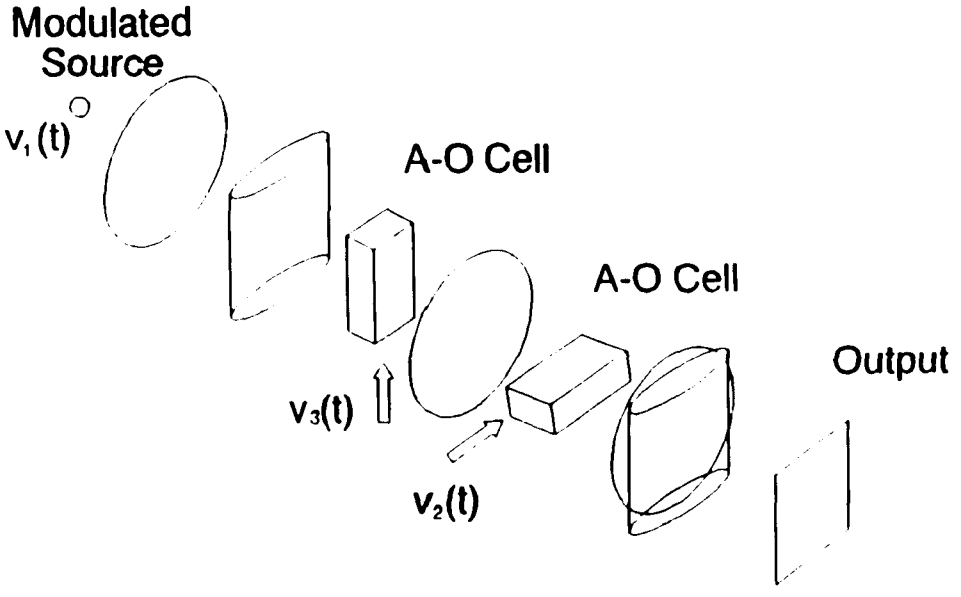

Fig.2.3.1. Kellman's optical tri-product integrator.

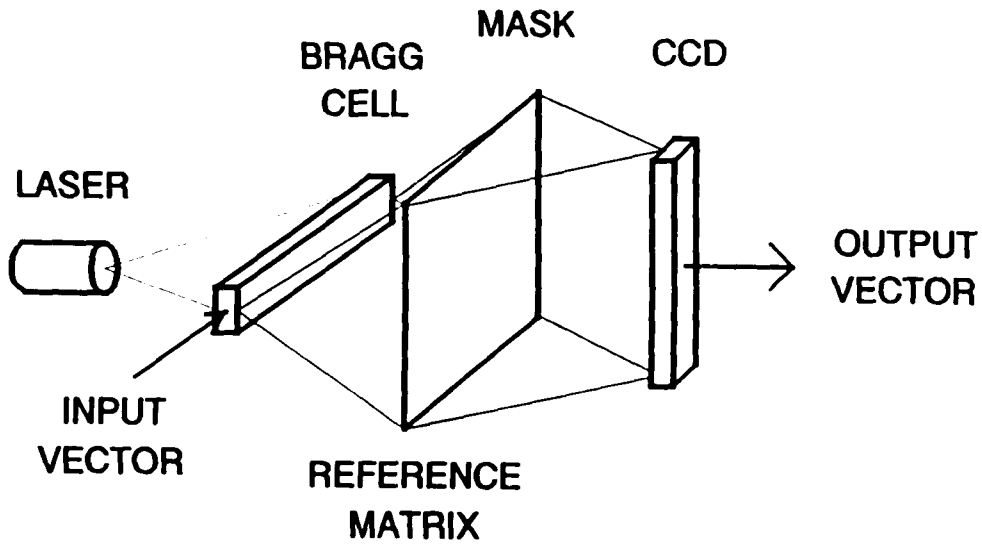

Fig.2.3.2. Mosca's optical vector-matrix multiplier.

3 OPTICAL REALIZATION OF LONG DATA STREAM CONVOLUTION/CORRELATION

3.1 Background

Because of its importance in communication, sensing and signal processing applications, methods of convolution and correlation of long data streams have been discussed in literatures. Many algorithms have been designed for electronic computers [3.1]-[3.5], which are based on Fast Fourier Transform (FFT) and Number Theory Transform (NTT). Although they were successfully used in many applications, due to the sequential processing nature of a conventional digital processor, convolution or correlation of long data streams at high speed is still difficult to perform.

To resolve this problem, concepts of parallel and distributed processing are needed. Optical systems with their inherent parallel processing capabilities are potential candidates for processing long data streams. Optical correlation of two signals with large time-bandwidth product was designed by Rhodes [3.6], who proposed to use a non-interlaced raster scan scheme to convert 1-D signals to their 2-D formats subject to an optical correlation suggested by Goodman [3.7]. Turpin [3.8] suggested a system which realizes an optical discrete Fourier transform of long sequence by first converting the original 1-D data sequence into a 2-D data array and then performing a 2-D optical Fourier transform on the 2-D pattern. A specially

designed phase-correcting prism was placed super accurately in the system to cancel an extra phase term. Various other interesting schemes of converting a 1-D sequence to its 2-D format suitable for optical processing were suggested by Stoner [3.9].

3.2 Chinese Remainder Theorem

The Chinese Remainder Theorem [3.10], well known in ancient China, states that it is possible to uniquely determine a non-negative integer given only its modulli with respect to each of several integers if the integer is known to be smaller than the product of modulli. As an example, consider the modulli

$$m_0 = 3$$

$$m_1 = 11$$

Their product is thus 33. Given a positive integer c, satisfying $0 \le c < 33$, let $c_i = c \bmod m_i$. The Chinese remainder theorem states that there is a one-to-one map between c and the corresponding c_i ($i = 0, 1$). Suppose that $c_0 = 1$, $c_1 = 2$ and $c_2 = 3$. Therefore, the set of c satisfying $c_0 = c \bmod m_0$ is

$$\{1, 4, 7, 10, 13, 16, 19, 22, 25, 28, 31\}$$

and the set of c satisfying $c_1 = c \bmod m_1$ is

$$\{2, 13, 24\}$$

The unique solution for c is thus 13. This example suggests that the residues uniquely determine the original integer. Generally, it may be proved:

Theorem 3.2.1:

Given a set of integers $m_0, m_1, \ldots, m_k$ that are pairwise relatively prime and a set of integers $c_0, c_1, \ldots, c_k$ with $c_i < m_i$, then the system of equations

$$c_i = c \mod m_i \qquad i = 0, 1, \ldots, k \qquad (3.2.1)$$

has at most one solution for c in the interval

$$0 \le c < \prod_{i=0}^{k} m_i$$

3.3 Index Mapping from 1-D to 2-D

Based on the above theorem, it is possible to generate an index mapping from 1-D to 2-D in order to design optically implementable algorithms. Consider a 1-D index

$$i = 0, 1, \ldots, N-1 \qquad (3.3.1)$$

where N is a composite number

$$N = r_1 r_2 \qquad (3.3.2)$$

with mutually prime factors r_1 and r_2. From the theorem in last section, there exists a one-to-one mapping

$$i \leftrightarrow (i_1, i_2) \qquad (3.3.3)$$

where i_1 and i_2 are defined by the congruent relations

$$i_1 = i \mod r_1 \qquad 0 \le i_1 < r_1$$

$$i_2 = i \mod r_2 \qquad 0 \le i_2 < r_2 \tag{3.3.4}$$

It is known from the Chinese remainder theorem that there is a unique solution i to the above congruent relations. The following theorem describes how to determine i from the known i_1 and i_2.

Theorem 3.3.1:

Let $N = r_1 r_2$ be a product of two mutually prime integers r_1 and r_2. Then the congruent relations of Eq.(3.3.4) is uniquely solved by

$$i = i_1 s_1 + i_2 s_2 \mod N \tag{3.3.5}$$

$$0 \le i < N$$

where

$$s_1 = 1 \mod r_1$$

$$s_2 = 1 \mod r_2 \tag{3.3.6}$$

$$s_1 = 0 \mod r_2$$

$$s_2 = 0 \mod r_1 \tag{3.3.7}$$

From the Chinese remainder theorem, it is known that there is only one solution to the congruent relations. So the question is to prove Eq.(3.3.4) is the solution. Modulo r_1 and r_2 operations are performed to Eq.(3.3.5), respectively, as follows

$$i \mod r_1 = i_1 s_1 + i_2 s_2 \mod r_1$$

$$i \mod r_2 = i_1 s_1 + i_2 s_2 \mod r_2$$

Since $0 \le i_1 < r_1$, $0 \le i_2 < r_2$, Eq.(3.3.6) and Eq.(3.3.7), the congruent relations in Eq.(3.3.4) are thus obtained.

To determine integers s_1 and s_2, it is found that

$$s_1 = n_1 r_2 = m_1 r_1 + 1 \tag{3.3.8}$$

and

$$s_2 = n_2 r_1 = m_2 r_2 + 1 \tag{3.3.9}$$

where n_1, n_2, m_1 and m_2 are positive integers. These two equations have to be solved. However, since there are four variables in two equations, an infinite number of solutions can be obtained. Only minimum values of n_1 and n_2 are selected as the final results. As a special case, when $r_1 = r_2 + 1$, it can be shown that the minimum n_1 and n_2 integers satisfying these equations are

$$n_1 = r_2$$

$$n_2 = 1$$

Therefore,

$$s_1 = r_2^2$$

$$s_2 = r_1$$

For example, when N=90, a selection of $r_1 = 10$ and $r_2 = 9$ results in

$$9n_1 = 10m_1 + 1$$

$$10n_2 = 9m_2 + 1$$

The minimum solution of these integer equations gives

$$s_1 = 81$$

$$s_2 = 10$$

which let Eq. (3.3.5) become $i = (81i_1 + 10i_2)_{90}$.

With this theorem available, algorithms which convert the convolution/correlation of long data streams to formats suitable for optical processing are ready to be constructed. In the following discussions, the computation of cyclic convolution

$$y(i) = \sum_{k=0}^{N-1} h(i-k)x(k) \qquad (3.3.10)$$

and cyclic correlation

$$z(i) = \sum_{k=0}^{N-1} h(k-i)x(k) \qquad (3.3.11)$$

are considered, where $i = 0, 1, 2, \ldots, N-1$ and integer N satisfies the condition in Eq.(3.3.2).

3.4 Conversion of 1-D Convolution/Correlation to Vector-Matrix Multiplications

To capitalize on the advantages of inherent ultra-high speed and parallel processing of an optical system , the convolution/correlation of Eqs.(3.3.10) and (3.3.11) are expressed in the form of large matrix-vector products:

$$y = Hx \tag{3.4.1}$$

$$z = H'x \tag{3.4.2}$$

which can be carried out by an optical matrix-vector multiplier.

3.4.1 Algorithm

In principle, for $N = r_1 r_2$ with mutually prime factors r_1 and r_2, the algorithm first shuffles and partitions the N-point data sequence into r_1 sub-sequences each with a length of r_2 while transforming the N-point reference sequence into r_1 matrices each with a scale of r_2^2. The convolution/correlation of Eqs.(3.3.10) and (3.3.11) are then converted into a group of vector-matrix multiplications and vector additions.

Based on the index mapping described in last section, the one-dimensional arrays of y_i / x_i, h_i, and x_i, where $i = 0, 1, \cdots, N-1$, can be indexed by the new index pair (i_1, i_2) governed by Eq.(3.3.5) and conceptually mapped onto the

respective two-dimensional arrays. Then the convolution/correlation Eqs.(3.3.10) and (3.3.11) become

$$y_{i_1,i_2} = \sum_{k_1=0}^{r_1-1} \sum_{k_2=0}^{r_2-1} h_{(i_1-k_1) \bmod r_1,(i_2-k_2) \bmod r_2} x_{k_1,k_2} \qquad (3.4.3)$$

and

$$z_{i_1,i_2} = \sum_{k_1=0}^{r_1-1} \sum_{k_2=0}^{r_2-1} h_{(k_1-i_1) \bmod r_1,(k_2-i_2) \bmod r_2} x_{k_1,k_2} \qquad (3.4.4)$$

which represent two-dimensional cyclic convolution and correlation[4], where the first dimension is of a length r_1 and the second dimension of a length r_2.

By combining Eq.(3.4.3) with relation (3.3.5), the convolution equation can now be written as

$$y_{(i_1 s_1 + i_2 s_2) \bmod N} = \sum_{k_1=0}^{r_1-1} \mathbf{h}_{(i_1-k_1) \bmod r_1} x_{k_1} \quad , \qquad (3.4.5)$$

4 In the following discussions, only convolution is described in detail. The derivation for correlation is similar.

where

$$\mathbf{h}_j = (h_{(js_1+t_2s_2)\bmod N} \quad h_{(js_1+(t_2-1)s_2)\bmod N} \quad \cdots \quad h_{(js_1+(t_2-r_2+1)s_2)\bmod N}) \tag{3.4.6}$$

$$j = (t_1 - k_1) \bmod r_1$$

and

$$\mathbf{x}_{k_1} = (x_{(k_1s_1)\bmod N} \quad x_{(k_1s_1+s_2)\bmod N} \quad \cdots \quad x_{(k_1s_1+(r_2-1)s_2)\bmod N})^T. \tag{3.4.7}$$

When the y_t is represented by

$$\mathbf{y}_t = (y_{(ts_1)\bmod N} \quad y_{(ts_1+s_2)\bmod N} \quad \cdots \quad y_{(ts_1+(r_2-1)s_2)\bmod N})^T, \tag{3.4.8}$$

where $t = 0, 1, \cdots, r_1 - 1$, the convolution can be regarded as

$$\mathbf{y}_t = \sum_{j=0}^{r_1-1} \mathbf{H}_{(t-j)\bmod r_1} \mathbf{x}_j \tag{3.4.9}$$

where

$$\mathbf{H}_t = \begin{pmatrix} h_{(ts_1)\bmod N} & h_{(ts_1+s_2)\bmod N} & \cdots & h_{(ts_1+s_2(r_2-1))\bmod N} \\ h_{(ts_1+s_2)\bmod N} & h_{(ts_1)\bmod N} & \cdots & h_{(ts_1+s_2(r_2-2))\bmod N} \\ \vdots & \vdots & \ddots & \vdots \\ h_{(ts_1+(r_2-1)s_2)\bmod N} & h_{(ts_1+s_2(r_2-2))\bmod N} & \cdots & h_{(ts_1)\bmod N} \end{pmatrix}. \tag{3.4.10}$$

With the help of Eq.(3.3.9), the above matrix can also be written as

$$\mathbf{H}_i = \begin{pmatrix} h_{(is_1)\bmod N} & h_{(is_1+(r_2-1)s_2)\bmod N} & \cdots & h_{(is_1+s_2)\bmod N} \\ h_{(is_1+s_2)\bmod N} & h_{(is_1)\bmod N} & \cdots & h_{(is_1+2s_2)\bmod N} \\ \vdots & \vdots & \ddots & \vdots \\ h_{(is_1+(r_2-1)s_2)\bmod N} & h_{(is_1+(r_2-2)s_2)\bmod N} & \cdots & h_{(is_1)\bmod N} \end{pmatrix}. \tag{3.4.11}$$

Thus, a set of standard vector-matrix multiplications is in order. Following exactly the same way, the correlation operation defined in Eq.(3.3.11) can be expressed as

$$\mathbf{Z}_i = \sum_{j=0}^{r_1-1} \mathbf{H}_{(j-i)\bmod N}\mathbf{X}_j \tag{3.4.12}$$

where

$$\mathbf{H}'_i = \begin{pmatrix} h_{(is_1)\bmod N} & h_{(is_1+s_2)\bmod N} & \cdots & h_{(is_1+(r_2-1)s_2)\bmod N} \\ h_{(is_1+(r_2-1)s_2)\bmod N} & h_{(is_1)\bmod N} & \cdots & h_{(is_1+(r_2-2)s_2)\bmod N} \\ \vdots & \vdots & \ddots & \vdots \\ h_{(is_1+s_2)\bmod N} & h_{(is_1+2s_2)\bmod N} & \cdots & h_{(is_1)\bmod N} \end{pmatrix}. \tag{3.4.13}$$

Suitable prime numbers r_1 and r_2 can be selected to make the length of each sub-sequence compatible with both the time-bandwidth product of the available Bragg cell devices and the scale of the matrix (3.4.11) or (3.4.13) for 2-D spatial light modulators.

People may wonder that, in order to represent a 1-D convolution by vector-matrix multiplication, the standard cyclic convolution can be directly written in the following format

$$\begin{pmatrix} y_0 \\ y_1 \\ y_2 \\ \cdot \\ y_{N-1} \end{pmatrix} = \begin{pmatrix} h_0 & h_{N-1} & h_{N-2} & \cdot & \cdot & h_1 \\ h_1 & h_0 & h_{N-1} & \cdot & \cdot & h_2 \\ h_2 & h_1 & h_0 & \cdot & \cdot & h_3 \\ \cdot & \cdot & \cdot & \cdot & \cdot & \cdot \\ h_{N-1} & h_{N-2} & h_{N-3} & \cdot & \cdot & h_0 \end{pmatrix} \begin{pmatrix} x_0 \\ x_1 \\ x_2 \\ \cdot \\ x_{N-1} \end{pmatrix}$$

(3.4.14)

This equation may be further converted into a group of vector-matrix multiplications by separating the input and output sequences to a group of shorter vectors in natural order. Although this seems more direct than the above derived algorithm, it contains r_1^2 different matrices. However, with the algorithm, there are only r_1 different sub-matrices needed to represent the reference sequences. Therefore a less memory requirement than that of using the partition in a natural order is resulted. Since a parallel optical matrix-vector multiplier treats each matrix-vector multiplication as one calculation and performs it on-the-fly, the total number of calculations here is in the order of r_1^2 which is much less than N^2. Also, it is noted that the convolution and correlation operations can share one optical setup because H'_i is simply the transpose of H_i. The flow chart of the basic convolution/correlation algorithm via partitioning and matrix-vector operation is shown in Fig.3.4.1. And a detail description of the algorithm for $r_1 = 3$ is depicted in Fig.3.4.2.

3.4.2 Computer Simulation

To demonstrate the above described algorithm, a 70-point data sequence x and a 20-point reference sequence h as shown in Fig.3.4.3 (a) and (b) are chosen

for convolution/correlation simulation. Using Eqs.(3.4.7) and (3.4.11)/(3.4.13), the sub-sequences of input data sequence x and sub-matrices H_i / H'_i of reference sequences are obtained by an installed data shuffle program in an AT&T 3B2 computer. Using these decomposed vectors and matrices in a system depicted in Fig.3.4.1, the computer simulation results for convolution and correlation are depicted in Fig.3.4.3 (c) and (d). Here, it should be noted that in order for the data to be in the form: $N = r_1 r_2$, where r_1 and r_2 are prime numbers, seven 0's are added to data sequence to make it to the length of 77 points, i.e. 7 times 11. The computer simulation results are exactly the same as the results obtainable from the conventional convolution or correlation definitions.

3.4.3 Opto-electronic Convolver/Correlator Architecture

As shown above, the convolution/correlation of long data streams can be converted using the new algorithm into a parallel set of vector-matrix multiplications and vector additions. To optically implement this algorithm, the restrictions associated with analog optical vector-matrix multiplication, i.e. its numeric accuracy is commonly limited to 8 bits [3.11], should be considered. This restriction can be used to determine the size of the sub-matrices to be partitioned. To accomplish high precision optical matrix multiplication, other practical problems including optical number encoding schemes should also be considered. Since only positive numbers can be directly expressed in an optical system,

conventional optical vector-matrix multipliers use the so called offset data representation, which represents a negative number by

$$a' = a + a_{offset} \qquad (3.4.15)$$

where a_{offset} is an appropriate offset value which makes a' positive [3.12]. This number representation causes problem for data correction in the case of multiple results. To bypass this problem, a data representation which only employs positive numbers or zero is used here. With this representation, a vector $\mathbf{x}$ is represented as

$$\mathbf{x} = \mathbf{x}^{+} - \mathbf{x}^{-} \qquad (3.4.16)$$

where $\mathbf{x}^{+}$ and $\mathbf{x}^{-}$ are its positive and negative parts, respectively, whose elements are either positive or zero. For example, vector $(1.,-1.2,-2.0,-3.4)$ can be expressed by

$$(1,0,2,0,0,0,4)-(0,1,0,2,0,3,0)$$

where

$$\mathbf{x}^{+} = (1,0,2,0,0,0,4)$$

and

$$\mathbf{x}^{-} = (0,1,0,2,0,3,0)$$

Apparently, there are no negative numbers in the resulted vectors. Similarly, the matrix $\mathbf{H}$ is also represented by a subtraction of its negative part from its positive part as

$$\mathbf{H}=\mathbf{H}^{+} - \mathbf{H}^{-} \quad . \qquad (3.4.17)$$

Based on this data representation and the rule of multiplication, $H^{+}x^{+}$ pair and $H^{-}x^{-}$ pair give the positive part of Hx while $H^{+}x^{-}$ pair and $H^{-}x^{+}$ give its negative part. A simple electronic subtraction of its negative from its positive part at the end will generate a correct result for $y = Hx$.

Now, based on the algorithm described in last section, a new opto-electronic convolver-correlator architecture is proposed, (see in Fig.3.4.4). Before the input data sequence enters the convolver-correlator, it is first shuffled in parallel using equation (3.4.7) with either an optical or an electronic routing processor and partitioned into r_1 shorter sub-sequences. Then, all these sub-sequences are separated into their positive and negative parts. This separation can also be performed in parallel. The thus preprocessed data are ready for matrix-vector processing in the system to be described. As the light source, the light beam generated from a pulsed laser is shaped by a spherical/cylindrical lens combination to a narrow beam bar. This light bar illuminates the apertures of both Bragg cell devices A and B, which are driven by RF signals carrying the positive and negative parts of input data sequence, respectively. The diffracted beams are then expanded using a group of spherical and cylindrical lenses in the direction perpendicular to the apertures. A light intensity pattern of Fig.3.4.5 is obtained at 2-D SLMs A and B, which carries reference data in the form of matrices specified by equation (3.4.10) or (3.4.12). At the other sides of the SLMs, a second spherical and cylindrical lens combination pairs collect the radiation from SLMs and direct them to the CCD detector arrays **a** to **d**. As an example, consider the branch **a** which performs the multiplication of $H^{+}x^{+}$

pairs. With the arrangement in Fig.3.4.4, the CCD array **a** is located at the center of a special plane, which is the image plane of SLM in vertical direction and Fourier transform plane in horizontal direction. The detected light intensity at each detector of the CCD array equals the summation of light intensity at an appropriate row of the SLM, which derives a pixel result of a vector-matrix multiplication. This is true because the location of the CCD array corresponds to a dc spatial frequency in horizontal direction. The combination of CCD arrays **a** to **d** will generate the correct vector-matrix multiplication. A reshuffling process of equation (3.4.8) will provide the final convolution or correlation result. The difference between the convolution and the correlation operations is simply the different feeding direction of shuffled reference sub-sequences as noted in equations (3.4.11) and (3.4.13).

3.5 Conversion of 1-D Convolution/Correlation to 2-D Convolution/Correlation

Utilizing the inherent parallel property of optical processing, the above algorithm can be used to optically perform convolution/correlation of long data stream at ultra-fast speed. However, the method relies on the use of a large number of optical vector-matrix multipliers which may not be practical in the near-future.

To overcome these problems while still enjoying parallel processing advantages that optics can offer, another algorithm which is efficient opto-electronically is presented in this section. The concept of this scheme was initially suggested by Stoner [3.9]. The algorithm first shuffles and transforms the original long data

sequences into 2-D data arrays. Then, with the aid of a 2-D Fourier transform, it generates the convolution result in a 2-D shuffled format. The algorithm is especially suitable for optical realization. Since the data permutations are based on the Chinese remainder theorem, the only other condition to validate the scheme is that the data point number should be separable into two mutually prime numbers. With these conditions being satisfied, the data shuffles could easily be realized by either appropriate opto-electronic scanning schemes or an optical geometrical transform. With its inherently ultra-high speed and parallel processing advantages, it is possible for an optical system equipped with the discussed algorithm to handle large scale data processing problems in real time.

Using the index mapping in Section 3.3, the 1-D cyclic convolution of Eq.(3.3.10) may also be expressed by a 2-D cyclic convolution in the form of

$$y(i_1, i_2) = \sum_{k_2=0}^{r_2-1} \sum_{k_1=0}^{r_1-1} h(i_1 - k_1, i_2 - k_2) x(k_1, k_2) \qquad (3.5.1)$$

where the indices of h are understood to be taken modulo r_1 and r_2 operations, respectively. Various algorithms have been developed based on this equation for the implementations in electronic computers [3.1][3.2],[3.4],[3.5],[3.10]. Also, this form of convolution expression is especially suitable to optical realizations.

3.5.1 Algorithm

Based on the properties of Fourier transform, it is known that the Fourier transform $Y(k)$ of the convolution result $y(i)$ defined by Eq.(3.3.10) is obtained as

$$Y(k) = X(k)H(k) \qquad (3.5.2)$$

$k = 0, 1, \ldots, N-1$

where $X(k)$, $H(k)$ and $Y(k)$ are the Fourier transforms of the input $x(i)$, the reference $h(i)$ and the convolution result $y(i)$, respectively, i.e.

$$X(k) = \sum_{i=0}^{N-1} x(i) e^{-j\frac{2\pi ik}{N}} \qquad (3.5.3)$$

$$H(k) = \sum_{i=0}^{N-1} h(i) e^{-j\frac{2\pi ik}{N}} \qquad (3.5.4)$$

$$Y(k) = \sum_{i=0}^{N-1} y(i) e^{-j\frac{2\pi ik}{N}} \qquad (3.5.5)$$

To start the derivation of the parallel and distributed convolution algorithm, first, the condition on N, i.e. $N = r_1 r_2$ where r_1 and r_2 are the two relatively prime numbers, is still observed. For those N's which do not satisfy this condition initially, zeros can be padded to either of their ends. Now, based on Theorem 3.3.1, a one-to-one mapping $i \Leftrightarrow (i_1, i_2)$ is defined, where i_1 and i_2. As an example,

consider $N = 90$ where $r_1 = 10$ and $r_2 = 9$. From the index mapping described in Section 3.3, the original 1-D data in a natural sequence of

$$(0,1,2,3,4,5,6,7,8,\ldots,85,86,87,88,89)$$

is mapped to the following 2-D index array

$$\begin{pmatrix} 0 & 81 & 72 & 63 & 54 & 45 & 36 & 27 & 18 & 9 \\ 10 & 1 & 82 & 73 & 64 & 55 & 46 & 37 & 28 & 19 \\ 20 & 11 & 2 & 83 & 74 & 65 & 56 & 47 & 38 & 29 \\ 30 & 21 & 12 & 3 & 84 & 75 & 66 & 57 & 48 & 39 \\ 40 & 31 & 22 & 13 & 4 & 85 & 76 & 67 & 58 & 49 \\ 50 & 41 & 32 & 23 & 14 & 5 & 86 & 77 & 68 & 59 \\ 60 & 51 & 42 & 33 & 24 & 15 & 6 & 87 & 78 & 69 \\ 70 & 61 & 52 & 43 & 34 & 25 & 16 & 7 & 88 & 79 \\ 80 & 71 & 62 & 53 & 44 & 35 & 26 & 17 & 8 & 89 \end{pmatrix}$$

by the congruent relation $t = 81t_1 + 10t_2 \mod 90$.

More generally, Fig.3.5.1 (a) and (b) show the 2-D patterns resulted by the shuffling process of Eq.(3.3.5) for (r_1, r_2) as (6,5) and (7,5), respectively. In each of the cases, it is observable that data sequence progresses sequentially along both horizontal and vertical coordinates until they hit the last row or column of the matrix and then hop to first row or column. For the case of Fig.3.5.1 (a) or $r_1 = r_2 + 1$, the matrix is in a format similar to a tilted non-interlaced scanning pattern. On the other hand, a one-line interlaced pattern is apparent in Fig.3.5.1 (b) or $r_1 = r_2 + 2$.

Based on this 1-D to 2-D transformation, the Fourier transforms of Eqs.(3.5.3)-(3.5.5) can be rewritten under the new index system, i.e.

$$X(k_1,k_2)=\sum_{i_1=0}^{r_1-1}\sum_{i_2=0}^{r_2-1}x(i_1,i_2)e^{-jf_{k_1,k_2}(i_1,i_2)} \qquad (3.5.6)$$

$$H(k_1,k_2)=\sum_{i_1=0}^{r_1-1}\sum_{i_2=0}^{r_2-1}h(i_1,i_2)e^{-jf_{k_1,k_2}(i_1,i_2)} \qquad (3.5.7)$$

$$Y(k_1,k_2)=\sum_{i_1=0}^{r_1-1}\sum_{i_2=0}^{r_2-1}y(i_1,i_2)e^{-jf_{k_1,k_2}(i_1,i_2)} \qquad (3.5.8)$$

where

$$f_{k_1,k_2}(i_1,i_2)=\frac{2\pi(s_1i_1+s_2i_2)(s_1k_1+s_2k_2)}{N}$$

Expanding $f_{k_1,k_2}(i_1,i_2)$,

$$f_{k_1,k_2}(i_1,i_2)=\frac{2\pi}{N}(s_1^2i_1k_1+s_2^2i_2k_2+s_1s_2(i_1k_2+i_2k_1)) \quad .$$

is obtained. The above equation, after using Eqs.(3.3.8) and (3.3.9), can be further simplified to

$$f_{k_1,k_2}(i_1,i_2)=\frac{2\pi s_1n_1i_1k_1}{r_1}+\frac{2\pi s_2n_2i_2k_2}{r_2}+2\pi n_1n_2(i_1k_2+i_2k_1) \quad . \qquad (3.5.9)$$

With the relations of

$$k'_1=s_1n_1k_1 \qquad \mathrm{mod}\, r_1 \qquad (3.5.10)$$

and

$$k'_2=s_2n_2k_2 \qquad \mathrm{mod}\, r_2 \qquad (3.5.11)$$

a substitution of Eq.(3.5.9) into Eqs.(3.5.6)-(3.5.8) leads to

$$X(k'_1, k'_2) = \sum_{i_1=0}^{r_1-1} \sum_{i_2=0}^{r_2-1} x(i_1, i_2) e^{-j2\pi\left(\frac{i_1 k_1}{r_1} + \frac{i_2 k_2}{r_2}\right)}$$

(3.5.12)

$$H(k'_1, k'_2) = \sum_{i_1=0}^{r_1-1} \sum_{i_2=0}^{r_2-1} h(i_1, i_2) e^{-j2\pi\left(\frac{i_1 k_1}{r_1} + \frac{i_2 k_2}{r_2}\right)}$$

(3.5.13)

$$Y(k'_1, k'_2) = \sum_{i_1=0}^{r_1-1} \sum_{i_2=0}^{r_2-1} y(i_1, i_2) e^{-j2\pi\left(\frac{i_1 k_1}{r_1} + \frac{i_2 k_2}{r_2}\right)} .$$

(3.5.14)

In order to prove the above $X(k'_1, k'_2)$, $Y(k'_1, k'_2)$ and $H(k'_1, k'_2)$ contains all points of the required Discrete Fourier Transform (DFT), it is shown that $k'_1 \in (0, 1, \ldots, r_1 - 1)$ and $k'_2 \in (0, 1, \ldots, r_2 - 1)$.

First of all, Eq.(3.3.8) is rewritten in the following format

$$m_1 = \frac{n_1}{r_1} r_2 + \frac{1}{r_1} \qquad (3.5.15)$$

From this, it is said that n_1 is not divisible by integer r_1 since, otherwise, no integer m_1 can be obtained when $r_1 > 1$. Now, the right side of Eq.(3.3.8) is substituted into Eq.(3.5.10) and

$$k'_1 = n_1 k_1 \qquad \text{mod } r_1 \qquad (3.5.16)$$

is resulted. Assume that two different values of k_1 (k_1^1 and k_1^2) deliver same value of k'_1. It may therefore be obtained that

$$n_1 k_1^1 - l_1 r_1 = n_1 k_1^2 - l_2 r_1$$

where l_1 and l_2 are the quotients of k_1^1 and k_1^2. It may also be expressed as

$$n_1 (k_1^1 - k_1^2) = (l_1 - l_2) r_1 \qquad (3.5.17)$$

Since n_1 is not divisible by r_1, the only way to let Eq.(3.5.17) correct is to set

$$k_1^1 - k_1^1 = q r_1 \qquad (3.5.18)$$

Because $k_1^1 \in (0, 1, \ldots, r_1 - 1)$ and $k_1^2 \in (0, 1, \ldots, r_1 - 1)$, the only correct solution to Eq.(3.5.18) is $q = 0$. This shows that $k'_1 \in (0, 1, \ldots, r_1 - 1)$. A similar derivation proves that $k'_2 \in (0, 1, \ldots, r_2 - 1)$. Therefore, it is concluded that the $X(k'_1, k'_2)$, $Y(k'_1, k'_2)$ and $H(k'_1, k'_2)$ in Eqs.(3.5.12)-(3.5.14) contains all points of the required DFT, which are in the form of 2-D discrete Fourier transforms of the size $r_1 \times r_2$. Although the obtained matrices are in a scrambled form known as Ruritanian format, their elements located at the same coordinates correspond to each other in a way identical to their original 1-D form. Thus, Eq.(3.5.2) can now be expressed in a form of multiplication of two images as

$$Y(k'_1, k'_2) = H(k'_1, k'_2) X(k'_1, k'_2) \qquad (3.5.19)$$

which gives the Fourier transform of the convolution result but in a permuted 2-D format. To obtain the convolution result, an inverse Fourier transform should be carried out on the above obtained matrix $Y(k'_1, k'_2)$. Because of Eq.(3.5.14), this inverse Fourier transform will give the required convolution result in the original 2D data arrangement.

From the above derivations, an N-point 1-D data convolution of Eq.(3.3.10) can be performed through the following procedures:

(a) convert both data and reference sequences into 2-D matrices of the scale $r_1 \times r_2$ based on the congruent relationship of Eq.(3.3.5);

(b) carry out Fourier transforms on the above 2-D matrices;

(c) obtain the product of the Fourier transform matrices;

(d) perform the inverse Fourier transform on the resulted matrix; and finally

(e) convert the above matrix back to a 1-D sequence by the congruent relationship of Eq.(3.3.5) to obtain the final convolution result.

Although a conventional electronic computer may execute, step-by-step, the above procedures, its inherent sequential processing nature can only promise the required 2-D Fourier transforms and matrix multiplications at relatively low speeds, which obviously inhibits applications where processing speed is very important. The use of very large scale integrated circuit chips can enhance the performance. However, the number of $r_1 + r_2$ individual FFT processors have to be employed. Optical processing, on the other hand, with its parallel processing characteristics, promises a speed-up by generating results concurrently in a 2-D parallel fashion.

3.5.2 Opto-electronic Convolver/Correlator

To perform the above operations, a coherent opto-electronic system based on the utilization of both massive optical interconnects and free-space optical

Fourier transformation is proposed (see Fig.3.5.2). Before the 1-D data and reference sequences are sent into the Fourier processor, they are first shuffled and converted to their corresponding 2-D patterns based on Eq.(3.3.5) by one of the schemes, which will be described in detail in Section 3.5.3. In this section, methods of processing the obtained permutation patterns are considered. Two mask like patterns shown in Fig.3.5.3 suitable for optical processing are obtained from the optical permutation devices and are loaded into spatial light modulators (SLM) B1 and B2, respectively. They carry the shuffled results where each data point is represented by a rectangular pixel. On the other side, the spatially filtered and expanded laser beam is split into two branches with equal intensity. They illuminate respectively the above spatial light modulators B1 and B2. Therefore, the 2-D patterns of the shuffled data and reference sequences intensity-wise modulate the output beams, which are then optically Fourier transformed.

3.5.2.1 Optical Fourier Transform

Mathematically, the mask pattern of data or reference sequence is described by

$$f(x,y)=\sum_{n=0}^{r_1-1}\sum_{m=0}^{r_2-1}s(n,m)\,rect\left(\frac{x-\left(n-\frac{r_1-1}{2}\right)d}{b}\right)rect\left(\frac{y-\left(m-\frac{r_2-1}{2}\right)c}{a}\right) \tag{3.5.20}$$

where, parameters a, b, c and d are the pixel widths and their intervals (see Fig.3.5.3), $s(n,m)$ $(n=0,1,\ldots,r_1-1, m=0,1,\ldots,r_2-1)$ represents the shuffled data or reference sequence in the form of matrix, $rect()$ is a standard gate function defined as $rect(x)=1$ when $-\frac{1}{2}\le x\le\frac{1}{2}$ and $rect(x)=0$ otherwise. For a coherent 4f optical system with a focal length f and optical wavelength λ, it can be shown as follows that the obtained optical pattern at the back focal plane of the corresponding transformation lens L_1 or L_2 is in the form of

$$F(\mu,\nu)=abe^{j\frac{\pi}{\lambda f}((r_1-1)\mu d+(r_2-1)\nu c)}sinc\left(\frac{\pi\mu b}{\lambda f}\right)sinc\left(\frac{\pi\nu a}{\lambda f}\right)$$
$$\sum_{n=0}^{r_1-1}\sum_{m=0}^{r_2-1}s(n,m)e^{-j\frac{2\pi}{\lambda f}(\mu nc+\nu md)}. \qquad (3.5.21)$$

For a coherent optical system with a focal length of f and optical wavelength of λ, the obtained optical pattern at Fourier plane (see Section 3.1) is proportional to the Fourier transform of input pattern, i.e.

$$F(\mu,\nu)=A\int_{-\infty}^{+\infty}\int_{-\infty}^{+\infty}f(x,y)e^{-j\frac{2\pi}{\lambda f}(\mu x+\nu y)}dxdy \qquad (3.5.22)$$

By substituting the mathematical expression of input mask pattern Eq.(3.5.20) into the above equation,

$$F(\mu,\nu)=\int_{-\infty}^{+\infty}\int_{-\infty}^{+\infty}\sum_{n=0}^{r_1-1}\sum_{m=0}^{r_2-1}s(n,m)$$

$$u\left(\frac{x-\left(n-\frac{r_1-1}{2}\right)d}{b}\right)u\left(\frac{y-\left(m-\frac{r_2-1}{2}\right)c}{a}\right)dxdy$$

(3.5.23)

is obtained. Applying the theorem that the linear transform of summation equals the summation of the linear transform,

$$F(\mu,\nu)=\sum_{n=0}^{r_1-1}\sum_{m=0}^{r_2-1}s(n,m)$$

$$\int_{-\infty}^{+\infty}\int_{-\infty}^{+\infty}u\left(\frac{x-\left(n-\frac{r_1-1}{2}\right)d}{b}\right)u\left(\frac{y-\left(m-\frac{r_2-1}{2}\right)c}{a}\right)e^{-j\frac{2\pi}{\lambda f}(\mu x+\nu y)}dxdy$$

(3.5.24)

is resulted. After letting new variables

$$\tilde{\mu}=\frac{r_1\mu d}{\lambda f} \qquad (3.5.25)$$

$$\tilde{\nu}=\frac{r_2\nu c}{\lambda f} \qquad (3.5.26)$$

Eq.(3.5.21) becomes

$$F(\tilde{\mu},\tilde{\nu}) = ab \cdot e^{j\pi\left(\frac{(r_1-1)\tilde{\mu}}{r_1}+\frac{(r_2-1)\tilde{\nu}}{r_2}\right)} \cdot sinc\left(\frac{\pi\tilde{\mu}b}{r_1 d}\right) sinc\left(\frac{\pi\tilde{\nu}a}{r_2 c}\right)$$

$$\cdot \sum_{n=0}^{r_1-1}\sum_{m=0}^{r_2-1} s(n,m)e^{-j2\pi\left(\frac{\tilde{\mu}n}{r_1}+\frac{\tilde{\nu}m}{r_2}\right)}$$

(3.5.27)

Now, the 2-D summation term of the above equation is the desired 2-D discrete Fourier transform of $s(n,m)$ when $\tilde{\mu}$ and $\tilde{\nu}$ are selected to be integers in the range of 0 to $r_1 - 1$ and $r_2 - 1$. The first constant term can be ignored. The second term may also be discarded since the linear phase shift will not affect the final results except for a position shift after the inverse Fourier transform is performed. Unfortunately, the third term must be considered seriously for the reason that it will distort the resulted Fourier transform by attenuating it as $\tilde{\mu}$ and/or $\tilde{\nu}$ increase. Also, the error of convolution-/correlation will be small when all useful data points are located inside the main lobe of the sinc function. To ascertain this condition, it is necessary to set

$$a < \frac{r_2 c}{r_2 - 1}$$

$$b < \frac{r_1 d}{r_1 - 1}$$

On the other hand, the size of each data point will spread to double the size of its original one after convolution or correlation. This phenomenon may

cause crosstalks between the neighbor points on the output plane. To prevent it, the size of each data point is restricted to

$$a < \frac{1}{2}\frac{r_2 c}{r_2 - 1} \tag{3.5.28}$$

$$b < \frac{1}{2}\frac{r_1 d}{r_1 - 1} \tag{3.5.29}$$

When these conditions are satisfied, theoretically, there will be no crosstalks between neighbor points. Unfortunately, any practical system suffers from the problems of blurring and defocusing. But with the above restriction, at least, the crosstalk may be limited to an acceptable level. For these reasons, it seems that a and b should be selected as small as possible. However, the fact that smaller values of a and b will correspond to lower optical power efficiency must also be considered since the display resolution of any SLM is limited. A tradeoff among the optical power efficiency, the data density around the origin of sinc function at Fourier plane and the level of crosstalk is thus necessary to obtain optimal ratios of b/d and a/c.

To solve the above described envelope distortion problem, an alternative method is to introduce a compensator placed at the Fourier plane with its optical transmittance as

$$T(\mu, \nu) = \frac{C_T}{sinc\left(\frac{\pi \mu b}{\lambda f}\right) sinc\left(\frac{\pi \nu a}{\lambda f}\right)} \tag{3.5.30}$$

With correct selections of parameters a, b, c and d, the required output pattern will remain inside the main lobe of the sinc function. Therefore, the worries of appearance of zeros in the denominator of Eq.(3.5.30) become unnecessary. A compensator can be simply realized by a fixed transparency with optical transmittance determined by Eq.(3.5.30). However, it may lower the entire optical intensity of the obtained image and may lead to slower response time of the photo-refractive crystal for multiplication.

3.5.2.2 Optical Multiplier

After the 2-D Fourier transform of data and reference sequences are obtained and compensated, they are subject to an optical multiplication. Such an optical multiplication can be performed in various ways. In the scheme of Fig.3.5.4, a four wave mixing in a nonlinear crystal is used. The beams A_{data} and $A_{reference}$ carrying the Fourier transforms of data and reference patterns interfere inside the photo-refractive crystal. The interference pattern thus obtained excites the charge carriers of the crystal causing them to redistribute through diffusion and drifting. This charge redistribution results in electric field variation in the crystal, which modulates through the electro-optic effect to produce a refractive index grating. When the readout beam A_{read} interacts with the obtained grating, the output beam A_{output} carries the required multiplication result represented by its complex amplitude proportional to $A_{data}A_{reference}A^{*}_{read}$. From a further analysis of the principle of the grating formation [3.13], it is noted that the

resulted index modulation Δn does not depend on the absolute intensity of the interference pattern. The effect of input optical field is only to redistribute the charge carriers based on the formed interference pattern. The maximum space charge field and Δn are limited by the total available charges inside the photo-refractive crystal. A higher optical intensity, however, corresponds to a faster speed to reach the steady state of index grating or to a shorter grating buildup time $\tau_{buildup}$. This grating build-up time is crucial to the speed of the convolution processor because a new frame of input data can be supplied to the SLM input only when the grating inside the crystal reaches its steady state and the corresponding information has been read by the readout beam. An upper bound of processing speed based on the grating buildup time for an input device resolution of $N \times M$ is thus determined by $N \times M / \tau_{buildup}$. The steady state diffraction efficiency which is important for the total efficiency of the optical system is determined by the index modulation Δn [3.14]. In order to obtain a high efficiency, a large Δn is desired which can be obtained either by using crystals with high electro-optic coefficients or by applying an external DC electric field.

The above multiplication is then subject to an optical inverse Fourier transform which generates a 2-D pattern related to the convolution result by the congruent relation after it is sampled by a sampling grid of Fig.3.5.5. For the final 1-D convolution result, the resulted 2-D pattern is either geometrically inversely transformed, imaged and read on a 2-D charge coupled device (CCD) array in a conventional way, or directly imaged on a

2-D CCD array and then recorded in the reverse sequence by the congruent relation. The convolution result in the 1-D form is thus obtained. Notice that the existence of a linear phase term associated with the desired Fourier transform at Fourier plane will cause shift of the output pattern corresponding to convolution result. To correctly locate the detector array, a displacement of $(N-1)d$ in horizontal direction and $(M-1)c$ in vertical direction from the optical axis of the setup should be observed. Another important issue to be considered is that the detector's dynamic range will determine the levels of intensity of the readout beam A_{read} of photorefractive crystal. For a maximum allowable intensity I_{max} by the detector without saturation, the intensity of A_{read} should not be larger than $I_{max}/\eta_{crystal}\eta_{output}$.

By recognizing the fact that the reference sequence is generally known beforehand such as in the cases of radar and sonar, a simplified system architecture is obtained. Shown in Fig.3.5.6, this simplified system will not use nonlinear crystal, which may cause lower processing speed in practical implementations. The reference sequence is first shuffled to form its corresponding 2-D pattern and then Fourier transformed to obtain the desired 2-D filtering mask described by Eq.(3.5.13). The pre-computed mask may either be represented using a SLM or be recorded as a fixed transparency.

3.5.3 Data Permutation Schemes

A serious challenge still remains, i.e. whether or not an efficient data permutation scheme can be obtained to support the 1-D to 2-D data conversion. An analysis of the permutation pattern from the congruent relation of Eq.(3.3.5) for two sets of r_1 and r_2 in Fig.3.5.1 reveals that some available techniques can be tailored to perform the data permutation from the original 1-D sequence to its 2-D matrix. The following is a brief description of two of the possible and efficient free-space opto-electronic shuffle schemes.

3.5.3.1 Special Purpose Cathode Ray Tube Scanning Scheme

In a conventional cathode ray tube (CRT) display, regardless of interlaced or non-interlaced model , images are formed in a raster scan fashion. The scanning voltages which control the beam deflections in X and Y directions are shown in Fig.3.5.7(a). A closer view of the patterns in Fig.3.5.1 and Fig.3.5.7(a) reveals their relation and the possibility of realizing the required 1-D to 2-D data conversion by using the scanning scheme on a conventional CRT with a modified voltage control system. To achieve this goal, the above scanning voltage relationship has to be changed to the one depicted in Fig.3.5.7(b), which should not be difficult to obtain by a specifically designed X- and Y- waveform generator shown in Fig.3.5.8. The conversion of 1-D into 2-D data array can thus be performed. For the convolution, the image on the screen of this modified CRT display is then coupled onto an optically

addressed SLM under a coherent illumination (laser beam) for further processing. The maximum data length of convolution by this scheme is mainly limited by the lowest resolution of CRT display and SLM employed in the system.

To ensure the system to work properly, the following relation between the CRT scanning rate, the resolution of the employed optical system and the data rate must be observed:

$$f_s = \frac{f_{max} f_f}{H_r} \qquad (3.5.31)$$

where f_s is the electron beam's scanning rate in lines per second, H_r is the resolution of the optical system, f_f is the frame rate of CRT display and f_{max} is the maximum number of data points per frame. In addition, the fly-back time must be kept much less than the interval between the two consecutive data points. For example, the scanning rate f_s, with a resolution of 1024 lines is approximately 977 Hz to handle 1 million point data. This rate should be standardized in cases of using commercial available devices.

3.5.3.2 Optical Geometrical Transform Based Scheme

In addition to the above direct scanning scheme, an opto-electronic interconnect scheme that uses an optical geometric transform in conjunction with a conventional CRT can also serve the purpose. This scheme as shown in Fig.3.5.9 (a) is built by using a conventional non-interlaced or interlaced

CRT display combined with an optically addressed SLM with an optical geometrical transform setup. This system is especially suitable for $N = r_1 r_2$ where $r_1 = r_2 + 1$. For the realization by a conventional 1-line-interlaced display, the input signal is first buffered and converted to a standard video signal by the system of Fig.3.5.10. However, a $\frac{1}{60}$second time delay will occur for NTSC standard video displaying system. In order to overcome this drawback, a non-interlaced video display can be used to obtain the required pattern without using the above buffering system.

Suggested by Lohmann et al [3.15], an optical system shown in Fig.3.5.9 (b) which is the content of the dashed box in Fig.3.5.9 (a) carries a geometrical transform of an image from a rectangular to a parallelogram shape. It was proven that coordinates (x_i, y_i) at the input plane will be mapped to coordinates (x_o, y_o) at the output plane by the following coordinate transformation

$$\begin{pmatrix} x_o \\ y_o \end{pmatrix} = \begin{pmatrix} x_i & + & a(y_i) \\ y_i & + & b(x_i + a(y_i)) \end{pmatrix} \qquad (3.5.32)$$

where $a()$ and $b()$ determine the phase shifts generated by phase filters PS1 and PS2. In order to realize the required geometrical transform, the following conditions on $a()$ and $b()$ must be observed

$$a(z) = 0 \qquad b(z) = -sz \qquad (3.5.33)$$

where s is a constant with $s > 1$ which is determined by the difference between integers r_1 and r_2. As an example, let's consider the selection of constant

s when $r_1 - r_2 = 1$. Consider the geometry of Fig.3.5.9 (c), where l_h and l_v are the width and height of optical pattern before the geometrical transformation. It can be shown that the relation between the shape of pattern and the related phase shift Θ is

$$\frac{\frac{l_v}{\tan\theta}}{r_2 - 1}(r_1 - 1) = l_h \qquad (3.5.34)$$

or

$$s = \tan\theta = \frac{l_v}{l_h}\left(\frac{r_1 - 1}{r_2 - 1}\right) \quad . \qquad (3.5.35)$$

Therefore, the phase shift inserted by PS2 can be calculated as

$$\Theta(\tilde{x}, \tilde{y}) = \frac{2\pi}{\lambda} s\tilde{x}\tilde{y} \qquad (3.5.36)$$

The above method of determining constant s can also be used when selecting other combinations of r_1 and r_2. Because of Eq.(3.5.33), the first phase filter PS1 in Fig.3.5.9 (b) will not be used here. Phase filter PS2 can be realized by a variety of techniques, e.g. a specially designed prism or a computer generated hologram.

After the conversion, a Hughes liquid crystal light valve (LCLV) illuminated by the uniform laser beam is used to create the coherent copy of the converted pattern such as the one shown in Fig.3.5.11(a), where the part in the dashed box is necessary for Fourier transform. Theoretically, this scheme is not restricted to $r_1 = r_2 + 1$. But for a pair of r_1 and r_2 with

difference other than unity, the optical system will become more complicated and lower power efficient. An example for $r_1 = r_2 + 2$ is also depicted in Fig.3.5.11(b), in which three copies of the geometrically transformed data image are needed to obtain the required permutation result. Similar to the above CRT scheme, the length of sequence which can be converted by this scheme depends on the resolution of the employed CRT.

3.5.3.3 Digital Image Processor Based Scheme

The commercial availability of high quality real-time pipelined image processor generates another possibility to perform the required data conversion in real-time. A system control diagram of Fig.3.5.12 is used. Buffering system of Fig.3.5.10 is necessary to convert the input data sequence to the standard TV format for some of the image processing units, which only adopts the interlaced signals. After this necessary conversion, two identical parallel systems process the transformation, that is, at one cycle, while data is being written from A/D converter to the FRAME A and the contents of FRAME B is being D/A converted to the conventional display, the pixels in FRAME C are read horizontally and written to the correct locations in FRAME D by a control program based on the congruent relationship. At the next cycle, the roles of FRAME A, FRAME B and FRAME C, FRAME D are interchanged to ensure a constant data flow. This requires a frame memory system which can store four frames of images each of which can be accessed independently. However, some changes in hardware may simplify

the system to only two frame memories as shown in Fig.3.5.13. The data is now being sequentially written to FRAME A by the congruent relation, while the contents of FRAME B is being read and D/A converted for the display purpose . At the next cycle, FRAME B accepts data from A/D converter while FRAME A outputs the converted pattern. This pipelined processing scheme with a fast clock speed may generate a real-time conversion of 1-D data or reference sequence into its corresponding 2-D array. The output image, which in fact is the resulted 2-D data array, is then displayed on a conventional TV or HDTV before coupled onto a resolution-wise compatible optically addressed SLM.

3.5.4 Discussions

3.5.4.1 About Cyclic Correlation

In addition to the cyclic convolution discussed above, cyclic correlation of the two very long data sequences $\{x_i\}$ and $\{h_i\}$ defined by Eq.(3.3.11) can also be performed by the proposed scheme. A comparison of $\{h_i\}$'s for convolution and correlation shows that the 2-D array corresponding to the reference sequence of the correlation is a transpose of that of the convolution. Thus the above correlation can be carried out with only a minor change, i.e. the direction of data feeding. In this case, either one of the 2-D patterns needs to be mirror-reflected.

3.5.4.2 About Signal Detection

When the designed correlator is used to detect and locate the desired signal as in the case of pattern recognition, variations to the optical correlator unit may improve the system performance. As can be seen that with the reference pattern fed into the correlator by the above described schemes the correlator itself is in fact in the form of the so called matched filter. Although it gives the highest possible signal-to-noise ratio when detecting a known signal corrupted by additive white noise, the correlation peak of this traditional form of correlator is not sufficiently sharp for a signal allocation. Several methods have been designed to solve the problem. Among them are a phase-only matched filter, a binary phase-only matched filter, a two-bit correlator and a joint transform correlator [3.7],[3.16]-[3.21]. Although these schemes were designed for image processing, they can be directly used to process shuffled pattern of the long stream 1-D signal.

As an example, a phase-only matched filter scheme is described briefly. The filter used in the system of Fig.3.5.6, which is similar to a VanderLugt correlator, is the 2-D Fourier transform of the shuffled reference pattern

$$F(u,v) = A(u,v)\exp(j2\pi\phi(u,v)) \qquad (3.5.37)$$

the phase-only filter is defined to be

$$F_o(u,v) = \exp(j2\pi\phi(u,v)) \qquad (5.5.38)$$

obtainable by setting $A(u,t)$ equal to unity. A deformable mirror device SLM can be used [3.17] to practically realize this phase-only filter. Detail discussion on phase-only filters can be found from Reference [3.16].

Another scheme mostly used in pattern recognition applications is an optical joint transform correlator (JTC) which principle diagram was shown in Section 2.3.2.

3.5.4.3 About Linear Convolution or Correlation

Although all the above discussions were made based on the cyclic convolution and correlation, linear convolution or correlation can also be carried out. Sufficient numbers of zeros have to be added to the original sequences before processing. Details of this zero-padding has already been fully discussed. Readers may refer to the book written by Oppenheim [3.22].

3.5.4.4 About Raster Scan Scheme

To convert data from 1-D to its 2-D form, raster scanning scheme is in common in both above mentioned permutation schemes as a final displaying technique. Because the time needed to establish one frame of image on the CRT display is much less than the grating buildup time in most available photo-refractive crystals, the processing speed of the entire system will be limited by $\tau_{buildup}$. However, when the simplified system of Fig.3.5.6 is used,

the scanning speed of CRT display becomes the limiting factor. One other issue, which is usually ignored and which is important when a scanning CRT or SLM is used as input device in an optical processing system, is the uniformity of the instantaneous 2D pattern. To visualize a frame of image on a CRT screen or a SLM generated by raster scan is not a problem because of the vision persistence of human eyes. However, this is not the case in optical system. Because of the fast transition time and finite life-time of flying spot on the screen at a given instant, only a slice of pattern is well illuminated (see example in Fig.3.5.14). Even with the thin-film transistor technique (TFT), which is used in liquid crystal TV (LCTV) to extend the addressing voltage and thus prevent the loss of contrast caused by the voltage relaxation effect [3.23], the instant image on the screen is still not uniform when all pixels are applied with the same voltage. A direct usage of this image to perform a convolution will obviously cause errors. Therefore, schemes which can strobe a image on the screen for the time of one frame is necessary in order to generate a uniform frame of image. For the case of using a LCTV with TFT, a compensator similar to what is discussed in Section 3.5.2.1 but with transmittance only varying in one dimension may also be used.

3.5.4.5 About Dynamic Range

To find the dynamic range of the proposed system, the electronic dynamic range of the input devices needs first to be considered as it obviously limits

the acceptable range of input signals. For example, when a conventional CRT display is selected as the input device in the second scheme, its input dynamic range will set an upper bound to the system dynamic range.

The dynamic range of the detector also needs to be considered, especially in the case when objects in a signal sequence have large difference in intensity. When correlation is performed, a strong signal will give rise to a strong correlation peak, while a weak signal will deliver a weak peak. Because of the limitation of dynamic range, the weak signal may not be detected when the system is tuned to detect a strong signal. On the other hand, the system may be saturated at strong signal when it is tuned to detect a weak signal. Although the newly suggested intensity-invariant JTC may improve the correlation efficiency by using differently polarized coherent beams to illuminate signal and reference images, it can not completely solve the above mentioned problem. When there are several targets with different intensity levels in the input image, the intensity-invariant JTC is able to cancel the pedestal term, but the interference pattern referring to each target is still proportional to the target's original intensity, which means that the problems of saturation of strong signals or loss of weak signals still remains. However, in many applications, the system dynamic range may not be required to be extremely large because of the following two reasons. First, no matter how good the quality of receiver is, the signal to be processed is contaminated by noise and is described by a finite signal-to-noise ratio. When the signal is weakened to a certain extent, the final correlation peak will be buried in

noise and can not be picked up. Second, a threshold is usually set before hand to determine the appearance of certain target at the output. Any correlation peak which is less than the preset threshold is considered as noise. Therefore the actual dynamic range required for the CCD detector is to cover the difference between an upper bound which is the correlation peak of the strongest signal and a lower bound which is the preset threshold or the noise level. Because of the linearity of convolution and correlation operations, the required dynamic range of the CCD detector should be kept at the ratio dividing the strongest signal level by the noise level of input signal. In other words, it should be determined by the difference between the strongest correlation peak and the preset threshold at output.

Other devices or components in the system may also have effects on the system dynamic range. With appropriate adjustments of the entire system, their influences can be kept at minimum. It is then appropriate to say that the system dynamic range is bounded by the smallest device dynamic range of its components.

3.5.4.6 About Data Rate

In the proposed systems, no matter what kind of data shuffle schemes is to be used, essential components such as a CRT display, a SLM and a CCD detector are employed. The resolutions of these devices are obviously less than that of other bulk optical components such as a lens, a beamsplitter,

etc. Therefore, they form the limit to the maximum data rate f_{max} achievable by the proposed system

$$f_{max} = \frac{r_h r_v p}{4} \qquad (3.5.38)$$

where $r_h \times r_v$ and p are the lowest 2-D resolution and the lowest frame rate the components in the system, respectively. As the input device of the proposed convolver, a conventional CRT with a resolution of 512×512 pixels delivers a input data rate of 250,000 points per frame. A near-future introduction of high definition TV (HDTV) with a resolution of over 1024×1024 [5] will improve the above input data rate to more than one million-point per frame. Also, as an output component, a 2-D CCD detector with a resolution of 1024×1024 are commercially available now. However, the resolution of 2-D SLM is still relatively low. Obviously, when a photo-refractive crystal is employed to perform the required multiplication operation, the lowest frame rate p in Eq.(3.5.38) is determined by the long response time of nonlinear crystal. Based on this analysis and Eq.(3.5.38), a group of maximum achievable data rates for different system configurations are listed in Table 3.1 for the purpose of comparison. Here, It is assumed that the CRT display and 2-D CCD detector with a resolution of 512x512 are operated at the video rate. Following conclusions may be obtained from the table. First of all, most existing SLM's are the source of limits to both the system resolution and frame rate. However, in the case

5 Fujitsu is seeking to develop a 2240×2240 HDTV.

of using megneto-optic SLM, because its frame rate is much higher (hundreds of microseconds per frame) than the video rate, the maximum data rate is determined by the resolution of the SLM together with the frame rate of CRT and CCD detector. When a magneto-optic SLM with a higher resolution, e.g. 512x512 as predicted, becomes available, the achievable data rate will be completely governed by the employed CRT display and CCD detector. Secondly, it is obvious that the maximum data rate drops drastically when a nonlinear crystal is included in the system for multiplication. For the case that a nonlinear crystal must be employed, BSO is preferred for its fast response time in order to keep the data rate sufficiently high. Although the shown scheme obtainable under current technology can not deliver the long data stream convolution / correlation operation in real-time or at video rate, they, at least, show the potential or near-future capabilities for this application. With the development of high resolution SLM [3.24]. And also, the discovery of high speed nonlinear wave-mixing crystals will result in real-time or video rate convolution of long 1D data sequences.

3.5.5 Computer Simulation Results

In order to verify the proposed processing scheme, computer simulations were carried out. A 1406-point convolution was selected as an example with its data and reference sequences shown in Fig.3.5.15 (a) and (b). The simulation program first solved integer equations of Eq. (3.3.8) and (3.3.9). With the selection of $r_1 = 38$ and $r_2 = 37$, minimum solutions for n_1 and n_2 were obtained, which

lead to the corresponding congruent relationship i.e. $t = (1369t_1 + 38t_2)_{1406}$ for the 1406-point convolution as shown in section 3.2. Shuffling process was carried out by the data conversion subroutine which was written based on the above congruent relation. The corresponding matrix was thus obtained. The 2-D patterns of data and reference sequences for optical processing were then generated which are shown in Fig.3.5.15 (c) and (d). Here each transparent box represents one datum and its transmittance is proportional to the corresponding data value. The 2-D Fourier transforms of the above 2-D patterns were performed by an FFT subroutine. Multiplication of the obtained images in the computer was followed to simulate what should happen in the nonlinear crystal. Inverse Fourier transform of the above obtained pattern produced the simulated output optical pattern. After data sampling on this pattern, which was written again based on the congruent relation, the simulated convolution result was obtained and is shown in Fig.3.5.16 (b). Comparison of this simulation result with cyclic convolution result generated by a conventional convolution subroutine as shown in Fig.5.5.16 (a) reveals the validity of the above proposed scheme. Errors shown in Fig.3.5.16 (c) are due to calculation accuracy and misalignment of compensator.

To compare the results generated by the proposed scheme but with the use of either a conventional or a phase-only matched filter, another simulation was performed. For the same reference sequence, only the phase term of 2-D Fourier transform of its shuffled pattern was preserved to form a phase-only filter. The result is shown in Fig.3.5.17, which is similar to standard correlation results

in Fig.3.5.16 except that apparently sharper correlation peaks appear in the resulted sequence to demonstrate the occurrence of signal and their accurate positions. An additional advantage of using this phase-only matched filter is its high optical efficiency. The simulations for data sequences contaminated by white noise with different levels were also performed. The results are shown in Fig.3.5.18 to Fig.3.5.20.

3.6 Summary

In summary, this chapter described two optically implementable algorithms based on the Chinese remainder theorem for the calculation of long data stream convolution / correlation. In the first algorithm, the convolution / correlation is converted into a group of vector-matrix multiplication. By using optical vector-matrix multiplier, the convolution / correlation is thus performed optically. However, because of technical problem, this algorithm is not very much practical under current technical condition. Therefore, an alternative algorithm was designed. In this algorithm, the input data and reference sequences are first shuffled to convert the original 1-D convolution to 2-D convolution. A subsequent optical 2-D convolver or correlator is then used to perform the operation. As the kernel unit for the realization of the system, three video rate data permutation schemes were discussed. Computer simulation results for both algorithms were also presented in this chapter. The schemes described in this chapter can not only be used to solve the long data stream convolution / correlation problems but also be used to

perform other long data stream operations where convolution / correlation is the basic function, e.g. the wavelet transform of long 1-D signal described in Chapter Five.

3.7 References

[3.1] R. C. Agarwal and C. S. Burrus, "Fast Convolution using Fermat Number Transforms with Applications to digital filtering," *IEEE Trans. Acoust., Speech, Signal Processing*, vol. ASSP-22, pp. 87-99, April 1974

[3.2] R. C. Agarwal and C. S. Burrus, "Number Theoretic Transforms to Implement Fast Digital Convolution," *Proc. IEEE*, vol. 63, pp.550-560, April 1975

[3.3] C. M. Rader, "Discrete Convolutions via Mersenne Transforms," *IEEE Trans. Comput.*, vol. C-21, pp. 1269-1273, Dec. 1972

[3.4] R. C. Agarwal and J. W. Cooley, "New Algorithms for Digital Convolution," *IEEE Trans. Acoust., Speech, Signal Processing*, vol. ASSP-25, no. 5, pp. 392-410, Oct., 1977

[3.5] R. C. Agarwal and C. S. Burrus, "Fast One-Dimensional Digital Convolution by Multidimensional Techniques," *IEEE Trans. Acoust., Speech Signal Processing*, vol. ASSP-22, pp. 1-10, Feb. 1974

[3.6] W. T. Rhodes, "One-Dimensional to Two-Dimensional and Two-Dimensional to One-Dimensional Mappings in Optical Signal Processing," *SPIE Proc.*, vol.128, pp. 322-331, 1977.

[3.7] C. S. Weaver and J. W. Goodman, "A Technique for Optically Convolving Two Function," *Appl. Opt.*, vol. 5, no. 7, pp. 1248-1249, July 1966

[3.8] T. M. Turpin, "Spectrum Analysis Using Optical Processing," *IEEE Proc.*, vol. 68, no. 1, pp. 79-92, Jan. 1981

[3.9] W. Stoner, "Review of 1-D Signal Processing Using the Optical Transfer Function," *SPIE Proc.*, vol.634, pp.64-79, 1986

[3.10] R. E. Blahut, *Fast Algorithm for Digital Signal Processing*, Addison-Wesley, Reading, 1985.

[3.11] J. A. Neff, R. A. Athale and S. H. Lee, "Two-Dimensional Spatial Light Modulators: A Tutorial," *Proc. IEEE*, vol. 78, no. 5, pp. 826-855, May 1990

[3.12] E. P. Mosca, R. D. Griffin, F. P. Pursel and J. N. Lee, "Acoustooptical Matrix-Vector Product Processor: Implementation Issues", *Applied Optics*, vol. 28, no 18, 15 Sept., 1989

[3.13] A. Yariv, *Quantum Electronics*, 3rd Edition, John Wiley & Sons, New York, 1989.

[3.14] H. M. Gibbs, G. Khitrova and N. Peyghambarian, *Nonlinear Photonics*, Springer-Verlag, Berlin, 1990.

[3.15] A. W. Lohmann and N. Streibl, "Map Transformations by Optical Anamorphic Processing," *Appl. Opt.*, vol. 22, no. 6, pp. 780-783, 15 March 1983

[3.16] J. L. Horner and P. D. Gianino, "Phase-Only Matched Filtering," *Applied Optics*, vol.23, no.6, pp.812-816, 1984

[3.17] J. M. Florence, "Design Consideration for Phase-Only Correlation Filters," *SPIE Proc.*, vol.1151, pp.195-202, 1989

[3.18] J. L. Horner and J. R. Leger, "Pattern Recognition with Binary Phase-Only Filters," *Applied Optics*, vol.24, no.5, pp.609-611, 1985

[3.19] J. L. Horner and H. O. Bartelt, "Two-Bit Correlation " *Applied Optics*, vol.24, no.18, pp.2889-2893, 1985

[3.20] B. Javidi and C. J. Kuo, "Joint Transform Image Correlation Using a Binary Spatial Light Modulator at the Fourier Plane," *Applied Optics*, vol.27, no.4, pp.663-665, 1988

[3.21] S. Jutamulia, K. Company and D. A. Gregory, "Intensity-Invariant Joint Transform Correlator," *Optics & Photonics News*, p.13, December 1991.

[3.22] A. V. Oppenheim and R. W. Schafer, *Digital Signal Processing*, Prentice-Hall, New Jersy, 1975.

[3.23] S. Morozumi, "Application to the Pocket Color T.V.-TFT Array," *Electron. Mag.*, vol. 30, p. 39, 1985

[3.24] J. A. Neff, R. A. Athale and S. H. L..., "Two-Dimensional Spatial Light Modulators: A Tutorial," *Proc. IEEE*, vol. 78, no. 5, pp. 826-855, May 1990

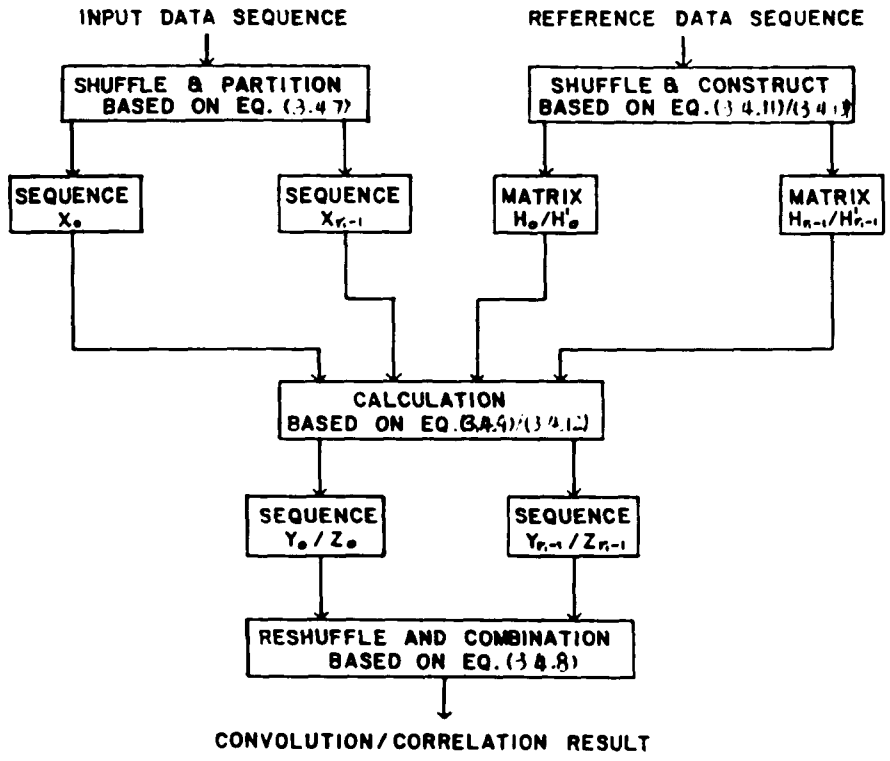

Fig.3.4.1. Principle diagram of the algorithm which converts long data stream convolution correlation to a group of relatively small scale vector-matrix multiplications.

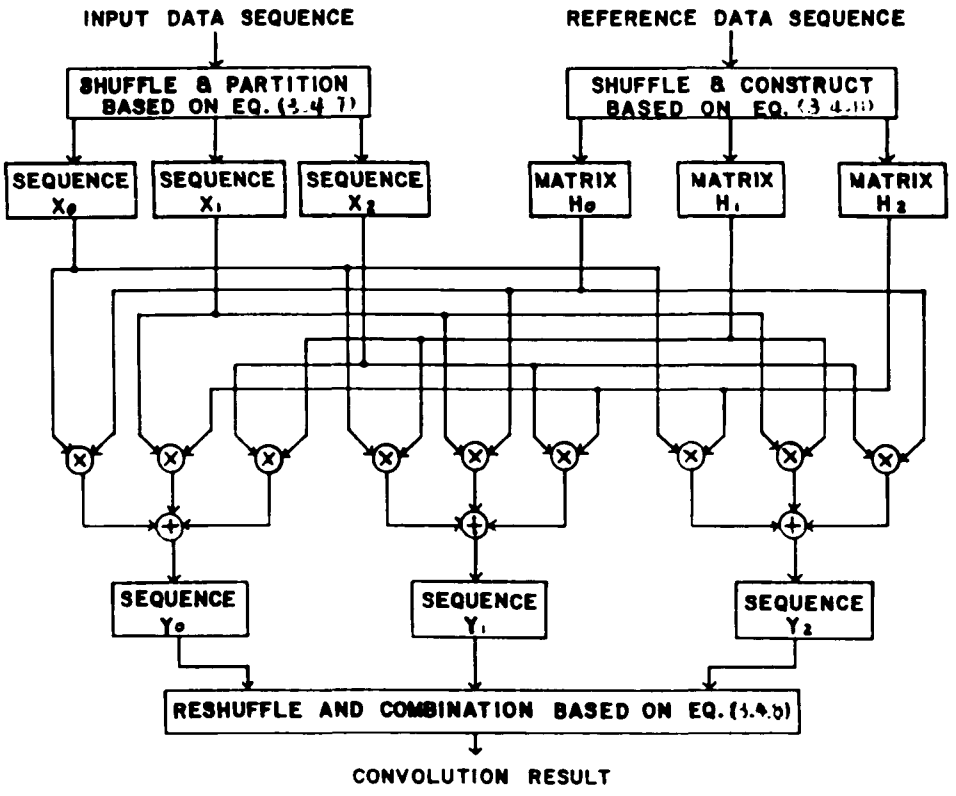

Fig.3.4.2. Flowing chart for computer simulation of the algorithm depicted in Fig.3.4.1.

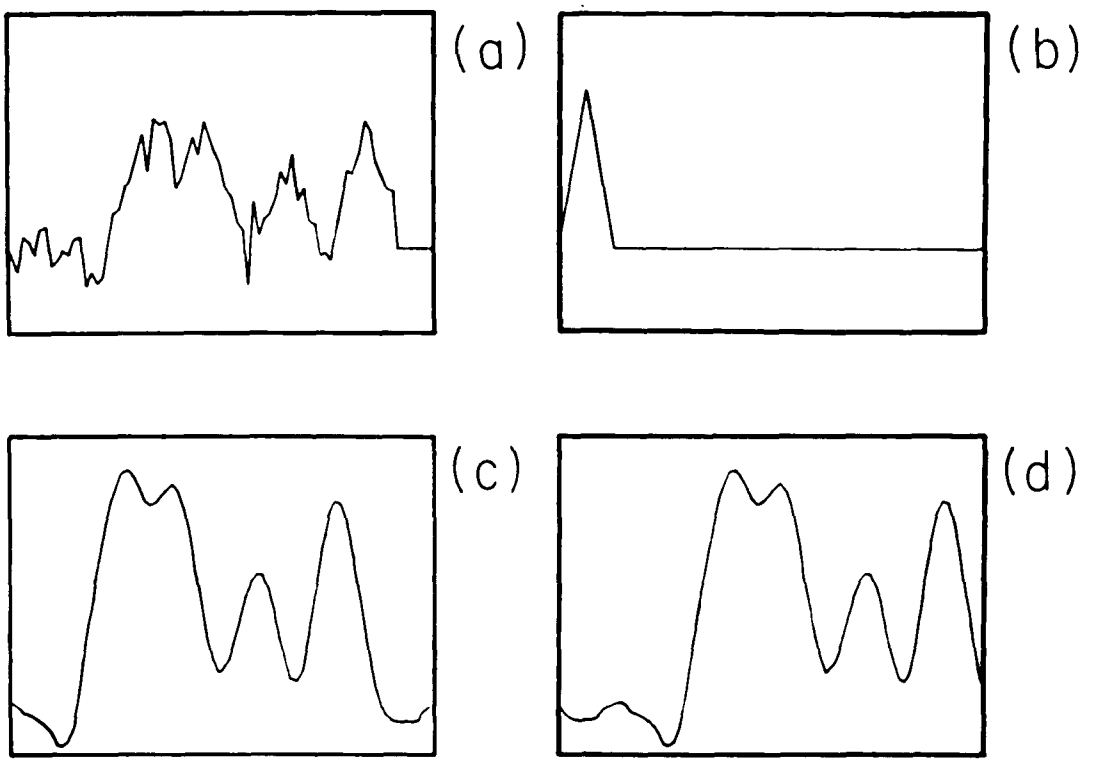

Fig.3.4.3. Results of computer simulation of the algorithm in Fig.3.4.1. (a) Input data sequence, (b) reference data sequence, (c) correlation result, and (d) convolution result.

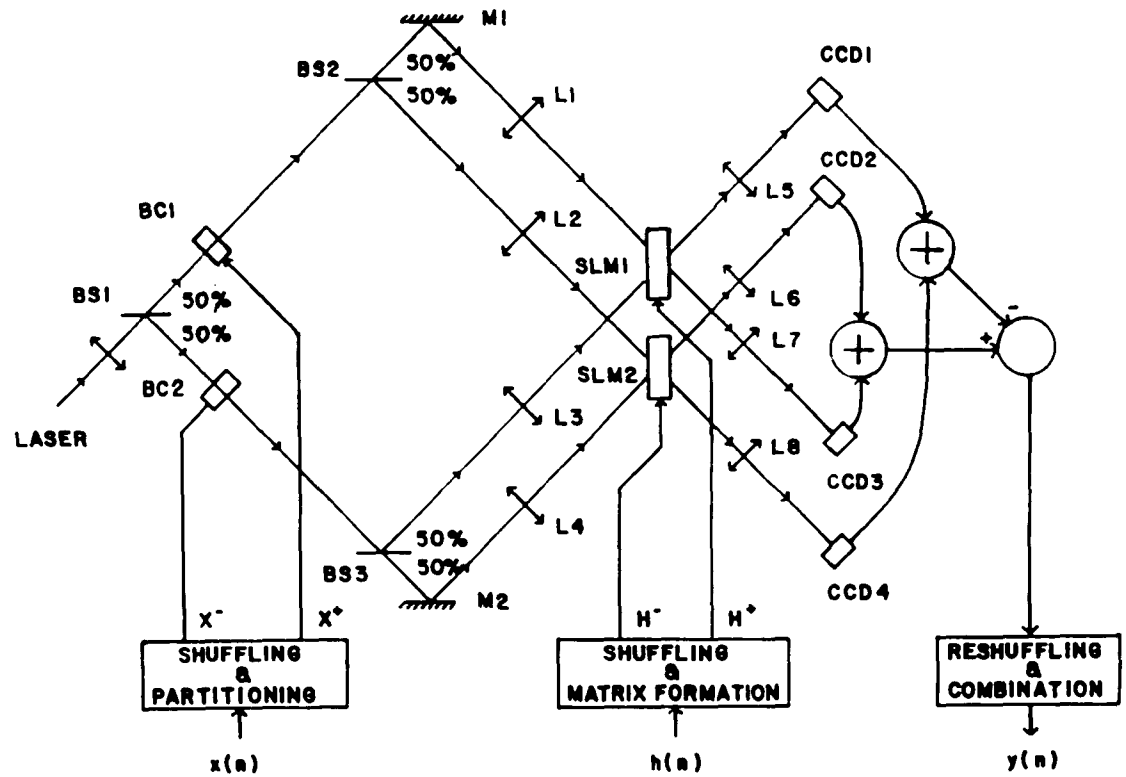

Fig.3.4.4. Proposed opto-electronic convolver correlator based on the algorithm in Fig.3.4.1. BS - beamsplitter, M - mirror and BS - Bragg cell device.

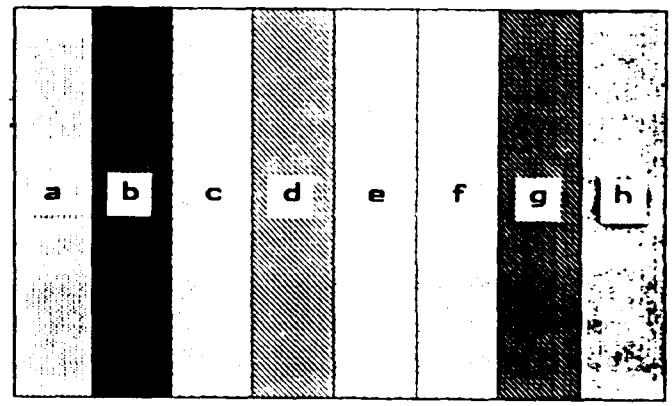

Fig.3.4.5. Light intensity pattern projected in SLMs.

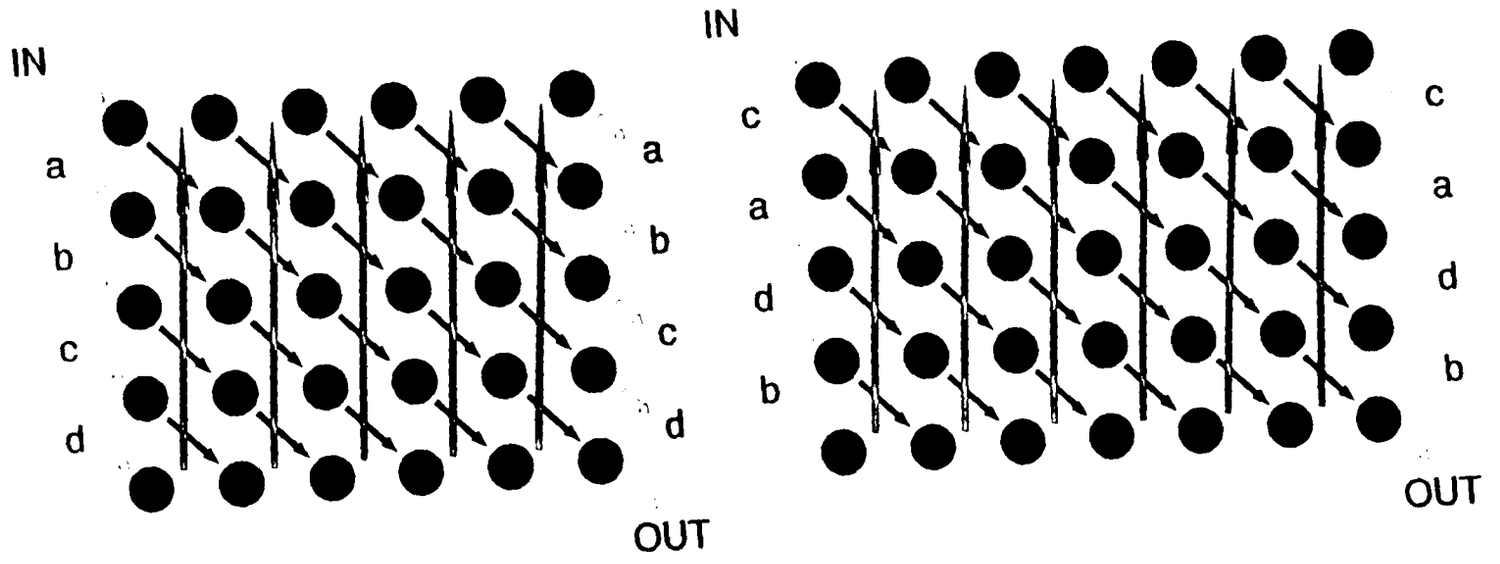

(a) (b)

Fig.3.5.1. Shuffle results for sequences with different selections of r_1 and r_2, where in (a) $r_1 = r_2 + 1$ and in (b) $r_1 = r_2 + 2$. The dark spots represent data points which run in the sequence from IN, to a, b, c, d, and OUT.

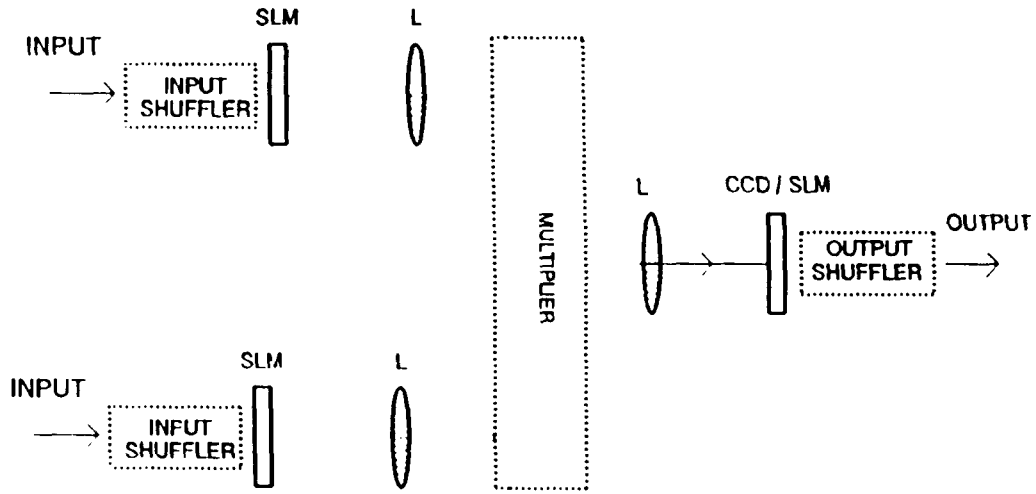

Fig.3.5.2. A proposed coherent opto-electronic processing system for performing convolution of long data sequences.

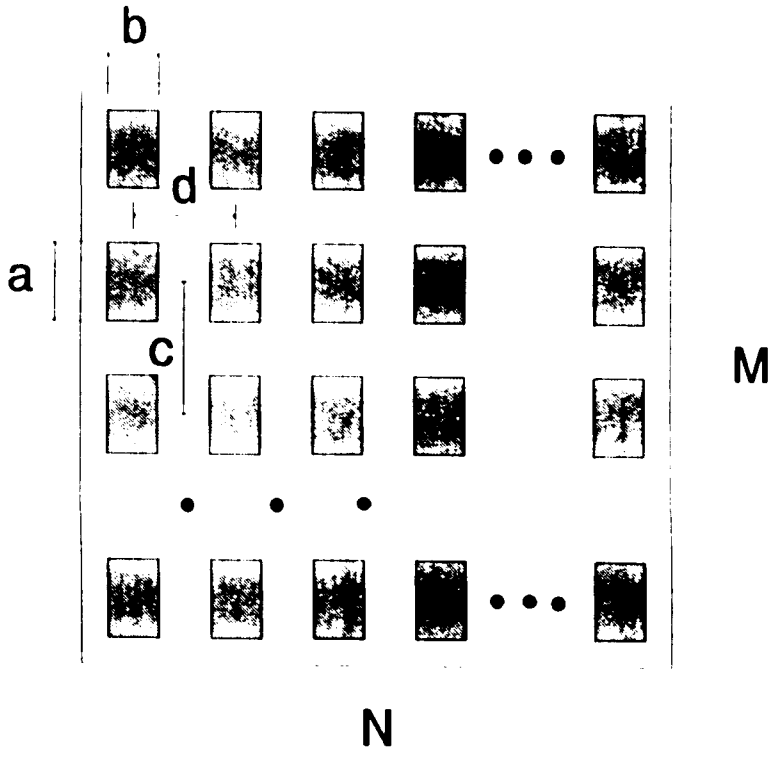

Fig.3.5.3. A mask like input pattern for r_1 = N and r_2 = M in which the shaded areas indicate intensity modulated data.

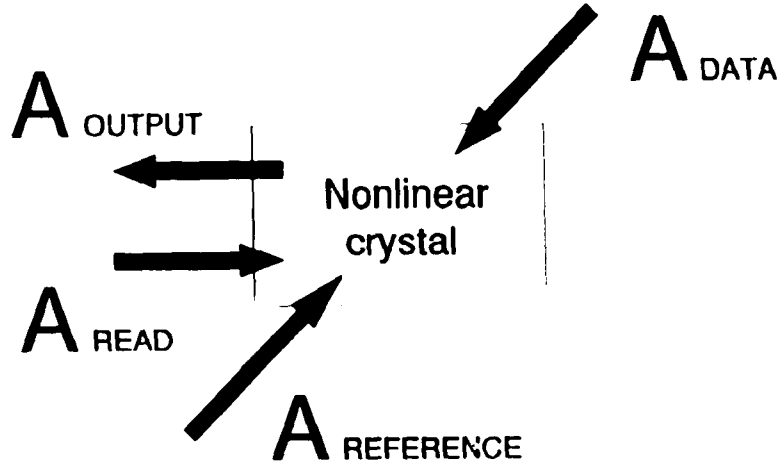

Fig.3.5.4. A principle diagram for multiplication of two optical patterns by a nonlinear four wave mixing in a photorefractive crystal.

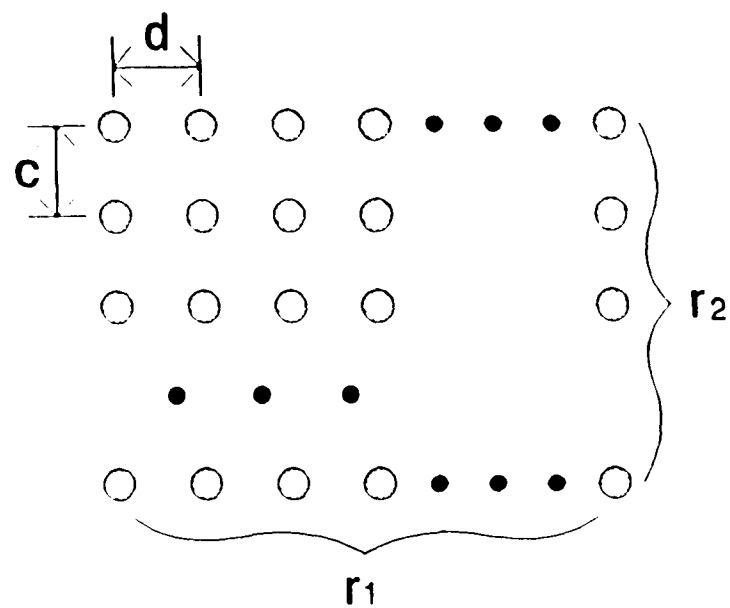

Fig.3.5.5. Sampling grid, where shaded circles indicate the sampling points. "c" and "d" are the same parameters used in Fig.3.5.3.

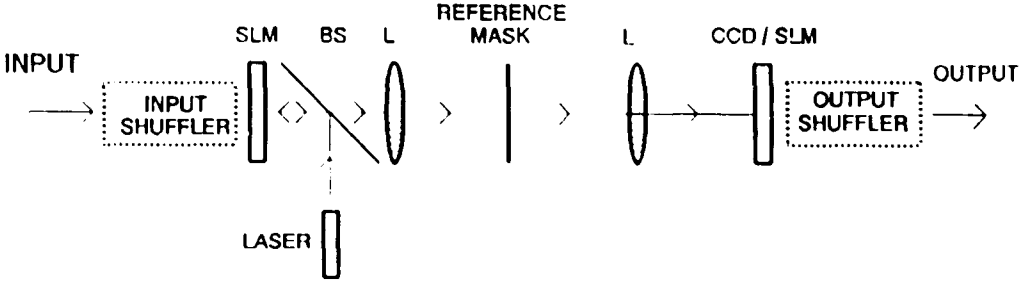

Fig.3.5.6. A simplified coherent opto-electronic processing system without using a photorefractive crystal.

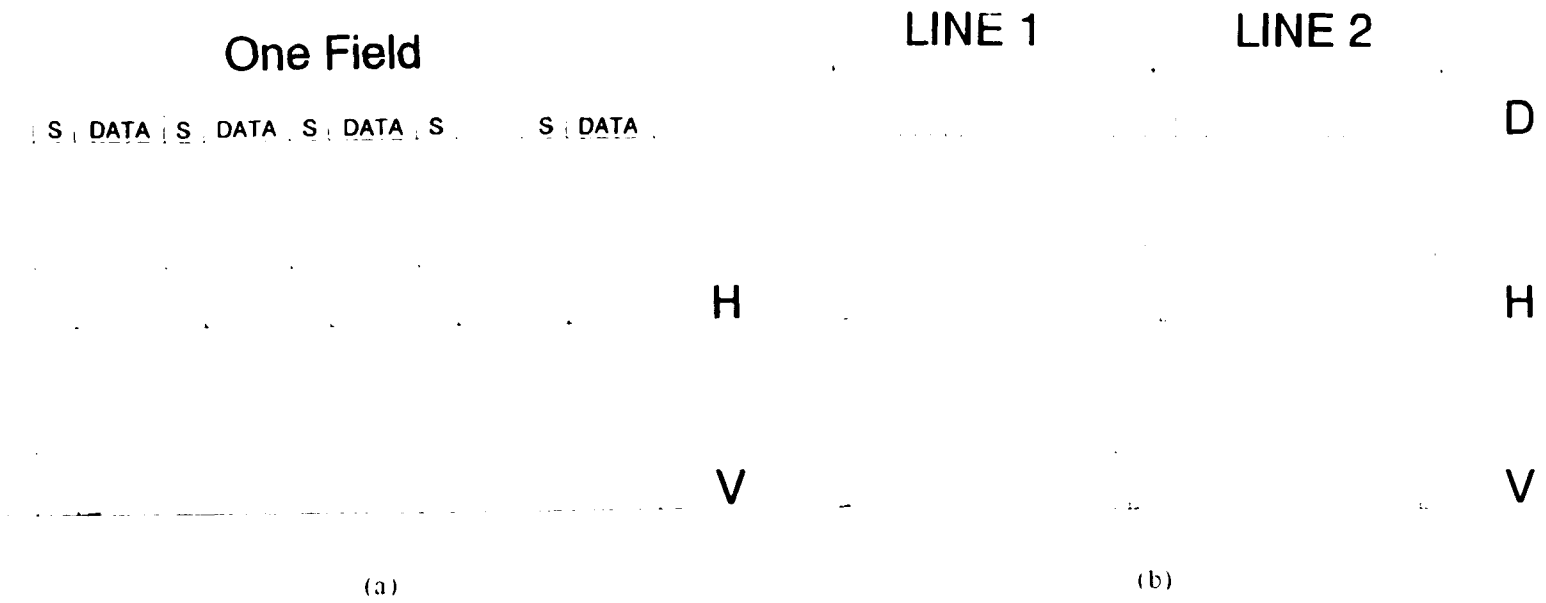

Fig.3.5.7. Scanning voltage relationships, (a) using a conventional CRT display and (b) using a special purpose CRT scanning system. S, synchronization signal; D, data; H, horizontal deflection voltage; V, vertical deflection voltage.

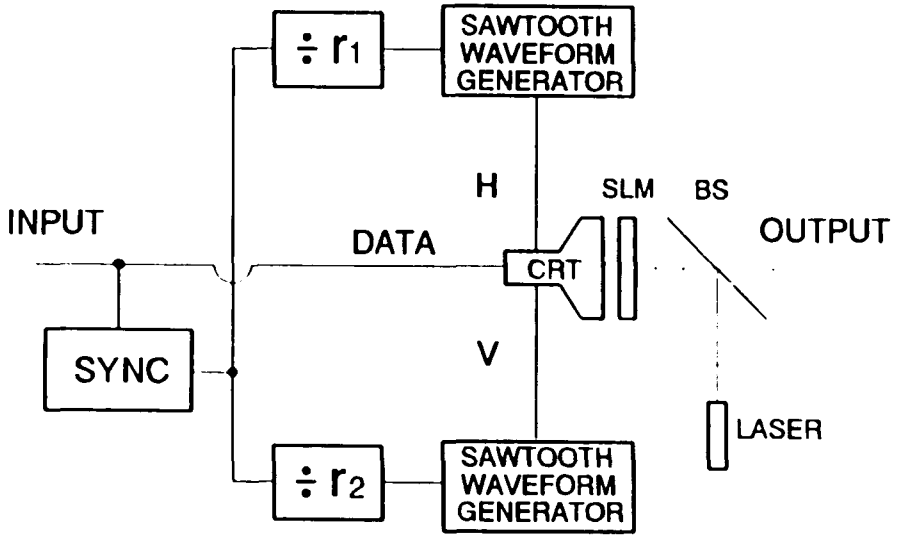

Fig.3.5.8. A schematic diagram of the shuffle scheme based on the special designed CRT display.

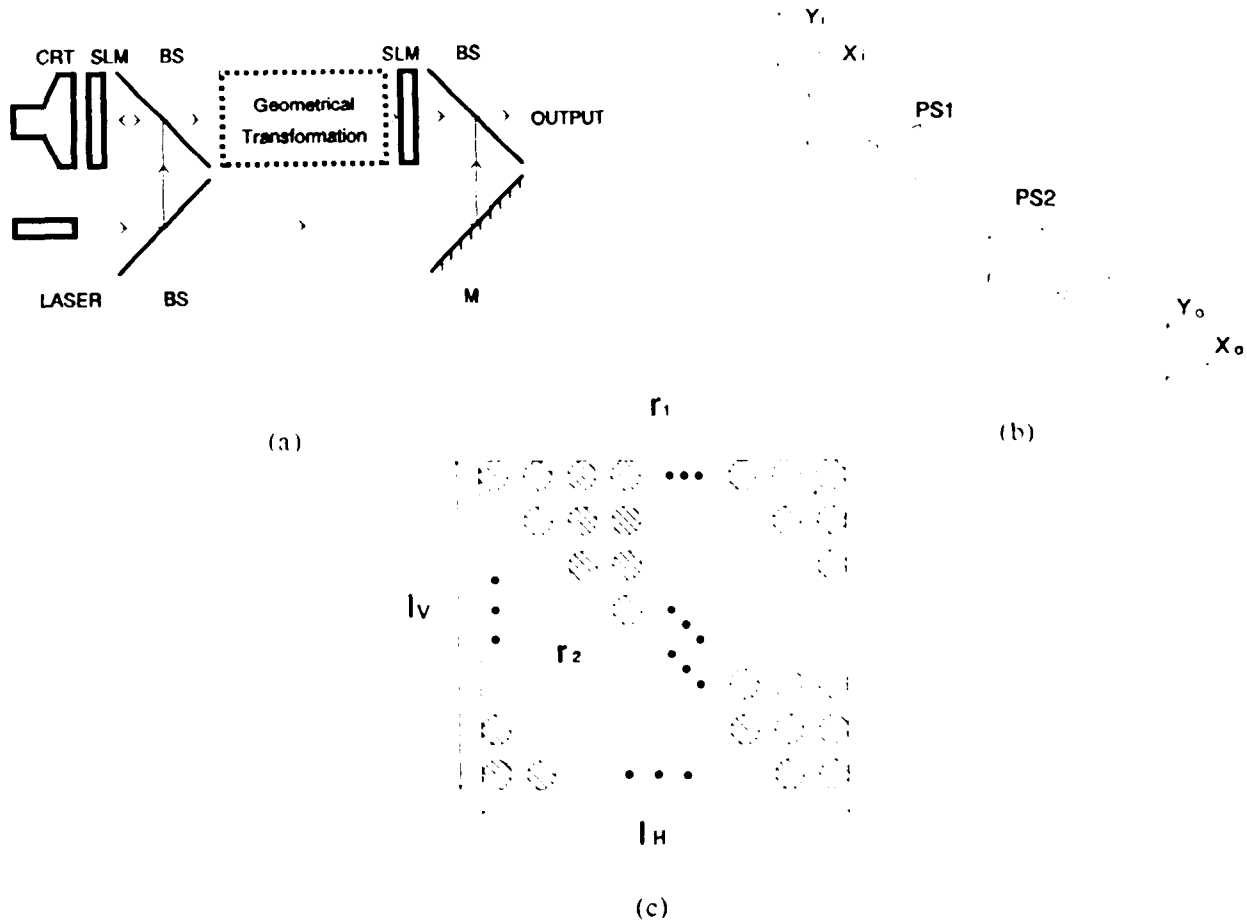

Fig.3.5.9. (a) A schematic show of an optical geometrical transform based shuffle system. M, mirror; (b) Lohman's setup for the optical geometrical transformation. PS, phase filter; and (c) geometry for determination of constant s, where l_H and l_V are widths in horizontal and vertical directions.

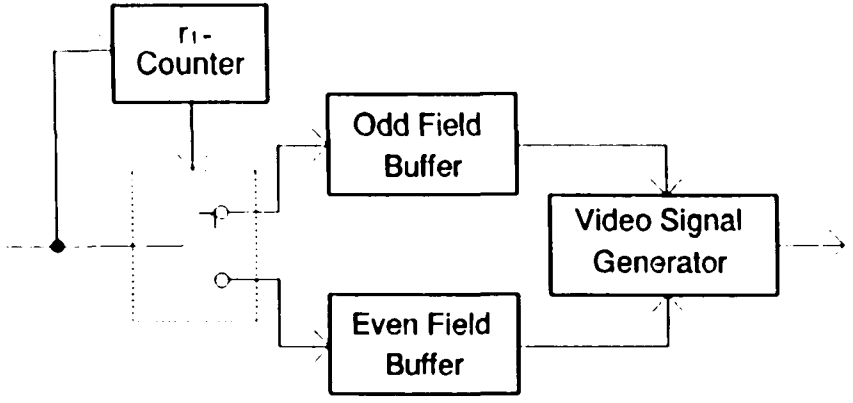

Fig.3.5.10. Buffer system which converts an input sequential signal to the form suitable for conventional 1-line-interlaced scanning system.

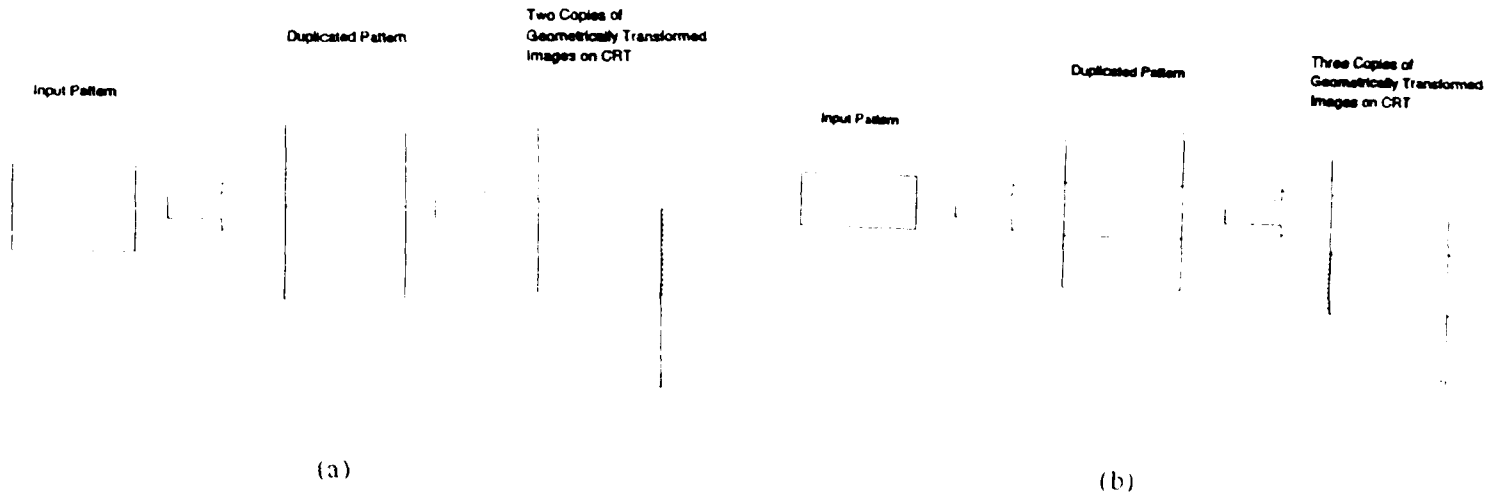

Fig.3.5.11. Procedures for generating 2-D shuffle patterns for the convolution and output patterns. (a) $r_1 = r_2 + 1$ and (b) $r_1 = r_2 + 2$. Dashed boxes contain the required shuffle results.

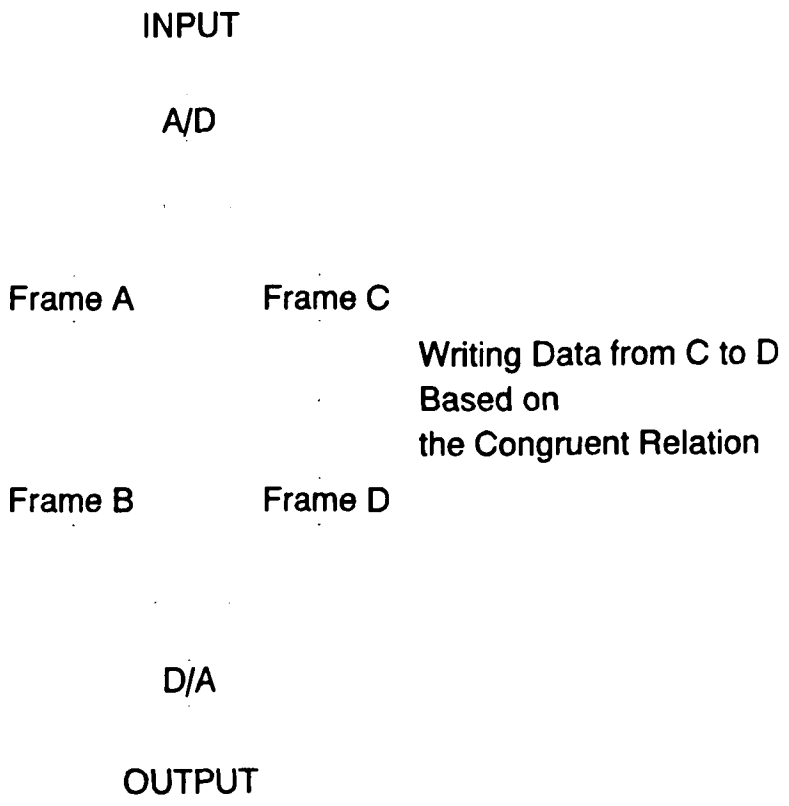

Fig.3.5.12. Principle diagram of image processing system based shuffle scheme.

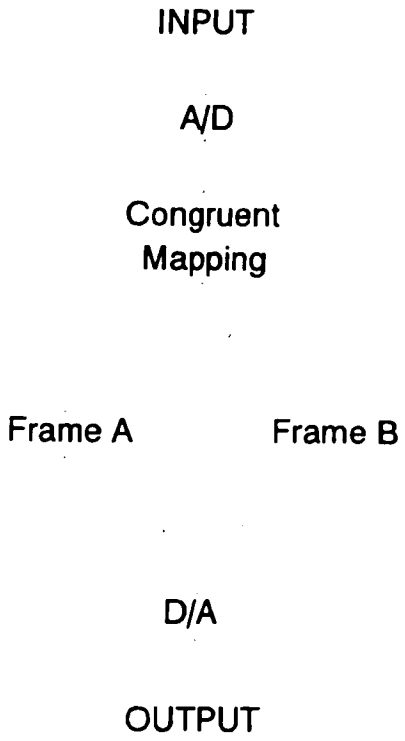

Fig.3.5.13. Simplified image processing system based shuffle scheme.

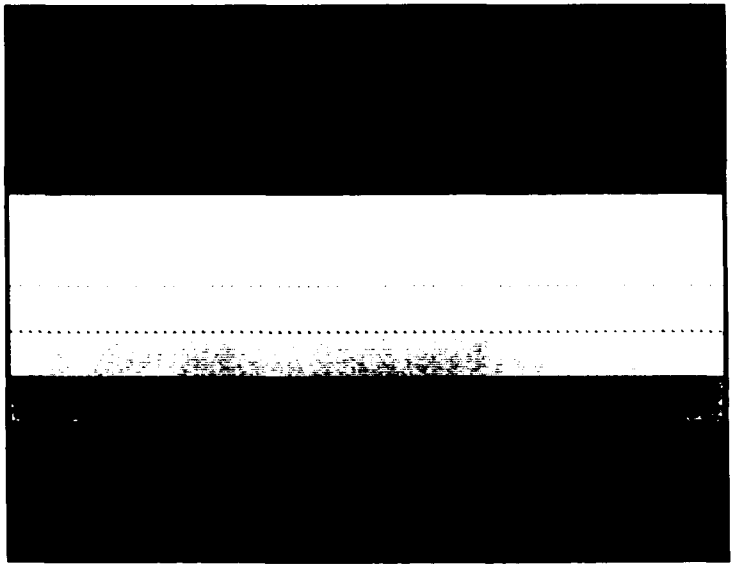

Fig.3.5.14. Instance pattern on a raster scan display.

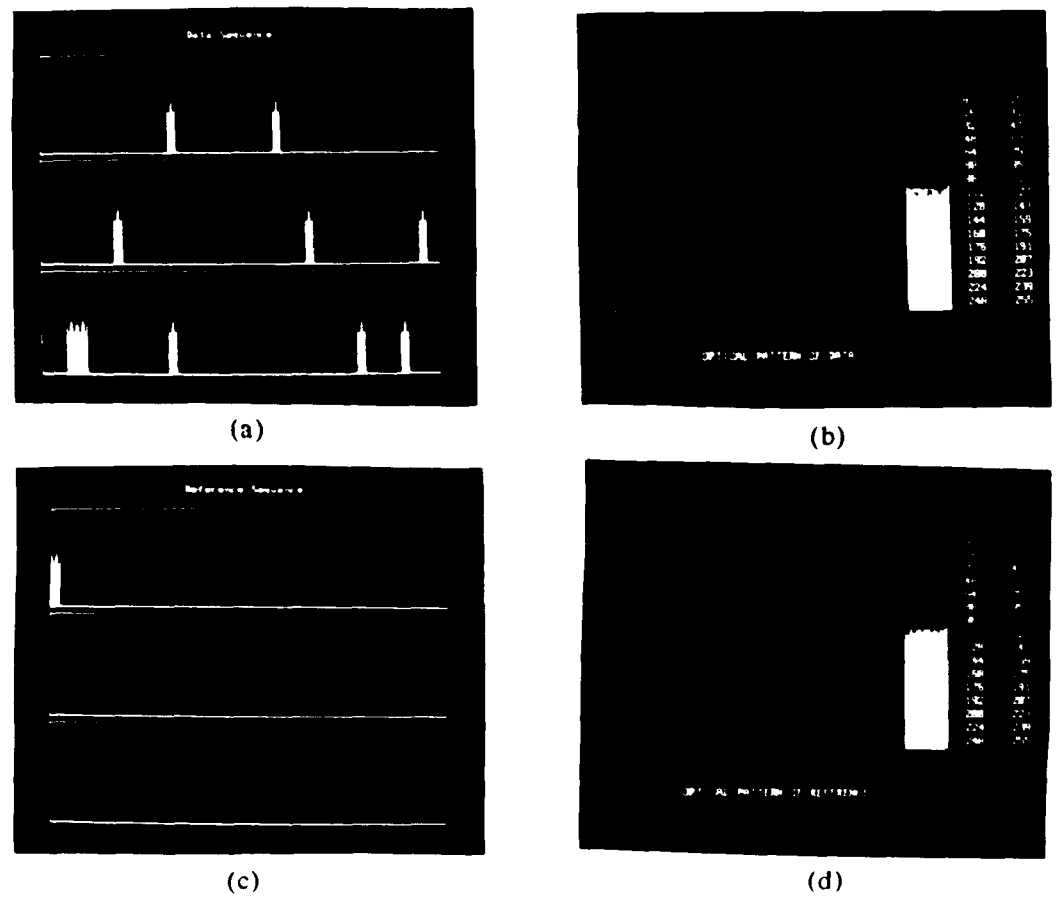

Fig.3.5.15. Noiseless input sequences. (a) The input data sequence to be shuffled; (b) its shuffled 2-D pattern of (a); (c) the reference sequence; and (d) its shuffled 2-D pattern.

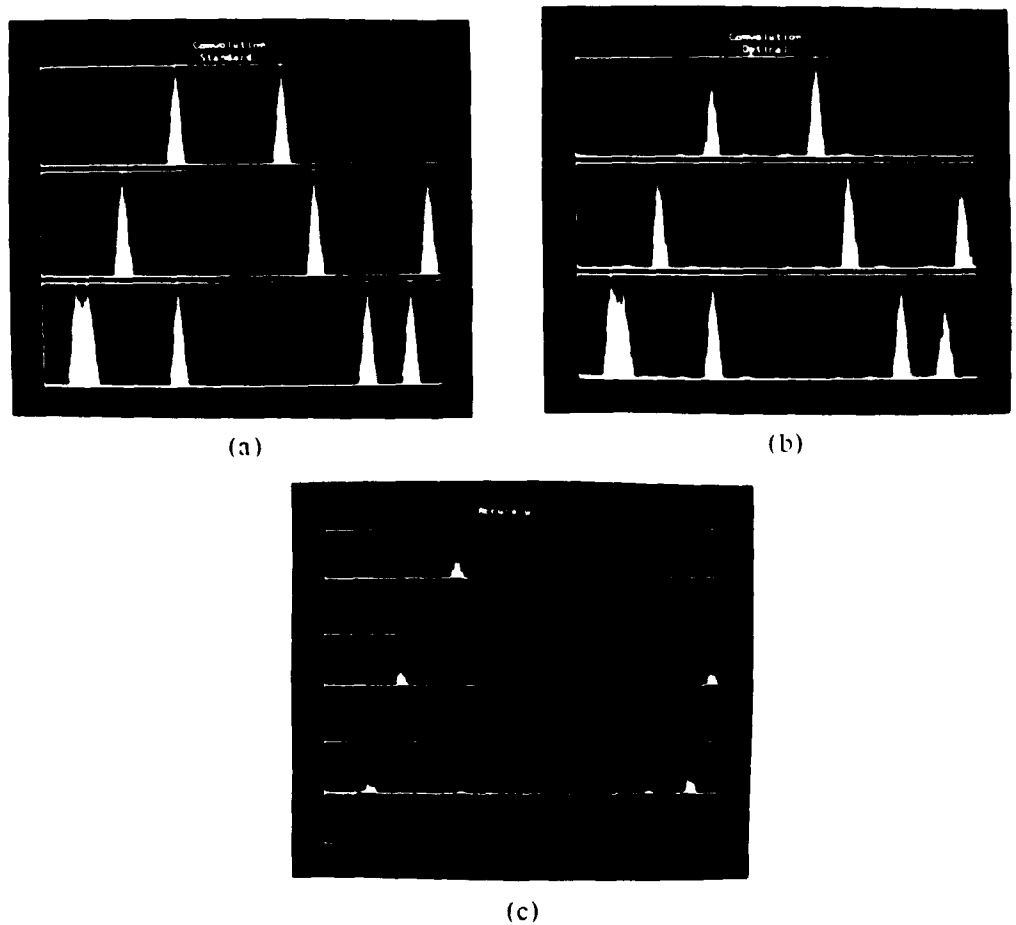

Fig.3.5.16. Simulation results for the sequences in Fig.3.5.15. (a) The conventional convolution result; (b) the simulation result of the algorithm which converts long data stream convolution correlation to 2-D convolution correlation; and (c) the errors between (a) and (b).

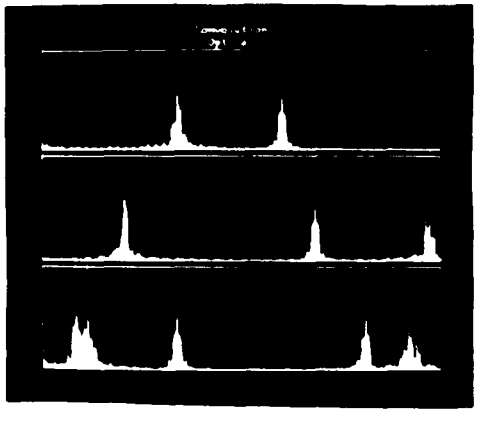

Fig.3.5.17. Simulation result for the sequences in Fig.3.5.15. when phase-only filtering scheme is employed.

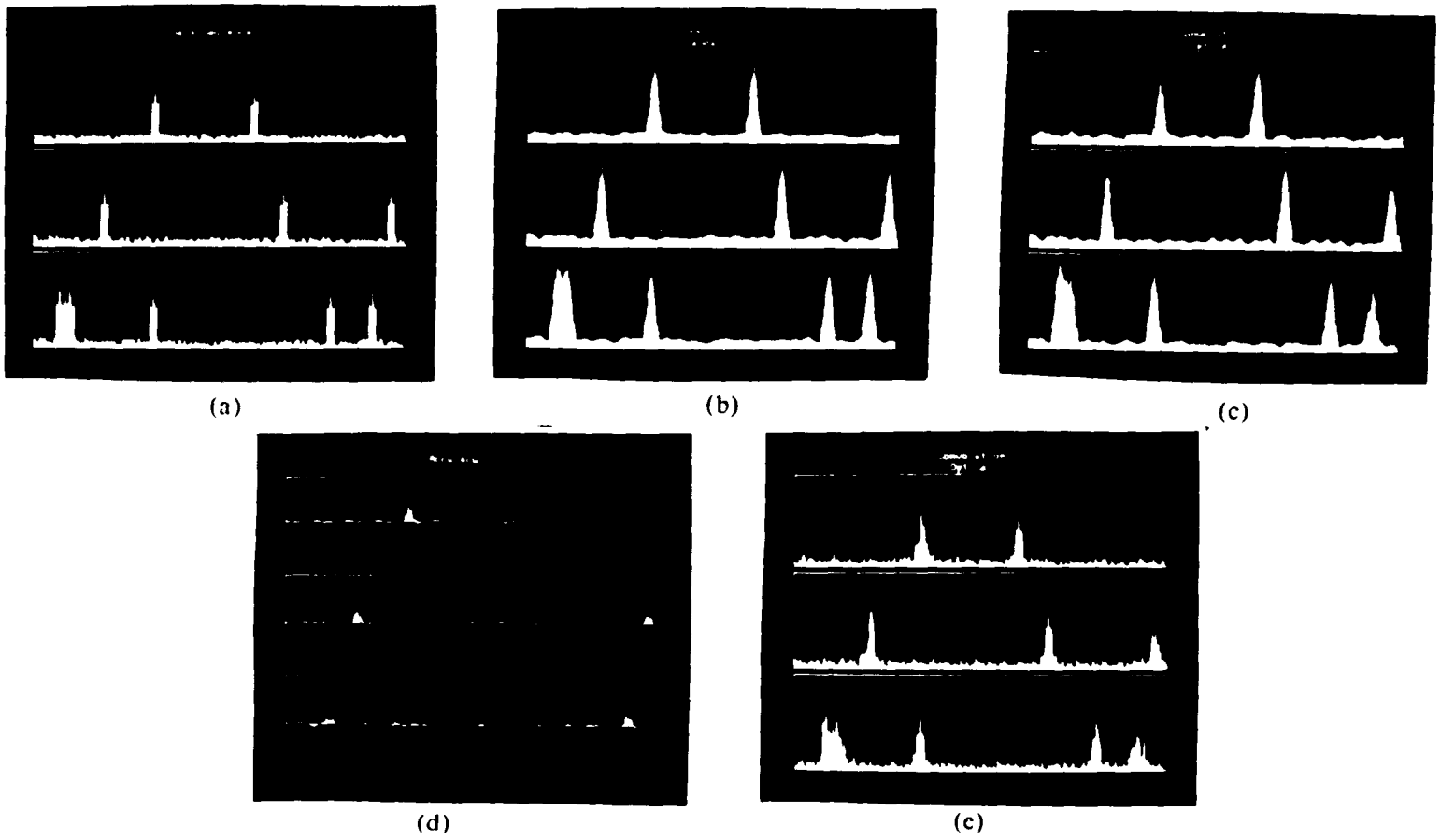

Fig.3.5.18. Simulation results for noise contaminated data sequence. The ratio of maximum signal level to maximum noise level is 5:1. (a) The input signal; (b) the conventional convolution result; (c) the simulated result of our scheme without phase-only filter employed; (d) the errors between (c) and (b); and (e) the simulated result by our scheme with phase-only filter employed.

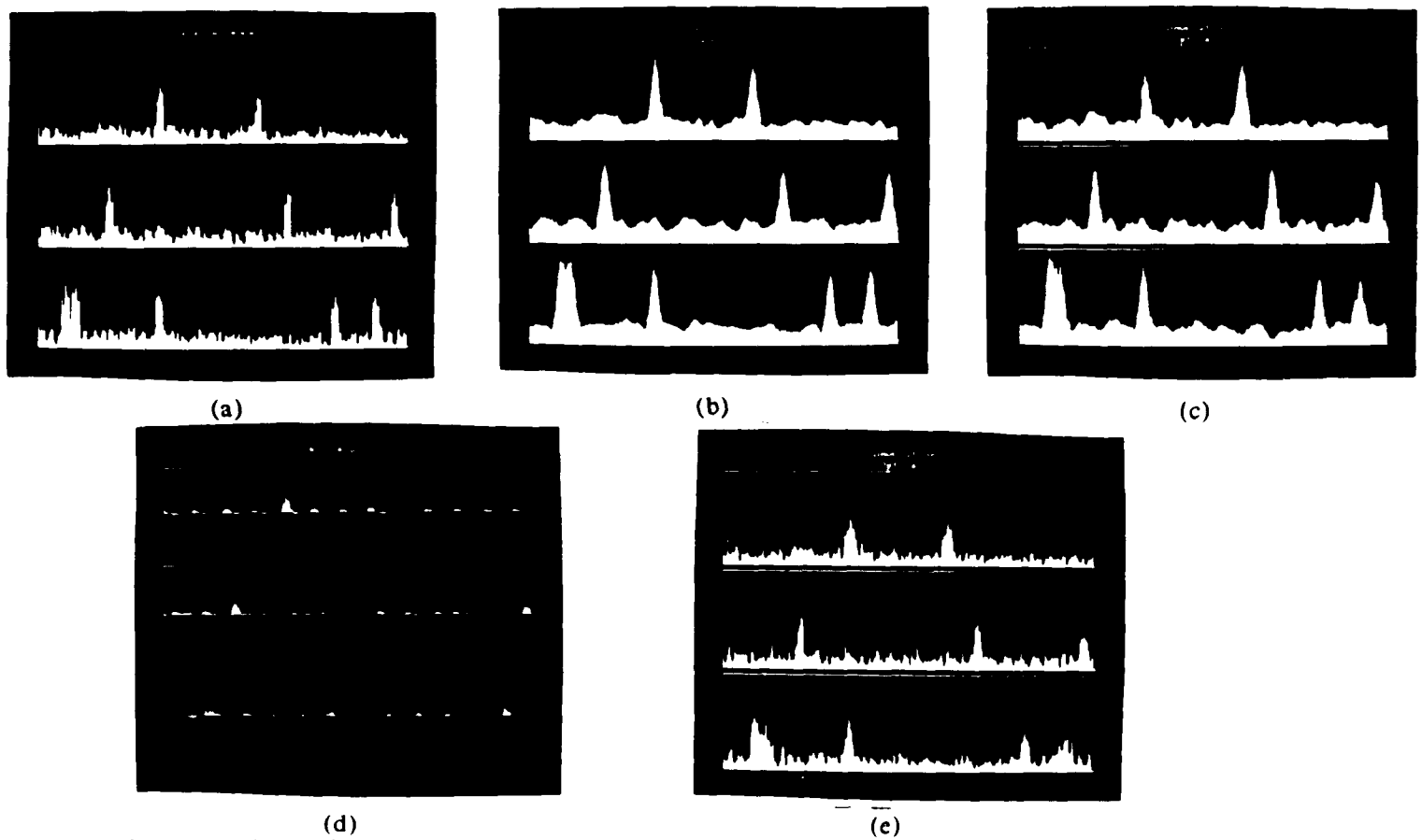

Fig.3.5.19. Simulation results for noise contaminated data sequence. The ratio of maximum signal level to maximum noise level is 5:2. (a) The input signal; (b) the conventional convolution result; (c) the simulated result of our scheme without phase-only filter employed; (d) the errors between (c) and (b); and (e) the simulated result by our scheme with phase-only filter employed.

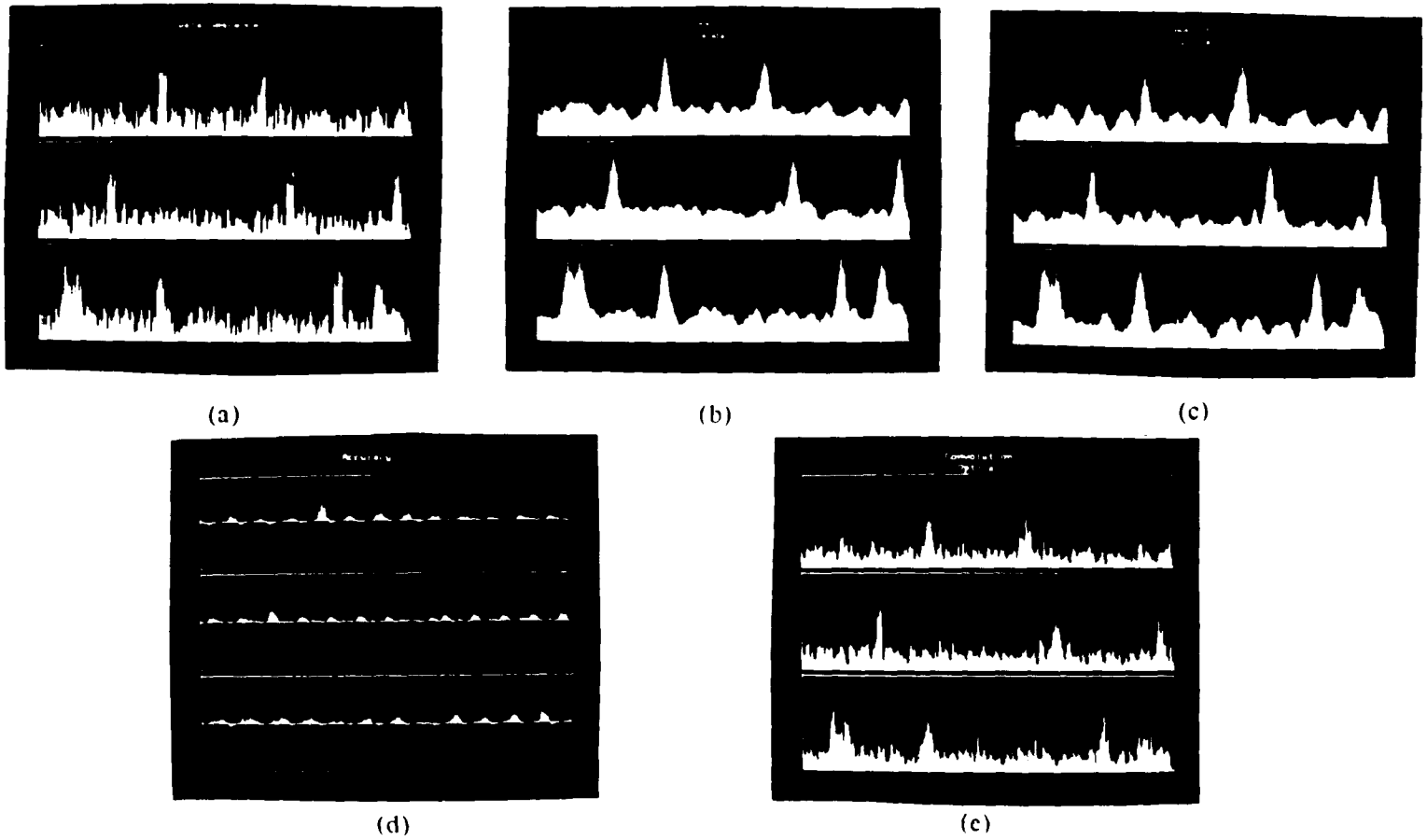

Fig.3.5.20. Simulation results for noise contaminated data sequence. The ratio of maximum signal level to maximum noise level is 5:3. (a) The input signal; (b) the conventional convolution result; (c) the simulated result of our scheme without phase-only filter employed; (d) the errors between (c) and (b); and (e) the simulated result by our scheme with phase-only filter employed.

Data Points Per Second

	LCLV ($2x10^4DF^a$)	MSLM ($200DF^a$)	EBSLM ($2x10^3DF^a$)	SIGHT MOD ($2x10^4DF^a$) ($7x10^4DF^{ab}$)	DMD ($4x10^3DF^a$)
No Crystal	$5x10^5$	$5x10^3$	$6x10^4$	$5x10^5$ $2x10^{6\,b}$	$1x10^5$
BSO	$2x10^5$	$2x10^3$	$2x10^4$	$2x10^5$ $7x10^{5\,b}$	$4x10^4$
$BaTiO_3$	$2x10^3$	540	200	$2x10^3$ $7x10^{3\,b}$	410

a) DF, data points per frame
b) Expected performance in near future.

Table 3.1 Maximum data rates achievable by our systems.

4 GABOR TRANSFORM

Since it was first described by Gabor in 1946 [4.1], Gabor representation as a time-frequency signal representation has been used in various applications such as signal detection [4.2], image representation [4.3]-[4.5], etc.

4.1 What is Gabor Transform?

In signal analysis, the short-time Fourier transform defined by

$$Y(\tau,\omega)=\int_{-\infty}^{\infty} y(t)w^{*}(t-\tau)e^{-j\omega t}dt \qquad (4.1.1)$$

delivers the frequency content in a neighborhood of τ, where w is a compactly supported window function. Closely related to this, the Gabor expansion of a 1-D signal $y(t)$ is expressed as [4.1],[4.3]

$$y(t)=\sum_{m=-\infty}^{\infty}\sum_{n=-\infty}^{\infty} C_{mn}w(t-n\tau)e^{j2\pi mf(t-n\tau)} \qquad (4.1.2)$$

where C_{mn} denotes the Gabor coefficients, f and τ are frequency and time resolutions with $f\tau \le 1$ in order to guarantee the above representation. On the other hand, the Heisenberg uncertainty also governs the determination of time and frequency resolutions [4.6]. The following inequality has to be satisfied

$$\tau f \ge \frac{1}{2(2\pi)} \qquad (4.1.3)$$

To determine the Gabor coefficient, Zak transform needs to be defined [4.7],[4.8]. As a joint time-frequency representation of signal $h(t)$, the Zak transform is given by [6]

$$H(z,\omega) = \sum_{k=-\infty}^{\infty} h(z-k)e^{-j2\pi k\omega} \qquad . \qquad (4.1.4)$$

Without loss of generality, it is assumed $\tau = f = 1$ in Eq.(4.1.2), since otherwise the time and frequency scale can be changed. Applying the Zak transform to Eq.(4.1.2),

$$Y(z,\omega) = \sum_{k=-\infty}^{\infty}\left(\sum_{n=-\infty}^{\infty}\sum_{m=-\infty}^{\infty} C_{mn}u(z-k-n)e^{j2\pi m(z-k)}\right)e^{-j2\pi k\omega}$$

$$= \sum_{n=-\infty}^{\infty}\sum_{m=-\infty}^{\infty} C_{mn}\left(\sum_{k=-\infty}^{\infty} u(z-k-n)e^{j2\pi mz}e^{-j2\pi k(\omega+m)}\right)$$

is obtained. By substituting $k' = k+n$ to the above equation,

$$Y(z,\omega) = \sum_{m=-\infty}^{\infty}\sum_{n=-\infty}^{\infty} C_{mn}e^{j2\pi mz}\left(\sum_{k'=-\infty}^{\infty} u(z-k')e^{-j2\pi(k'-n)(\omega+m)}\right)$$

$$= \sum_{m=-\infty}^{\infty}\sum_{n=-\infty}^{\infty} C_{mn}h'(z,\omega)e^{j2\pi(mz+n\omega)}$$

is in sequence, where $h'(z,\omega)$ is the Zak transform of the window function $u(t)$. After dividing both sides of the above equation by $h'(z,\omega)$,

$$\frac{Y(z,\omega)}{h'(z,\omega)} = \sum_{m=-\infty}^{\infty}\sum_{n=-\infty}^{\infty} C_{mn}e^{j2\pi(mz+n\omega)}$$

---

6 See Appendix B for more information about Zak transform.

is resulted. Multiplying this equation by $e^{-j2\pi(m'x+n'\omega)}$ and performing integration to both variables x and ω result in

$$\int_0^1\int_0^1 \frac{Y(x,\omega)}{h'(x,\omega)} e^{-j2\pi(m'x+n'\omega)}dx\,d\omega$$

$$= \sum_{m=-\infty}^{\infty}\sum_{n=-\infty}^{\infty} C_{mn}\int_1^1\int_0^1 e^{j2\pi((m-m')x+(n-n')\omega)}dx\,d\omega \quad .$$

It is known that

$$\int_0^1\int_0^1 e^{j2\pi((m-m')x+(n-n')\omega)} = 1 \qquad m=m' \qquad n=n'$$

$$= 0 \qquad m\neq m' \qquad n\neq n'$$

Therefore, the Gabor coefficients C_{mn} of signal $y(t)$ is determined by

$$C_{mn} = \int_0^1\int_0^1 \frac{Y(x,\omega)}{h'(x,\omega)} e^{-j2\pi(mx+n\omega)}dx\,d\omega \qquad (4.1.5)$$

Although this procedure of calculating C_{mn} is realizable using an electronic computer, it is inconvenient for its optical implementation.

To find a solution which is better for an optical realization, the biorthogonal function $\hat{u}(t)$ of window function $u(t)$ is used, which is defined in the following way

$$\int_{-\infty}^{\infty} u(t-n)\hat{u}^*(t-l)e^{j2\pi(k-m)t}dt = \delta(n-l)\delta(m-k)$$

$$(4.1.6)$$

Multiplying both sides of Eq.(4.1.2) by the product of the time-shifted version of function $\hat{u}(\cdot)$ and $e^{-j2\pi m t}$, and performing the integral operation to variable t in interval $(-\infty, \infty)$,

$$\int_{-\infty}^{\infty} y(t)\hat{u}^{*}(t-n')e^{-j2\pi m t}dt$$

$$= \sum_{m=-\infty}^{\infty}\sum_{n=-\infty}^{\infty} C_{mn}\int_{-\infty}^{\infty} u(t-n)\hat{u}^{*}(t-n')e^{j2\pi(m-m')t}dt$$

is obtained. Based on the definition of the biorthorgonal function,

$$C_{mn} = \int_{-\infty}^{\infty} \hat{u}^{*}(t-n)y(t)e^{-j2\pi m t}dt \qquad (4.1.7)$$

is thus achieved. Because of its close relationship with the Fourier transform, it is said that this is the more suitable formula for an optical implementation.

To determine the biorthogonal function from a given Gabor window function, the following derivation is described. The Zak transform of the signal $y(t)$ is first substitute in Eq.(4.1.5), which results in

$$C_{mn} = \int_0^1\int_0^1 \frac{\sum_{k=-\infty}^{+\infty} y(x-k)e^{-j2\pi k\omega}}{Z_y(x,\omega)} e^{-j2\pi(mx+n\omega)}dx\,d\omega$$

$$= \sum_{k=-\infty}^{+\infty}\int_0^1 y(x-k)\left[\int_0^1 \frac{e^{-j2\pi(n-k)\omega}}{Z_y(x,\omega)}d\omega\right]e^{-j2\pi mx}dx$$

Using Property 2 (see Appendix B for detail) of the Zak transform, the above equation is further simplified as

$$C_{mn} = \sum_{k=-\infty}^{+\infty} \int_0^1 y(x-k) \left[\int_0^1 \frac{1}{Z_u^*(x-k-n,\omega)} d\omega \right] e^{-j2\pi m x} dx$$

Because of the periodicity of an exponential function with a complex index, it can be shown that

$$e^{-j2\pi m x} = e^{-j2\pi m(x-k)}$$

for k being any integer. If a new variable $x' = x - k$ is assigned, the combination of summation about k and integration about x is now an integration about this new variable x' from negative infinity to positive infinity. The following equation is thus obtained

$$C_{mn} = \int_{-\infty}^{+\infty} y(x') \left[\int_0^1 \frac{1}{Z_u^*(x'-n,\omega)} d\omega \right] e^{j2\pi m x'} dx'$$

By comparing this with Eq.(4.1.7), the biorthogonal function of the window function is determined by

$$\hat{u}(x) = \int_0^1 \frac{d\omega}{Z_u^*(x,\omega)} \qquad (4.1.8)$$

where $Z_u^*(x,\omega)$ is the Zak transform of the elementary window function $u(t)$. This equation was also given by Friedlander and by Bastiaans in their papers [4.2],[4.9].

An further inspection of Eq.(4.1.7) reveals that the Gabor coefficients are, in fact, samples of a cross ambiguity function of $y(t)$ and $\hat{u}(t)$ [4.2],[4.10],[4.11],[4.12],[4.13]. And therefore, the optical setups for the implementation of the cross ambiguity

function could be used to perform the optical Gabor transform.

4.2 Window Selection

Analyzing the definition of Gabor representation shows that each Gabor coefficient describes the amplitude of the corresponding time-shifted and frequency-modulated version of the chosen Gabor window. These coefficients occupy rectangular cells in the joint time-frequency domain. Each cell provides a discrete quantum of information about the signal that is independent of the coefficients in any other cell. To reach a high representation resolution, a window which is highly concentrated jointly in both time and frequency domains is expected. It was shown by Weyl in 1932 that a Gaussian function reaches the equality in Heisenberg uncertainty inequality [4.14]. This is the reason that Gaussian function is widely used in image representation. On the other hand, Eq.(4.1.2) may also be used in applications related to pattern recognition. If the time-shifted and/or frequency-modulated version of certain known waveform is going to be allocated in a received signal, the window function is better to be chosen as the desired waveform. By doing this, whenever a waveform exists in the received the signal, the corresponding Gabor coefficient will be the corresponding strength of the target and its position will delivers the information of time delay and the carrier frequency. An example of this is in the application of radar signal processing (detailed in section 4.5). For the applications of transient signal detection, a

one-sided exponential function is preferred since it is considered more matched with the non-symmetric and abrupt transition properties of natural transient signals [4.2] than a symmetric two-sided Gaussian function.

4.3 Example of Gabor Window

As a traditional Gabor window, the Gaussian function was discussed by Bastiaans [4.14],[4.15]. It was him who gave the expressions of the biorthogonal function of the Gabor window function the first time. As he described for a Gaussian function of

$$u_g(t) = \left(\frac{\sqrt{2}}{T}\right)^{\frac{1}{2}} e^{-\pi\left(\frac{t}{T}\right)^2} \qquad (4.3.1)$$

the corresponding biorthogonal function was determined as

$$\hat{u}_g(z) = \left(\frac{1}{\sqrt{2}T}\right)^{\frac{1}{2}} \left(\frac{K_0}{\pi}\right)^{-\frac{3}{2}} e^{\pi\left(\frac{z}{T}\right)^2} \sum_{n-\frac{1}{2}\geq\frac{z}{T}} (-1)^{-n} e^{-\pi\left(n-\frac{1}{2}\right)^2} \qquad (4.3.2)$$

where K_0 is a constant which equals 1.85407468. The Gaussian Gabor window and its biorthogonal function are also graphically shown in Fig.4.3.1.

To demonstrate the derivation of the biorthogonal function of a given Gabor window, here the one-sided exponential function is considered since it is going to

be used in the following proof-of-concept experiments. Mathematically, a one-sided exponential function is expressed as

$$u(t) = \sqrt{2\lambda}\exp(-\lambda t)u(t) \qquad (4.3.3)$$

where λ is a decay parameter and $u(x)$ is a unit step function. To calculate its biorthorgonal function, the Zak transform is first performed on it.

$$\begin{aligned} h^{*}(x,\omega) &= \sum_{k=-\infty}^{\infty} \sqrt{2\lambda}\, e^{-\lambda(x-k)} u(x-k) e^{-j2\pi k\omega} \\ &= \sqrt{2\lambda}\, e^{-\lambda x} \sum_{k=-\infty}^{Z} e^{-k(j2\pi\omega-\lambda)} \\ &= \frac{\sqrt{2\lambda}}{1-e^{j2\pi\omega-\lambda}} e^{j2\pi\omega-\lambda(x-Z)} \end{aligned} \qquad (4.3.4)$$

where Z is the largest integer which is smaller or equal to x. From this result and Eq.(4.1.8), the biorthorgonal function is derived as

$$\begin{aligned} \hat{u}(x) &= \int_0^1 \frac{d\omega}{h^{*}(x,\omega)} \\ &= \frac{e^{\lambda(x-Z)}}{\sqrt{2\lambda}} \left\{ \int_0^1 e^{-j2\pi\omega Z} d\omega - e^{-\lambda} \int_0^1 e^{-j2\pi\omega(Z+1)} d\omega \right\} \\ &= \frac{e^{\lambda x}}{\sqrt{2\lambda}} \left\{ e^{-\lambda Z} \frac{1-e^{-j2\pi Z}}{j2\pi Z} - e^{-\lambda(Z+1)} \frac{1-e^{-j2\pi(Z+1)}}{j2\pi(Z+1)} \right\} \end{aligned} \qquad (4.3.5)$$

It can be proved that

$$e^{-\lambda Z}\frac{1-e^{-j2\pi Z}}{j2\pi Z} = 1 \qquad Z = 0$$

$$= 0 \qquad Z \neq 0 \qquad (4.3.6)$$

Therefore, the biorthogonal function of one-sided exponential function is

$$\hat{u}(x) = \frac{\exp(\lambda x)}{\sqrt{2\lambda}}[-u(x+1) + 2u(x) - u(x-1)]. \qquad (4.3.7)$$

which is graphically shown in Fig.4.3.2 together with the original window function. Using this function with Eq.(4.1.7), the Gabor coefficients of transient signals may be determined. Here, it is mentioned that the above obtained $\hat{u}(x)$ is a real function. And therefore, the operation to generate the complex conjugate of the biorthogonal function is not necessary in this case.

4.4 Optical Gabor Coefficient Processor for Short 1-D Signals

4.4.1 System Architecture

To evaluate the Gabor coefficients in real time, an opto-electronic Gabor coefficient processor for short 1-D signal depicted in Fig.4.4.1 was proposed and experimentally tested [4.16]-[4.19]. The length of the 1-D signals is limited to the aperture time of the input acousto-optic modulator, e.g. Bragg cell device.

In the setup, an input pulsed laser beam is first spatially filtered and one-dimensionally focused to form a narrow bar onto the window of an acousto-optic modulator. Since no negative values can be directly expressed by the inherently positive optical intensity, a DC term has to be employed to lift all negative values to the positive side. However, this will cause a strong DC component to inhibit the detection of signal components around DC. Therefore, in the system, the input signal $s(t)$ is first mixed with an internal carrier $\cos(2\pi f_c t)$ before sent to the A-O modulator by an RF driver. The Bragg cell's output is then amplitude modulated by this composite signal and is horizontally imaged and vertically expanded by a group of spherical and cylindrical lenses to form a pattern described as

$$p(x,y) = s\left(\frac{ax}{v_A}\right)\cos\left(2\pi\frac{f_c ax}{v_A}\right) \qquad (4.4.1)$$

where v_A is the acoustic wave velocity and a is an optical imaging constant, respectively. This pattern is then projected onto a SLM carrying a intensity mask which is related to the biorthogonal function of the selected Gabor window function by

$$T_{SLM}(x,y) = \hat{w}\left(\frac{a(x-y)}{v_A}\right)\cos\left(2\pi\frac{f_c ax}{v_A}\right) + b, \qquad (4.4.2)$$

where b, guarantees $T_{SLM}(x,y) \geq 0$. The light amplitude of the pattern generated from the SLM is now in the form of

$$f(x,y)=\frac{1}{2}\hat{u}\left(\frac{a(x-y)}{l_A}\right)s\left(\frac{ax}{l_A}\right)\left(1+\cos\left(2\pi\frac{2f_c ax}{l_A}\right)\right)$$

$$+b_r s\left(\frac{ax}{l_A}\right)\cos\left(2\pi\frac{f_c ax}{l_A}\right) \qquad (4.4.3)$$

A second astigmatic optical system located at side b of beamsplitter is used to perform a one-dimensional Fourier transform in x-direction and an imaging operation in y-direction, which results in an optical pattern at the plane where a 2-D detector array is located as

$$F(x_f,y_f)=\frac{1}{2}\int_{-\infty}^{\infty}\hat{u}\left(\frac{a(x-y_f)}{l_A}\right)s\left(\frac{ax}{l_A}\right)\exp\left(-j2\pi\frac{xx_f}{\lambda l_f}\right)dx$$

$$+\frac{1}{2}\int_{-\infty}^{\infty}\hat{u}\left(\frac{a(x-y_f)}{l_A}\right)s\left(\frac{ax}{l_A}\right)\cos\left(2\pi\frac{2f_c ax}{l_A}\right)\exp\left(-j2\pi\frac{xx_f}{\lambda l_f}\right)dx$$

$$+\int_{-\infty}^{\infty}b_r s\left(\frac{ax}{l_A}\right)\cos\left(2\pi\frac{f_c ax}{l_A}\right)\exp\left(-j2\pi\frac{xx_f}{\lambda l_f}\right)dx$$

(4.4.4)

where λ and l_f are the optical wave length and focal length of optical transform system, respectively. It can be seen that the first term in the above equation generates the Gabor coefficients and this term can be separated from other terms than a dc bias provided that a condition

$$f_c \geq 2B_s \qquad (4.4.5)$$

where B_s is signal bandwidth, be satisfied. When

$$t = \frac{a(x - y_f)}{v_A} \tag{4.4.6}$$

is assumed and a low-pass spatial filter is placed to pick up only the first term, then, the filtered signal $F_G(x_f, y_f)$, where

$$F_G(x_f, y_f) = rect(x_f, y_f)\frac{v_A}{2a}\exp\left(-j2\pi\frac{x_f y_f}{\lambda l_f}\right) \cdot \int_{-\infty}^{\infty} \hat{w}(t)s\left(t + \frac{a y_f}{v_A}\right)\exp(-j2\pi x'_f t)dt \tag{4.4.7}$$

is thus obtained on the output plane, where

$$x'_f = \frac{x_f v_A}{\lambda l_f a} \quad . \tag{4.4.8}$$

$F_G(x_f, y_f)$ is identical to Eq.(4.1.7) except for a complex coefficient $\exp\left(-j2\pi\frac{x_f y_f}{\lambda l_f}\right)$ and a constant amplitude, which is only related to system parameters and can be corrected using a look-up table in case that the values of the Gabor coefficients are necessary.

To detect the resulted coefficients, a 2-D detector has to be appropriately mounted and electronically controlled in order to preserve all information. Comparison of Eq.(4.4.8) with Eq.(4.1.7) shows that at the output plane the

sampling grid should be governed by the following physical requirements. The sampling intervals along the x_f and y_f directions are determined by

$$\Delta x_f = \frac{f \lambda l_f a}{v_A} \tag{4.4.9}$$

and

$$\Delta y_f = \frac{\tau v_A}{a} \tag{4.4.10}$$

for a given frequency resolution f and a time resolution τ, where $f\tau \leq 1$. The sampling grid is schematically shown in Fig.4.4.2. Although a custom made 2-D detector array built by, for example, photodiodes based on the above interval specifications can be used for the case of relatively low resolution, a 2-D CCD array is suggested for the general case where the sampling periods are reconfigurable. By an appropriate designed optical imaging system, the intervals in Eqs.(4.4.9) and 4.4.10 may be rescaled to match the physical size of a CCD detector.

To assure that the system works properly, a time matching of the modulations of the pulsed laser and of the Bragg cell must be established. First of all, only the shaded part of the 2-D pattern of Eq.(4.4.8) as shown in Fig.4.4.3 (a) is detected and sampled by the 2-D detector array. Then, for an A-O modulator with an aperture time of τ_a, the pulsed laser firing interval is kept at $\tau_a - \tau$. With the aid of the synchronization diagram shown in Fig.4.4.3 (b), it is obvious that the detector can always correctly determine the signals' arrival times no

matter when they arrive and how long they last. Consider the case that a transient signal arrives at the exact end of one sampling window, because of the window overlap in time diagram, it may be missed by the current window, however it will be caught by the following window. In the case where a signal lasts more than one window time, because only the shaded area of the output pattern will be detected, those false arrival peaks caused by the edges of each window will be ignored by the system. Finally, to freeze the traveling of the acoustic wave in Bragg cell during a laser strobe, the duration of the laser pulse must also be substantially short.

For the final determination of the appearance of certain target, a conventional threshold based decision can be made. If the amplitudes of the coefficients are required, a lookup table may be established before hand to get rid of those undesired complex constants. However, as for the reason that optical processing is more qualitative than quantitative, it is suggested to use the system to allocate the interested targets rather than to mathematically determine its Gabor coefficients under current technical conditions.

4.4.2 Preliminary Experimental Results

A proof-of-concept hybrid system was built in our laboratory and some preliminary experiments were performed to confirm the principle of the proposed optical Gabor coefficient processor. The Fig.4.4.1's architecture was slightly modified. The input A-O modulator was replaced by a fixed

transparency and a spherical lens was thus used to substitute the lens group L_2-C_2. Also, an Ar^+ Ion laser was used as the input light source instead of the pulsed laser. The window pattern was projected by a Hughes liquid crystal SLM through a FG-100-AT image processor installed in an IBM PC-AT compatible computer. A SONY CCD Video Camera was located at the output plane to pick up the resulting pattern and to transfer it to the computer for sampling and further processing. The input and Gabor window masks are shown in Fig.4.4.4

Two transient signals were used to test the system. The first signal contains a single pulse as shown in Fig.4.4.5 (a), using the above described setup, an optical pattern at the output plane was picked up by the CCD, which is shown in Fig.4.4.5 (b). In the photo, vertical direction corresponds to the frequency axis in a downward direction while the time axis is in horizontal direction from right to left. The apparent bright spot pointed by the arrow indicates the existence of a carrier modulated pulse. The distance from the right side of photo to the spot is proportional to the arrival time of the pulse while the distance from the DC to the spot is proportional to the carrier frequency. To sample the output pattern, the image is post-processed by a image processing software called IMAGEPRO II. The sampling result is given in Fig.4.4.5 (c). By measuring the light intensities at each sampled point, the Gabor coefficients of this transient signal was obtained. A 3-D graph generated by GRAPHTOOL is shown in Fig.4.4.5 (d). A sharp peak corresponding to the signal is seen. Errors because of the imperfect optical system are also noticed without big

effects. In a second example, an input signal containing two pulses with different carrier frequencies and different arriving times (see Fig.4.4.6 (a)) was also tested. The resulted optical pattern and the 3-D graphic show of Gabor coefficients clearly display their different arrival times and carrier frequencies (see Fig.4.4.6 (b)-(d)).

4.5 Optical Gabor Coefficient Processor for Long 1-D Signals

In the above described Gabor coefficient processor architecture, the length of the signal is limited by the space-bandwidth product of the input 1-D acousto-optic modulator. However, in many applications such as radar signal processing and seismic signal analysis, the processing of long 1-D signals in the range 10^4 to 10^6 data points is desired. To accommodate this, methods which fully utilize the available space-bandwidth product of 2-D optical processor are required.

Bastiaans suggested a scheme (Fig.4.5.1) to perform Gabor transform on a long 1-D signal. In the proposed system, the input 1-D signal $y(t)$ is first converted into a 2-D raster-scan format, which is described by

$$f_1(x_{t1}, x_{t2}) = rect\left(\frac{x_{t1}}{X}\right)\sum_{n=0}^{N-1} y(x_{t1} + nX)\delta(x_{t2} - n\alpha X) \qquad (4.5.1)$$

where $rect(t)$ is the gate function which equals one when $-\frac{1}{2} < t \leq \frac{1}{2}$ and zero otherwise. In the above equation X is the width of each raster line and αX is the space between

the raster lines. With Eq.(4.5.1) modulating the light field just behind the input device and a transparency with its transmittance of

$$T(x_{t1}, x_{t2}) = rect\left(\frac{x}{X}\right) rect\left(\frac{y}{Y}\right) X \sum_{m=-\infty}^{\infty} \hat{u}^{*}(x_{t1} + mX) e^{-i2\pi m x_{t2}/X}$$

(4.5.2)

located at the middle plane, where $Y = \frac{f\lambda l_f}{2\pi a}$, it was proved that at the output plane, the required Gabor coefficients may be obtained by sampling the optical pattern in the following way

$$C_{mn} = \int_{-\infty}^{\infty} \int_{-\infty}^{\infty} Y(x_{o1}, x_{o2}) \, \delta\left(x_{o1} - \frac{m l_f \lambda}{X}, x_{o2} - n\alpha X\right) dx_{o1} dx_{o2}$$

(4.5.3)

The sampling interval is thus determined by

$$\Delta x_{o1} = \frac{l_f \lambda}{X} \tag{4.5.4}$$

$$\Delta x_{o2} = \alpha X \tag{4.5.5}$$

in horizontal and vertical directions, respectively. Apparently, the interval in horizontal direction is small generally. For example, when $f = 0.5 \ (m)$, $\lambda = 6328 \ \text{Å}$ and $X = 50 \ (mm)$, the corresponding sampling interval in horizontal direction is $\Delta x_{o1} = 6.33(\mu m)$, which may cause some troubles in optical implementation. Although lenses may be chosen with long focal length and a laser may be selected

with long wavelength, the sampling space is still at the level of microns. It may probably be tried to decrease the size of input image, however, this effort will sacrifice the input space-bandwidth product.

To overcome the inherent implementation difficulty in Bastiaans's architecture, a modified scheme for long signals is now proposed. Unlike the Bastiaans's architecture which can generate all the required Gabor coefficients by just one shot, the proposed scheme needs to feed the time-shifted versions of the biorthogonal function to the processor in sequence. Therefore, the processing speed is fast but not real-time. Now the principle of the processor is described briefly.

In the system depicted in Fig.4.5.2, the biorthogonal function of the selected Gabor window is first generated off-line. When processing starts, the input signal is converted to 2-D pattern by raster scan and inserted into optical path by SLM A. The following spherical lens images the input pattern on SLM B which carries one of the time-shifted versions of the biorthogonal function in the raster scan format. Multiplication operation is thus resulted. It was proved by Turpin [4.23] that, by performing a 2-D Fourier transform on this pattern and with the aid of a prism, the 1-D Fourier transform of the multiplication of the input signal and the time-shifted version of the biorthogonal function is thus obtained at the output plane also in a raster scan format but rotated ninety degree. Therefore, by applying a sequence of time-shifted versions of the biorthogonal function to the processor, the required Gabor coefficients are obtained. As shown by Turpin, all the resulted data points can be easily detected.

However, in some applications where long 1-D signal is to be processed, if only the input signal is too long to fit in one window time while the length of the reference is within the window time, it is not necessary to use the above described schemes. From the analysis in Section 4.4.1, it is known that the Gabor coefficient processor for short 1-D signal may also be used in these applications without any loss of coefficients or false coefficients, as long as the timing diagram and the detected area depicted in Fig.4.4.3 are observed.

4.6 Optical Gabor Coefficient Processor for 2-D Signals

Similar to the case of considering 1-D signals, a 2-D signal, e.g. an image, may also be described by Gabor expansion. Mathematically, 2-D Gabor expiation is given by

$$y(x_1, x_2) = \sum_{m_1=-\infty}^{\infty} \sum_{n_1=-\infty}^{\infty} \sum_{m_2=-\infty}^{\infty} \sum_{n_2=-\infty}^{\infty} C_{m_1 n_1 m_2 n_2} u(x_1 - n_1\tau_1, x_2 - n_2\tau_2) e^{j2\pi(m_1 f_1 x_1 + m_2 f_2 x_2)} \tag{4.6.1}$$

where f_1 and f_2 are the frequency resolutions in the two dimensions while τ_1 and τ_2 are the time resolutions. Apparently, under this case, the Gabor coefficients are in a four dimensional (4-D) space. A similar derivation as in section 4.1 delivers that the Gabor coefficients of 2-D signal are determined by

$$C_{m_1 m_2 n_1 n_2} = \int_{x_1} \int_{x_2} u^*(x_1 - n_1, x_2 - n_2) y(x_1, x_2) e^{-j2\pi(m_1 x_1 + m_2 x_2)} dx_1 dx_2 \qquad (4.6.2)$$

where

$$\hat{u}(x_1, x_2) = \int_0^1 \int_0^1 \frac{d\omega_1 d\omega_2}{h^*(x_1, \omega_1, x_2, \omega_2)} \qquad (4.6.3)$$

is the biorthogonal function of the selected window function[7].

Because of its application in image processing, an optical Gabor coefficient processor for 2-D signals is interested. However, the dimensionality of the Gabor coefficients for 2-D signal really causes a serious problem of result representation.

One of the existing techniques to display a 4-D signal on a 2-D plane is based on the principle that the 4-D signal is represented by a time sequence of 2-D images where two out of the four dimensions are sampled in time. Therefore, a system shown in Fig.4.6.1 could be used to perform 2-D Gabor transform. It should be pointed out that this system can only perform the required 2-D Gabor transform at a fast speed rather than a real-time processing. How fast the processing speed is depends on the number of samples required in the two time dimensions and the

---

7 In Eq.(3.5.3), $h^*(x_1, \omega_1, x_2, \omega_2)$ is the 2-D Zak transform of the window function, which is defind as

$$h^*(x_1, \omega_1, x_2, \omega_2) = \sum_{k_1=-\infty}^{\infty} \sum_{k_2=-\infty}^{\infty} u(x_1 - k_1, x_2 - k_2) e^{-j2\pi(k_1\omega_1 + k_2\omega_2)}$$

rate of SLM. In principle, the 2-D biorthogonal function of the selected Gabor window is first generated based on Eq.(4.6.3) off-line. The image to be processed is carried into the processor by SLM A. The input image is then imaged on SLM B, which carries one of the time-shifted versions of the Gabor window function. A multiplication result is thus obtained right behind SLM B. This pattern is then subject to 2-D Fourier transform by spherical lens L3. The Gabor coefficients corresponding to current time-shifting parameters is obtained. To get the Gabor coefficients of other time-shifting parameters, the pattern on SLM B is updated by the time-shifted versions of the biorthogonal function in sequence.

Number of other methods have also been developed to solve the problem. They are based on the utilization of an optical 2-D to 4-D interconnect [4.21] and a phase grating with an optical lenslet array [4.18]. Compared with the scheme based on sequential display, the processing performed by these schemes is in real-time. However, the available space-bandwidth product of an optical processing system limits their resolution [4.18] to be less than that of sequential display based scheme.

4.7 Applications

As a time-frequency signal representation, there are various applications of using the Gabor signal representation. As an example, the applications to signal detection are discussed here. By means of signal detection, certain targets are

going to be detected and located in the received signal. The problem falls into two categories, i.e. detection of signal with known waveform and the detection of signal with unknown waveform.

For the first class of problem, the determination of the time-shift and frequency-shift version of a known waveform are considered, such as in radar signal processing. Consider a pulsed radar system shown in Fig.4.7.1. In principle, a known signal pulse is first modulated by a carrier generated by a local oscillator and then sent out by radar transmitter from the antenna. The returned echo from the remote target is then detected and displayed in certain format by the radar receiver. The target modifies the reflected signal (echo) in the following ways. The time delay of the received echo is proportional to the distance between the radar station and the detected target. The Doppler shift of echo referring to the original radar pulse contains the information of target speed. Since it is known that in the Gabor representation the coefficients correspond to the intensities of time-shifted and frequency-modulated (shifted) version of the original Gabor window, their indices are used to determine the time shift and frequency modulation. The desired parameters are thus obtained by the Gabor representation with an appropriately chosen Gabor window function. The waveform of signal pulse originally sent out by radar transmitter is chosen as the Gabor window function. This is reasonable since the purpose is just to determine the time-shifted and frequency-modulated version of this signal. By analyzing the resulted Gabor coefficients pattern, the existence of non-zero Gabor coefficients indicate the appearance of echo. The position of a non-zero coefficient in time direction

delivers the delay time which is proportional to the distance of target form the radar station. Its position in frequency direction can be used to calculate the Doppler shift, which is determined by the target speed.

For the second class of signal detection problem, the detection of transient signals with unknown waveform by Gabor transform is considered. The transient signals are those with unknown waveform, unknown arrival time and overlapped waveforms. Many techniques exist for the detection of transient signals such as matched filter and maximum likelihood detection. Although they are theoretically possible to solve the problem, it is difficult for them to be practically implemented. The above discussed Gabor expansion is a possible candidate to solve the problem. It was shown that, with a proper selection of an elementary window function, Gabor representation may represent the signal in a better time and frequency separability [4.6]. Since the envelopes of the transient signals are more or less the one-sided exponential functions, a relevant way of representing a transient signal by its Gabor expansion series is to expand it by a set of one-sided exponential window functions [4.2]. A Gabor coefficient processor for 1-D signals described in sections 4.4 and 4.5 is used to determine the Gabor coefficients of the received signal. With the obtained Gabor coefficients, the presence of signals can be detected by the observation of non-zero Gabor coefficients. For the detection of a single pulse, an appropriate thresholding similar to the conventional binary detector will yield the location of non-zero Gabor coefficients on the output time-frequency plane, which provides information leading to the arrival time and carrier frequency of the received signal. To detect the received signal with waveforms other than

a pulse, the signal synthesis [4.20] based on the obtained Gabor coefficients is necessary. In this case, the location of the Gabor coefficients provide the arrival time of the target while a Gabor expansion using these coefficients and the window function gives rise to the signal's waveform. On the other hand, if the arrival time of a signal, e.g. as in the case of radar signal detection, is to be determined for the signal with certain known waveform, the Gabor coefficients of the known waveform are first used to generate a 2-D pattern. The thresholding result of the correlation of this pattern with the output pattern of the received signal will locate the position of correlation peak on the output plane. The position corresponding to the time axis will give the information of distance while the position corresponding to frequency axis will deliver the Doppler shifter which can be used to determine the speed of target.

Technically, it is possible to reach the case that the signal arrives between two consecutive sampling points. It can be mathematically proved that the width of Gabor coefficient pulse is 2τ in time direction and $2f$ in frequency direction in analog sense (see Fig.4.7.2). To determine the arrival time of signal appropriate interpolation has to be employed to allocate the pulse peak. Similar scheme may solve the problem that the carrier frequency does not match with one of the sample points.

Before this chapter is closed, the time and frequency resolutions of Gabor transform for signal detection need to be re-evaluated because of the practical case described in last paragraph. The puzzles are:

(1) When two consecutive non-zero Gabor coefficients in time direction are obtained, is there one pulse arriving between the two consecutive sampling times or are there two pulses arriving sequentially?

(2) When two consecutive non-zero Gabor coefficients in the frequency direction are obtained, is there only one frequency between the two consecutive sampling frequencies or are there two frequency components?

To solve the puzzle, it is said that the actual time and frequency resolutions for the application to signal detection are 2τ and $2f$, respectively, rather than τ and f as described in section 4.1.

4.8 Summary

In summary, this chapter studied optical implementation of Gabor transform on both 1-D and 2-D signals. A Gabor coefficient processor for short 1-D signal was described. Preliminary experimental results were also shown to demonstrate the feasibility of the system. Possible system architectures for processing long 1-D signals and 2-D signals were also briefly described. Application of Gabor transform to signal detection was also discussed.

4.9 References

[4.1] D. Gabor, "Theory of Communication," *J.I.E.E.*, vol.93, pp.429-459, 1946.

[4.2] B. Friedlander and B. Porat, "Detection of Transient Signals by the Gabor Representation," *IEEE Trans. on Acoust., Speech and Sig. Proc.*, vol.37, no.2, pp.169-180, February 1989.

[4.3] G. Eichmann, C. Lu, M. Jankowski and R. Tolimieri, "Shape Representation by Gabor Expansion," *Technical Note.*

[4.4] J. Daugman, "Complete Discrete 2-D Gabor Transforms by Neural Networks for Image Analysis and Compression," *IEEE Trans. Acoust., Speech and Sig. Proc.*, vol.36, no.7, pp.1169-1179, July 1988.

[4.5] Z. Y. Zhu, "Neuron-Like Textural Processing Based on Gabor Representation and Neural Networks," *Doctoral Thesis Proposal*, City University of New York, New York, 1991.

[4.6] H. Wechsler, *Computational Vision*, Academic Press, San Diego, 1990.

[4.7] A. J. E. M. Janssen, "The Zak Transform: A Signal Transform for Sampled Time-Continuous Signals," *Philips J. Res.*, vol.43, pp.23-69, 1988.

[4.8] J. W. M. Bergmans and A. J. E. M. Janssen, "Robust Data Equalization, Fractional Tap Spacing and the Zak Transform," *Philips J. Res.*, vol.42, pp.351-398, 1987.

[4.9] M. J. Bastiaans, "Gabor's Signal Expansion and Degrees of freedom of a Signal," *OPTICA ACTA*, vol.29, no.9, pp.1223-1229, 1982.

[4.10] D. Casasent and B. V. K. V. Kumar, "Optical Image Plane Correlator for Ambiguity Surface Computation," *Applied Optics*, vol.18, no.10, pp.1673-1678, 15 May 1979.

[4.11] R. J. Marks II, J. F. Walkup and T. F. Krile, "Ambiguity Function Display: An Improved Coherent Processor," *Applied Optics*, vol.16, no.3, March 1977.

[4.12] P. N. Tamura, J. J. Rebholz and T. C. Lee, *J. Opt. Soc. Am.*, vol.69, p.1451, 1979.

[4.13] K. H. Brenner and A. W. Lohmann, *Opt. Com.*, vol.42, p.310, 1982.

[4.14] M. J. Bastiaans, "Gabor's Expansion of a Signal into Gaussian Elementary Signals," *Proc. IEEE*, vol.68, no.4, pp.538-539, April 1980.

[4.15] M. J. Bastiaans, "A Sampling Theorem for the Complex Spectrogram, and Gabor's Expansion of a Signal in Gaussian Elementary Signals," *Opt. Eng.*, vol.20, no.4, pp.594-598, July/August 1981.

[4.16] Y. Zhang and Y. Li, "Optical Determination of Gabor Coefficients of Transient Signals," *Opt. Lett.*, vol.16, no.13, pp.1031-1033, 1 July 1991.

[4.17] Y. Zhang, Y. Li, R. Tolimieri, E. G. Kanterakis, A. Katz, X. J. Lu and N. P. Caviris, " Opto-Electronic Gabor Detector for Transient Signals," *Proc. SPIE*, vol.1981, pp.23-31, April 1991.

[4.18] Y. Li and Y. Zhang, "Optical Implementation of Gabor and Wavelet Expansions of 1- and 2-D Signals," *Proc. SPIE*, vol.1702, 1992.

[4.19] A. Katz, X. J. Lu, E. G. Kanterakis, Y. Li, Y. Zhang and N. P. Carivis, "Real-Time Optoelectronic Gabor Detection of Transient Signals," *OSA 1991 Annual Meeting Technical Digest*, p.12, 1991, San Jose.

[4.20] W. Krattenthaler and F. Hlawatsch, "Improved Signal Synthesis from Pseudo-Wigner Distribution," *IEEE Trans. Signal Processing*, vol. SP-39, pp. 506-509, February 1991.

[4.21] H. J. Caulfield and H. H. Szu, "Optical Wavelet Transform in Higher Dimensions," Proc. SPIE, vol.1705, April 1992.

[4.22] Y. Li and Y. Zhang, "Optical Gabor and Wavelet Expansions of One and Two Dimensional Signals," in preparation.

[4.23] T. M. Turpin, "Spectrum Analysis Using Optical Processing," *IEEE Proc.*, vol. 68, no. 1, pp. 79-92, Jan. 1981

4.10 Figures

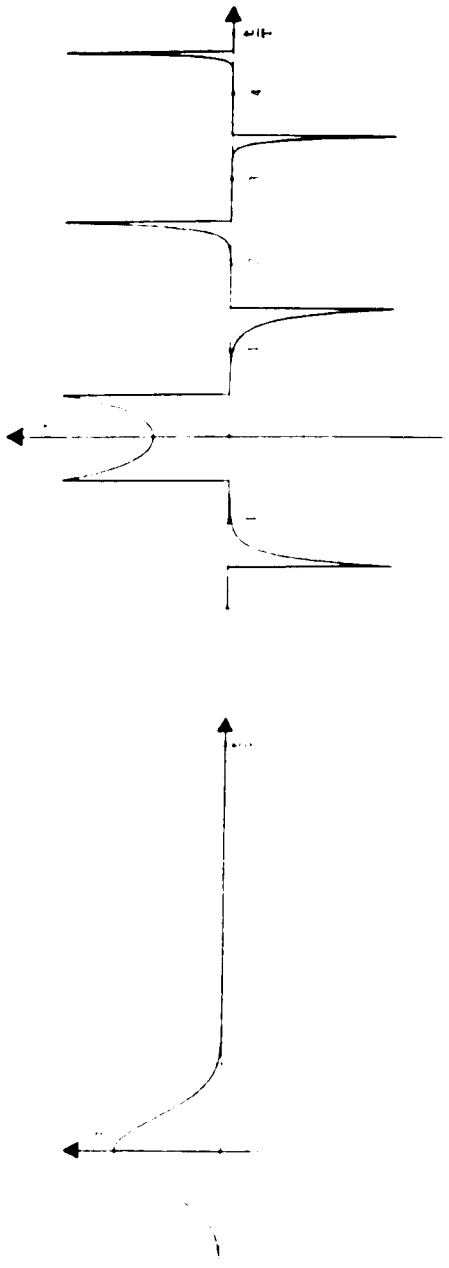

(b)

(a)

Fig.4.3.1. (a) A Gaussian window function and (b) its biorthogonal function.

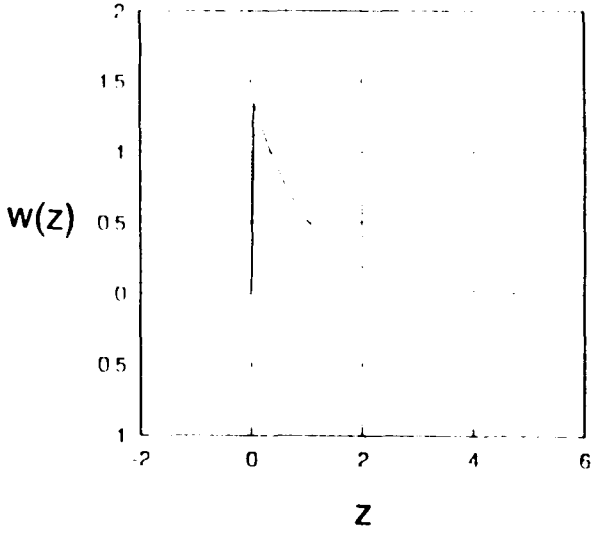

(a)

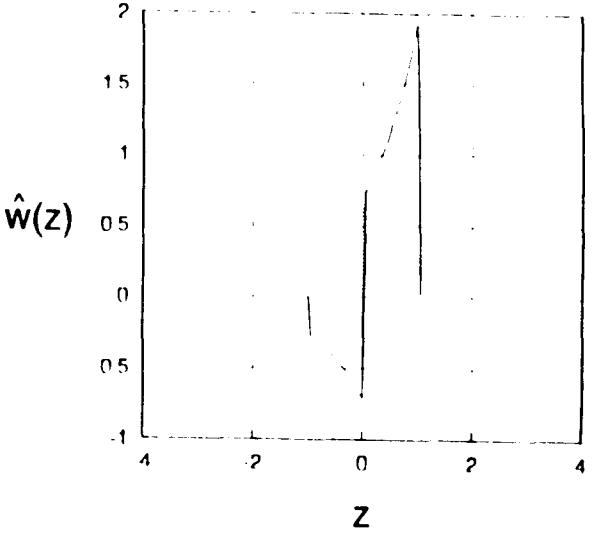

(b)

Fig.4.3.2. (a) A single sided exponential window function and (b) its biorthogonal function.

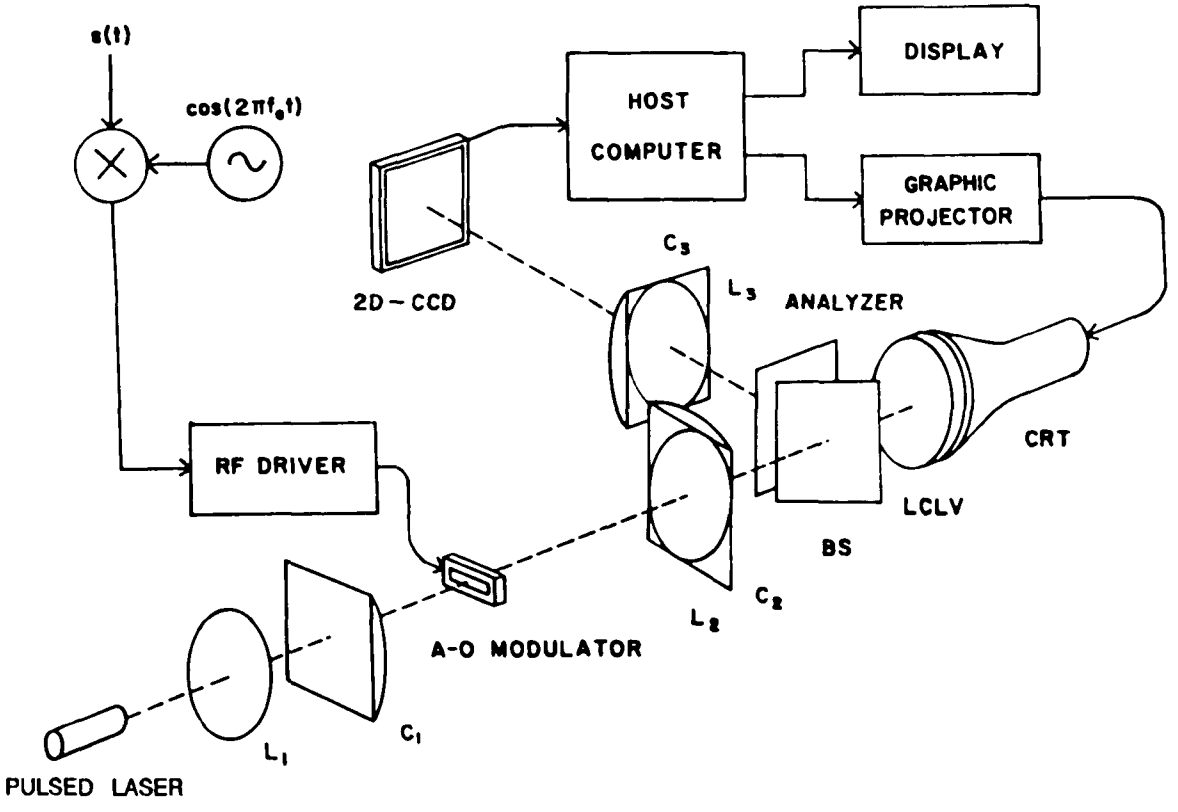

Fig.4.4.1. Proposed Gabor coefficient processor for short 1-D signals.

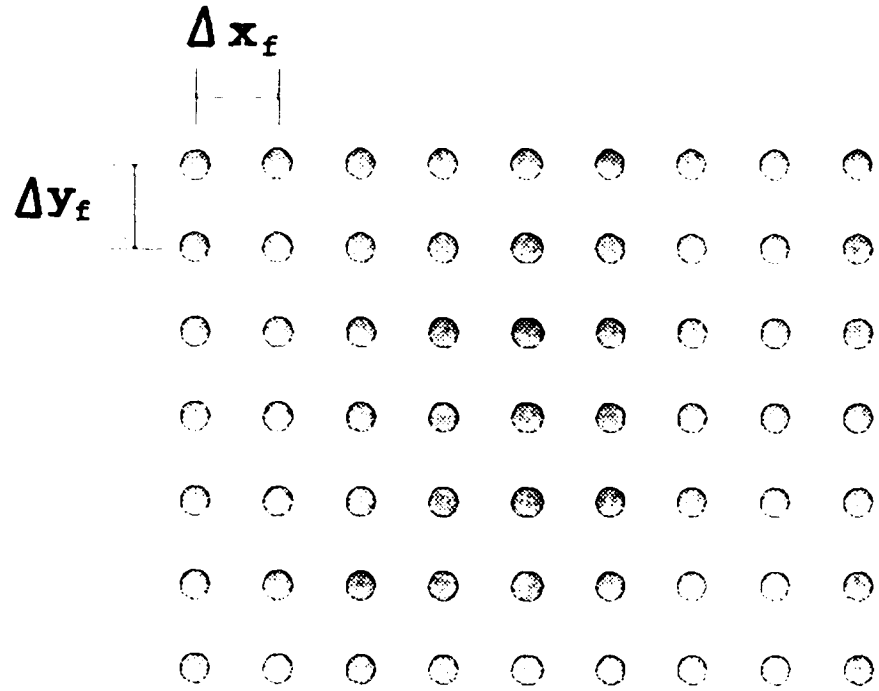

Fig.4.4.2. Sampling grid.

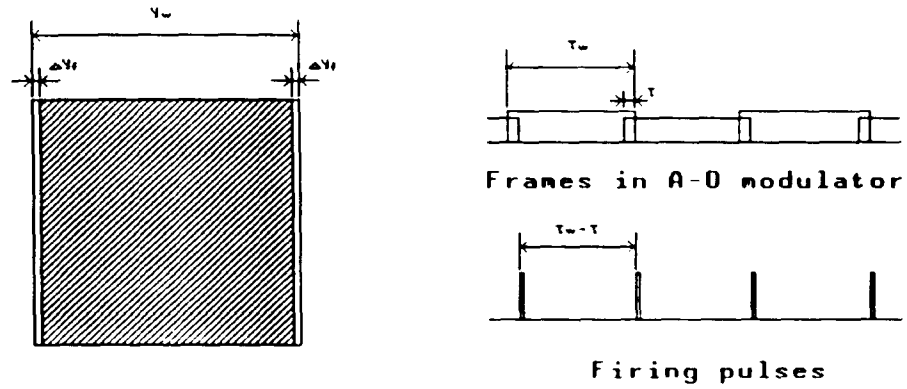

(a) (b)

Fig.4.4.3. Detection area and synchronization diagram. (a) Detection area (shaded), where y_w is the image width in the y direction corresponding to the A-O modulator aperture time τ_w. (b) Synchronization diagram.

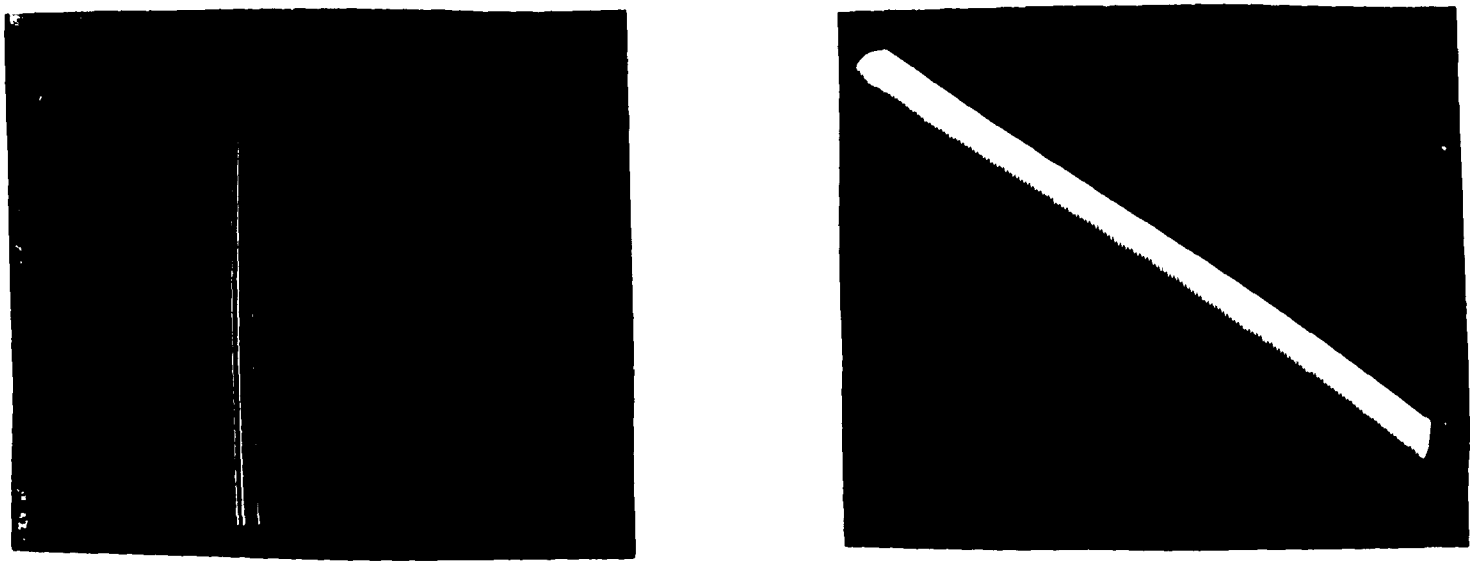

(a) (b)

Fig.4.4.4. Input signal and Gabor window masks used in the proof-of-concept experiment. (a) Mask of single pulse input and (b) mask of the time-shifted versions of modulated biorthogonal function.

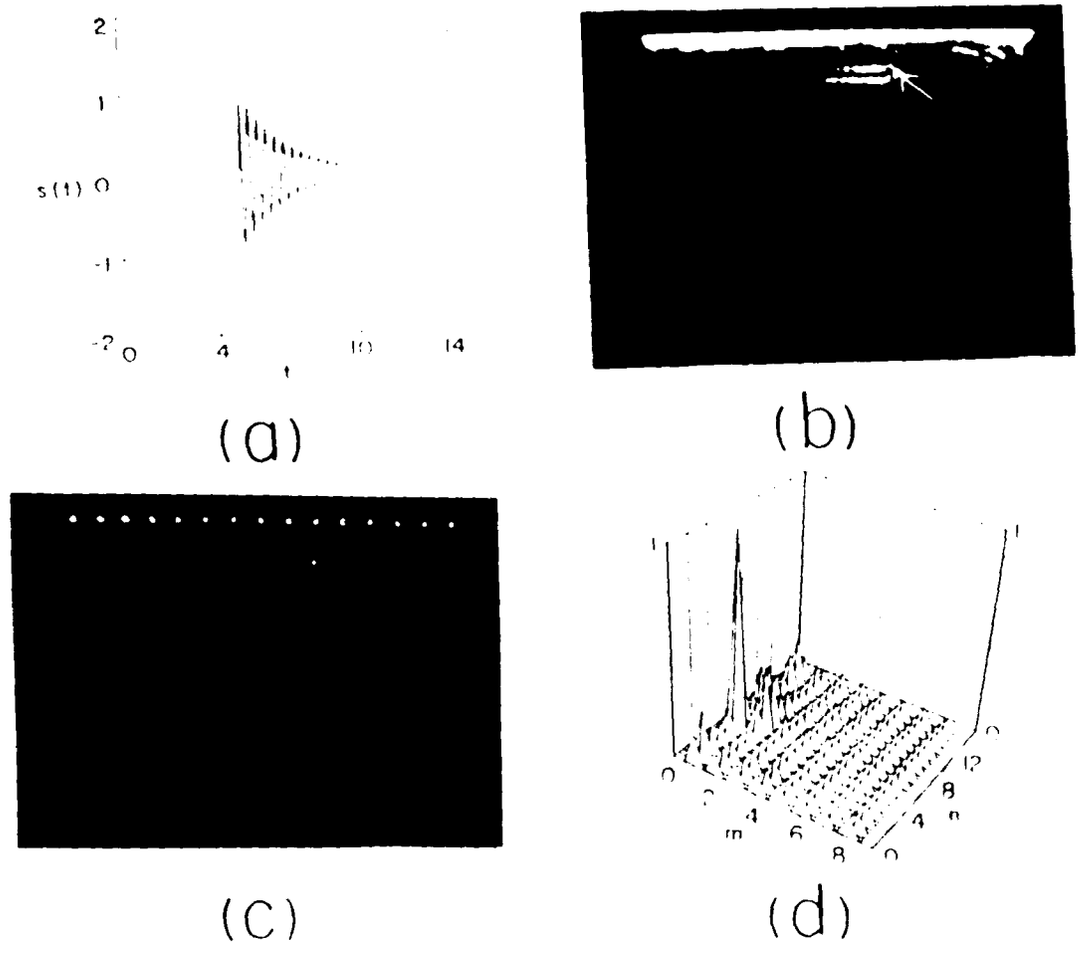

Fig.4.4.5. Experimental results for an input signal containing a single pulse. (a) Input signal waveform, (b) unsampled output optical pattern, (c) sampled result of (b) and (d) the plotted Gabor coefficients.

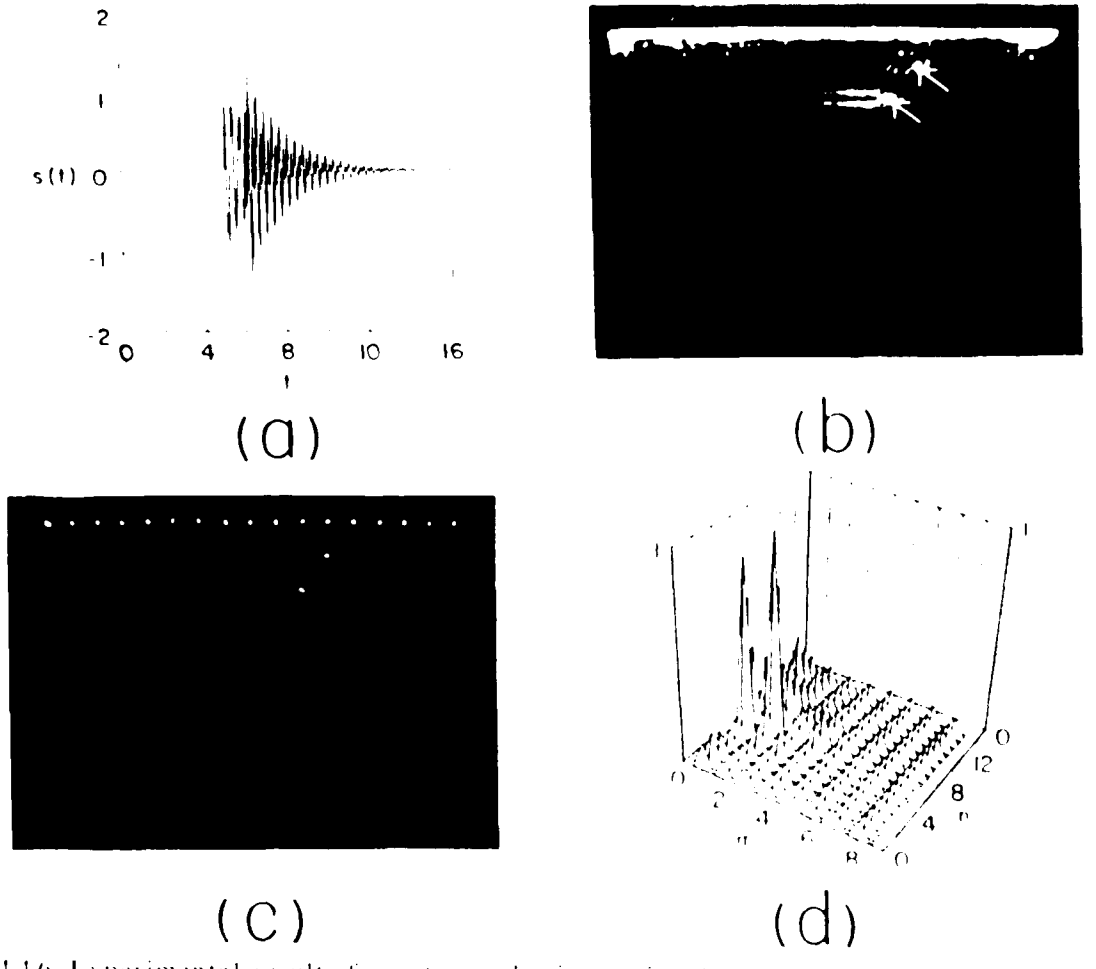

Fig 4.16. Experimental result for a two-pulse input signal. (a) Input signal waveform, (b) unsampled output optical pattern, (c) sampled result of (b), and (d) the plotted Gabor coefficients.

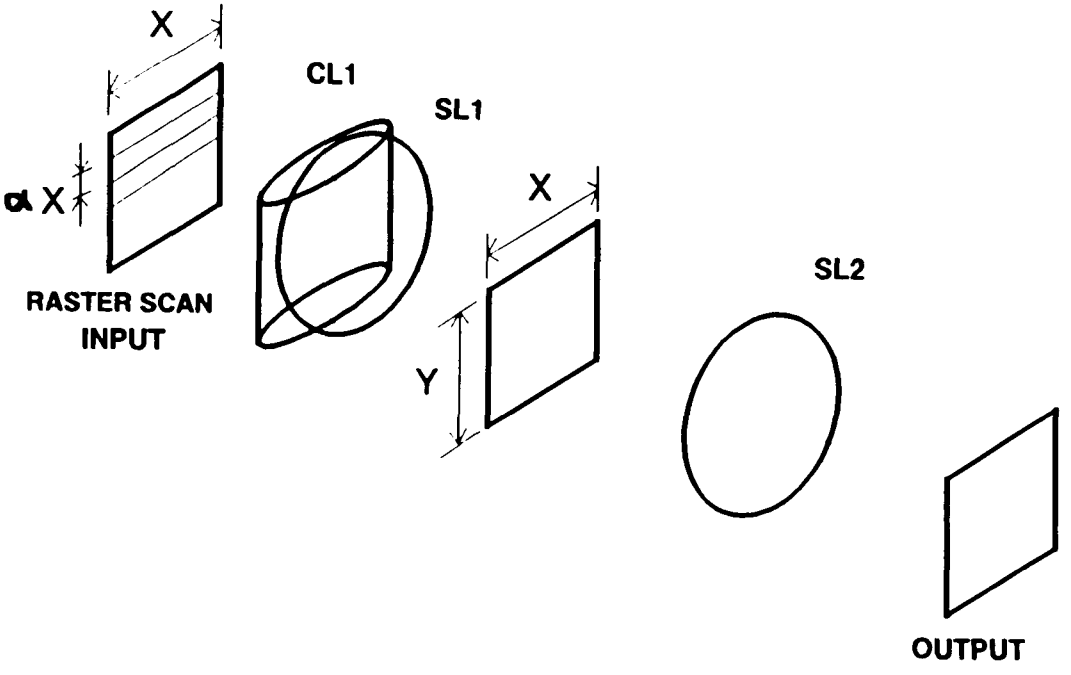

Fig.4.5.1. Bastiaans' Gabor coefficient processor.

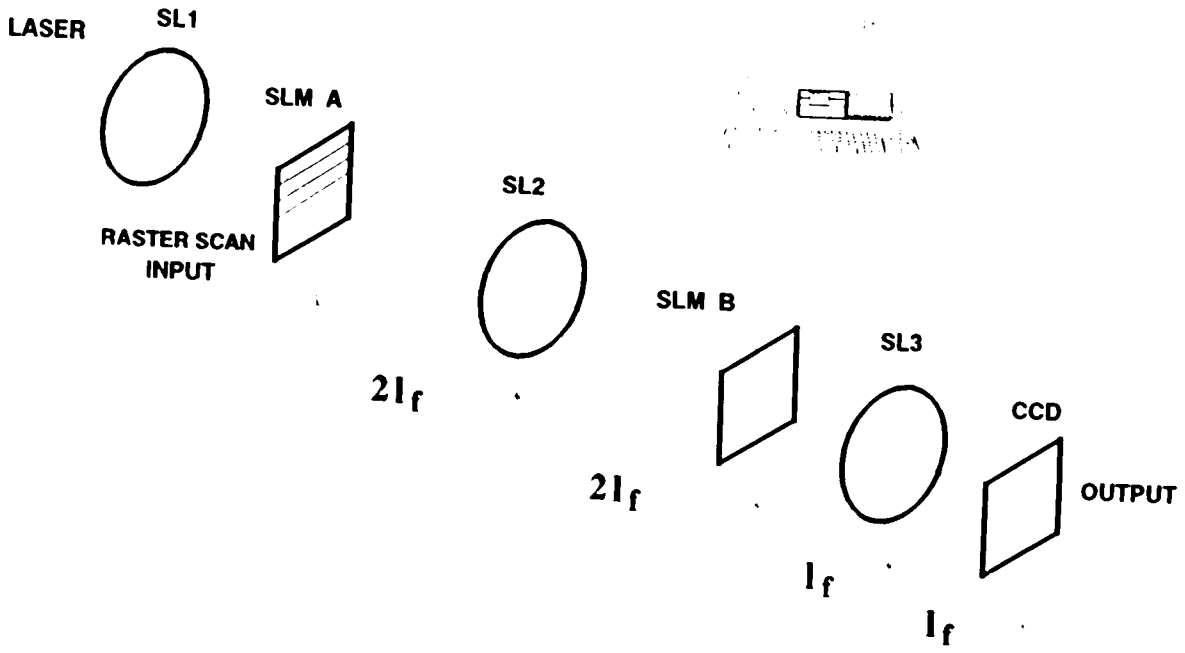

Fig.4.5.2. Gabor coefficient processor for long 1-D signals. A phase compensator is combined with SLM B.

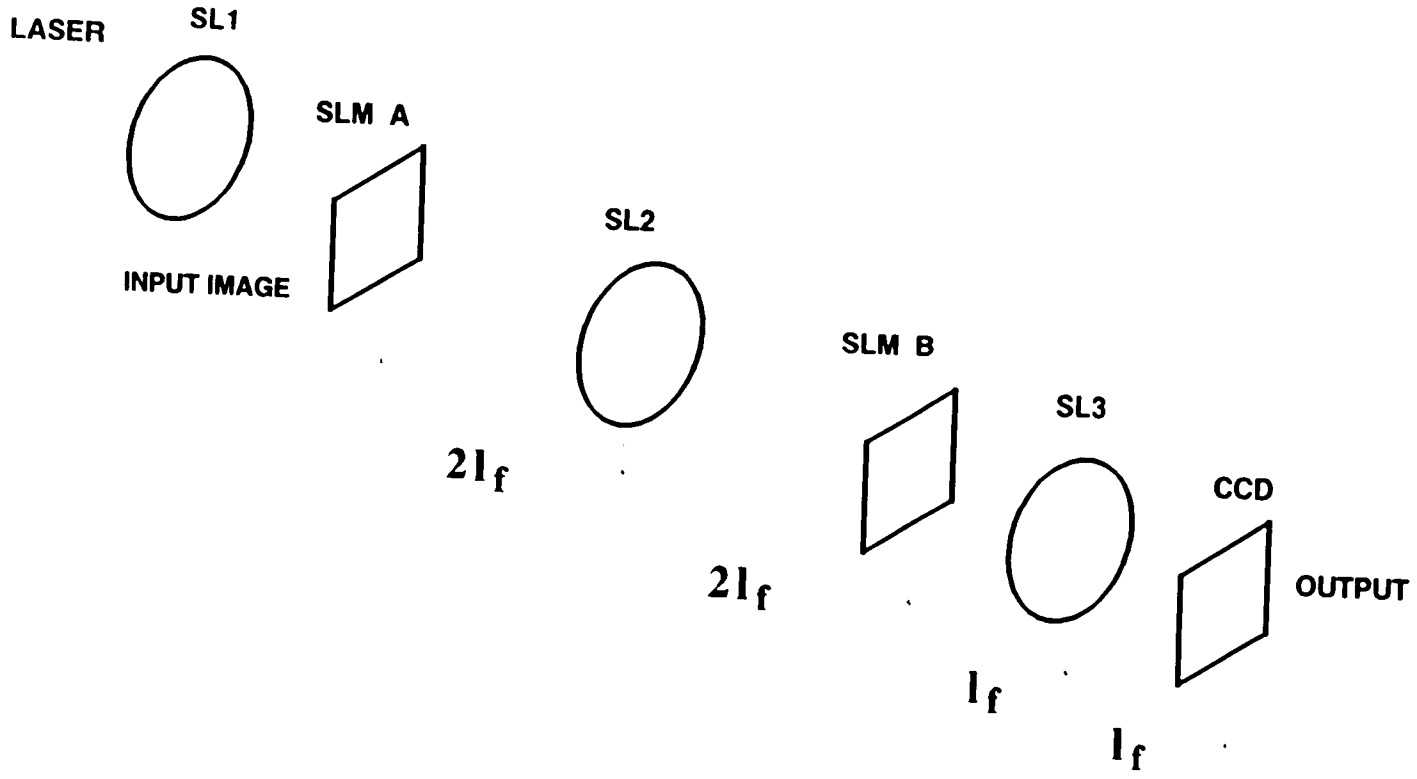

Fig.4.6.1. 2-D Gabor coefficient processor.

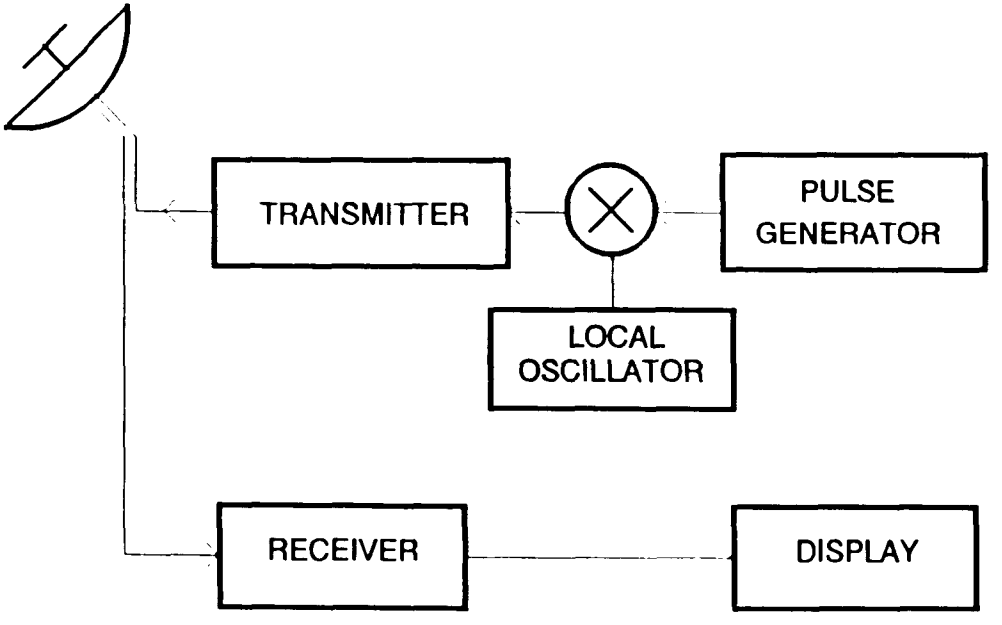

Fig 4.7.1. Principle diagram of a pulsed radar.

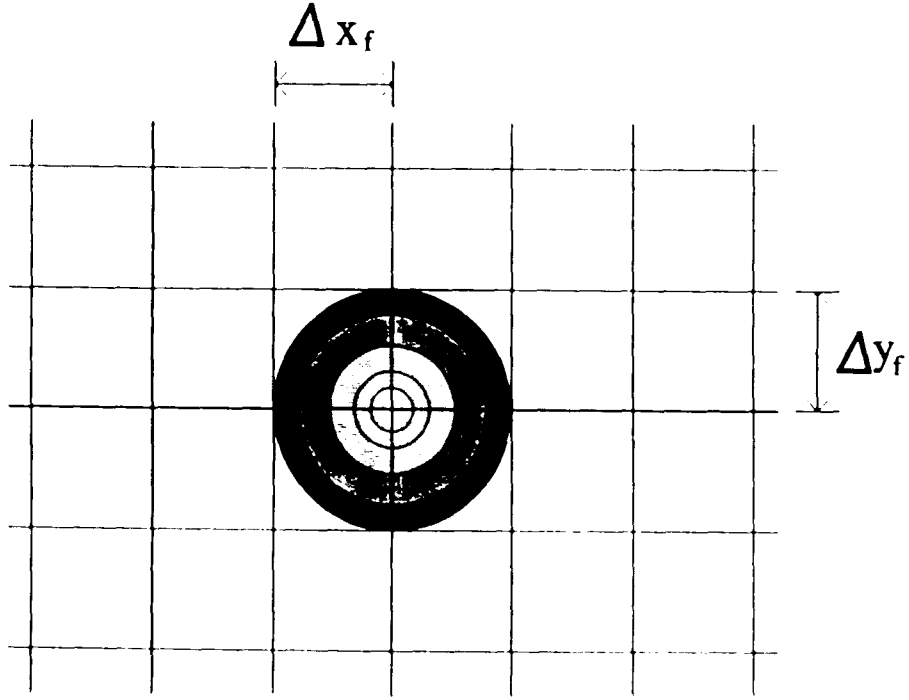

Fig.4.7.2. Gabor coefficient pulse peak, where Δx_f and Δy_f are the sampling intervals determined by Eqs.(4.4.9) and (4.4.10).

5 WAVELET TRANSFORM

The above mentioned Gabor transform has been found wide range of applications in signal detection, image representation and pattern recognition. However, from the properties of the Gabor transform, it is known that, once the Gabor window function is selected, the time and frequency resolutions are fixed, which are determined by the standard deviations of window function in time (space) and frequency domains [5.1],[5.2]. Also, the minimum resolutions are governed by the Heisenberg uncertainty inequality. Consider the analysis of the two pulses shown in Fig.5.0.1 with different time width. To represent the pulse in Fig.5.0.1(a) of a very narrow time width with high fidelity and less Gabor coefficients, the appropriate Gabor window function should be close to the envelope of the pitch signal. Therefore, if the same Gabor window is used to describe the pulse in Fig.5.0.1(b) of relatively long time width, an extremely large number of Gabor coefficients has to be employed. On the other hand, if a Gabor window is chosen to represent the pulse with large time width, it is not appropriate to establish the Gabor representation for the pulse with short time width since the representation series will either be too long to be useful or be divergent itself. Because of this, the Gabor representation may not be an optimal solution to the applications where the signals cover a wide frequency range.

Suggested by Grossmann and Morlet [5.3] in 1984, the wavelet representation offers a method to solve the problem [5.2],[5.4]-[5.9]. It was shown [5.4] that the resolution of the wavelet transform is not constant but varies with the scale parameter, which makes the wavelet transform an appropriate tool to process signals with features of

different scales. Also, while it is difficult, if not impossible, for other time(space)-frequency representations to form an orthogonal base, such a base can be obtained with an appropriately selected wavelet function easily [5.27]. Furthermore, wavelet method, with its successive layers only including the additional details which are not available at the preceding layer, represents a signal efficiently.

5.1 What is wavelet transform?

Wavelet representation is a multiresolution signal decomposition which describes signals in a hierarchical structure. As defined by Grossmann and Morlet [5.3], the signal's wavelet representation is the signal's decomposition into a family of functions which are the translation and dilation of a single unique function $\psi(x)$, which is called the basic wavelet. The wavelet transform of a function $f(x)$ is formulated as

$$Wf(a,b) = \int_{-\infty}^{+\infty} f(x)\psi_a(x-b)dx \qquad (5.1.1)$$

where a and b are a dilation and a shift parameters, $\psi_a(x)$ is a real dilated wavelet function [8] and expressed by

$$\psi_a(x) = \sqrt{a}\,\psi(ax) \quad . \qquad (5.1.2)$$

---

8 For some applications, the wavelet transform is defined for complex functions as

$$Wf(a,b) = \int_{-\infty}^{+\infty} f(x)\psi_a^*(x-b)dx$$

For the simplicity, only real functions are considered in the following analysis. Extension of the results to complex functions is not difficult.

In the dilated version of the wavelet function, a factor $\sqrt{a}$ is included right before the functions $\psi(a\,x)$ to ensure energy conservation [5.10],[5.11]. On the other hand, based on the property of the Fourier transform, the frequency domain representation of the dilated wavelet is given by

$$\Psi_a(\omega) = \frac{1}{\sqrt{a}}\Psi\left(\frac{\omega}{a}\right). \qquad (5.1.3)$$

To visualize the waveforms of the dilated wavelets corresponding to different dilation parameters, a Gaussian basic wavelet is used in Fig.5.1.1 for demonstration. In the figure, only the frequency domain representation of the wavelets are shown. Some important points of the wavelet transform are exposed by the figure. Based on the spectra of the dilated wavelets with different dilation parameters and the definition of wavelets transform (Eq.(5.1.1)), the set of wavelets may be explained as a bank of bandpass filters with different central frequency and bandwidth. Further more, it is not difficult to find out that the bandwidth of the bandpass filter generated by a dilated wavelet is determined by the product of the dilation parameter and the bandwidth of the bandpass filter given by the basic wavelet. As the dilation parameter is applied to the basic wavelet, both the central frequency and the bandwidth of the resulted dilated wavelet are increased by a factor of the dilation parameter referring to the basic wavelet. Therefore, the Quality (Q) Factors [9] of these bandpass filters are a constant value regardless of the dilation

9 In electronics [4.12], the Quality (Q) Factor of a frequency selective circuit is defined to be the ratio of the resonant frequency (central frequency for a bandpass filter) to the bandwidth, which physically means the sharpness of the circuit selectivity. This sharpness of the selectivity is, in fact, a measure of the circuit quality.

parameters. Apparently, a larger dilation parameter corresponds to a narrower and sharper pulse in time domain, and a bandpass filter of higher central frequency and wider bandwidth. Using wavelet transform to analyze the two pulses in Fig.5.0.1, an exciting result arrives. A single basic wavelet can be chosen for the two pulses. A larger dilation parameter applied to the basic wavelet generates the representation for the more narrow pulse while a smaller dilation parameter gives out the expression for the wider pulse. Therefore, the "constant Q" property indicates that wavelet transform is fair to all the frequency components of a signal covering a broad frequency range.

To reconstruct a signal from its wavelet transform $Wf(a,b)$, an inverse wavelet transform was also derived [5.2],[5.3] and is mathematically formulated as

$$f(x) = \frac{1}{C_\psi}\int_{-\infty}^{+\infty}\int_{0}^{+\infty} Wf(a,b)\psi_a(x-b)\,da\,db \qquad (5.1.4)$$

where the constant

$$C_\psi = \int_0^{+\infty}\frac{|\Psi(\omega)|^2}{\omega}d\omega \qquad (5.1.5)$$

A restriction to the selection of the basic wavelet function has thus to be observed for the validity of the inverse wavelet transform, which states that the Fourier transform $\Psi(\omega)$ of the basic wavelet $\psi(x)$ must satisfy

$$C_\psi < +\infty$$

since an infinity C_ψ will never deliver a reconstructed function. This restriction implies that $\Psi(0) = 0$ and that $\Psi(\omega)$ is small enough in the neighborhood of $\omega = 0$.

Although the above direct and inverse wavelet transform are formulated somewhat different from those given by Grossmann and Morlet [5.3] , they are linked by the following one-to-one mapping $a = e^u$ and $b = \frac{t}{e^u}$ between the space $\{a > 0, -\infty < b < +\infty\}$ and the space $\{-\infty < u < +\infty, -\infty < t < +\infty\}$, where u and t are the dilation and shift parameters in their original paper.

The above continuous forms of forward and inverse wavelet transforms uniquely describe all the functions belonging to $L^2(R)$. However, they are redundant because of the used continuous variables. To decrease the redundancy of the signal representation, variable "a" is discretized. Together with the selection of $a = 2^j$ ($j = -\infty, \ldots, -1, 0, 1, \ldots, +\infty$), the discretization happened to generate an orthonormal basis [5.2],[5.4],[5.13], which allows a signal to be uniquely expressed as a linear combination of the orthogonal wavelets. Mathematically, Eq.(5.1.4) now becomes

$$f(x) = \sum_{j=-\infty}^{+\infty} \int_{-\infty}^{+\infty} W f(2^j, b)\psi_{2^j}(x-b)\,db. \qquad (5.1.6)$$

This equation is interpreted as a decomposition of function $f(x)$ into a set of discrete frequency channels centered at $2^j\omega_0$, where ω_0 is the central frequency of the bandpass filter generated by the basic wavelet. The signal component in each channel may further be sampled at a rate proportional to 2^j. And the final version of the discrete wavelet representation of signal $f(x)$ is thus given by

$$f(x) = \sum_{j=-\infty}^{+\infty} \sum_{n=-\infty}^{+\infty} W f(2^j, n2^{-j})\psi_{2^j}(x - n2^{-j}). \qquad (5.1.7)$$

It is this equation the base of the so called multiresolution analysis suggested by Mallat. However, for the ease of optical implementation, the translation variable b will be kept continuous as in Eq.(5.1.6) in the following analysis.

A trouble caused by the above described discrete wavelet representation for practical applications is that infinity terms are required to describe the signal faithfully. Fortunately, a lowpass filtering effect exists in natural world. And also for many applications, the signal's information to certain resolution level is enough because of the resolution of optical components. Therefore, a lowpass filter may be selected to pre-filter the signal without loss of useful information. If this effect corresponds to the filtering of signal $f(x)$ by the low-pass filter with an impulse response $\phi(x)$, which is sometimes called scaling function, it can be shown by induction that this signal can now be expanded [5.5] as [10]

$$f(x) = \int_{-\infty}^{+\infty} A f_{2^{-(N-1)}}(b)\phi_{2^{-(N-1)}}(x-b)db$$

$$+ \sum_{l=-N}^{0} \int_{-\infty}^{+\infty} h_l f(2^l, b)\psi_{2^l}(x-b)db \qquad (5.1.8)$$

10 Here, the non-discretized form of variable b is preserved for the later optical implementation.

To explain the above expansion, it is found that, in the first term,

$$Af_{2^{-(N-1)}}(b) = \int_{-\infty}^{+\infty} f(x)\phi_{2^{-(N-1)}}(x-b)dx \qquad (5.1.9)$$

is the coarse information of signal $f(x)$ where the employed lowpass filter is determined by

$$\phi_{2^{-(N-1)}}(x) = \sqrt{2^{-(N-1)}}\,\phi(2^{-(N-1)}x) \quad . \qquad (5.1.10)$$

Those terms of $Wf(2^j,b)$ where $j = -N,\ldots,0$, are the wavelet transforms of the signal defined by Eq.(5.1.1), where variable a is discretized. They contain all the details of the signal.

To determine the basic wavelet function based on the impulse response of the lowpass pre-filter, it was proved by Mallat [5.5] that the selected wavelet $\psi(x)$ and the impulse response $\phi(x)$ of the original lowpass filter are linked together in frequency domain by

$$\Psi(\omega) = e^{-j(\omega/2)}H\left(\frac{\omega}{2}+\pi\right)\Phi\left(\frac{\omega}{2}\right) \qquad (5.1.11)$$

where

$$H(\omega) = \sum_{n=-\infty}^{+\infty}\left\{\int_{-\infty}^{+\infty}\phi_2^{-1}(b)\phi(b-n)db\right\}e^{-jn\omega} \qquad (5.1.12)$$

which is called the quadrature filter.

One remark is made before the next section that the integral limits in Eq.(5.1.8)

can only range from -w/2 to +w/2 because of the limitation optical window size. Therefore, exact forward and backward wavelet transforms should not be expected. Even if it is like this, the optical generated results are still accurate enough for most applications.

5.2 A Wavelet Example

Recommended by Mallat [5.5], a wavelet function which has a good localization in both time (space) and Fourier domains is described in frequency domain by

$$\Psi(\omega) = \frac{e^{-j(\omega/2)}}{\omega^N} \sqrt{\frac{\Sigma_{2N}\left(\frac{\omega}{2}+\pi\right)}{\Sigma_{2N}(\omega)\Sigma_{2N}\left(\frac{\omega}{2}\right)}} \qquad (5.2.1)$$

where

$$\Sigma_N(\omega) = \sum_{k=-\infty}^{+\infty} \frac{1}{(\omega+2k\pi)^N} \qquad (5.2.2)$$

This wavelet is called analytic wavelet or Mallat's wavelet. Its corresponding scaling function is given by

$$\Phi(\omega) = \frac{1}{\omega^N \sqrt{\Sigma_{2N}(\omega)}} \qquad (5.2.3)$$

in frequency domain. Their waveforms and spectra are plotted in Fig.5.2.1.

This wavelet function was selected as the basic wavelet to test the optical wavelet processor described in section 5.4.

5.3 Comparison with Gabor Transform

To qualitatively compare the Gabor and wavelet transforms, the waveforms of the corresponding Gabor window and wavelet functions are considered first. They are first compared in time domain (see Fig.5.3.1). Apparently, all the Gabor kernels are equal height and have exactly same envelope, which is the original Gabor window function, except that they are modulated by carriers with different frequencies. Unlike this, all the dilated wavelet functions have same shape but shrinked or expanded on time axis by the dilation parameters. Their heights are proportional to the dilation parameters. In the frequency domain (see Fig.5.3.2), the filters generated by the Gabor kernels are equal bandwidth. The central frequencies of the filters are equal spaced. This indicates that the set of filters generated by Gabor kernels is not a "constant Q" system, which further means that a Gabor representation can never be expected to have a good performance to describe an object covering a wide frequency range. However, as described in section 5.1, the set of filters delivered by the dilated wavelets forms a "constant Q" system. Therefore, good performance may be found uniformly across a broad band of frequency. In the wavelet set, the bandwidth and central frequency of the resulted bank of bandpass filters are proportional to the dilation parameters. Overlaps between channels also usually exist, which is considered as a reason to guarantee the recovery of signal from its wavelet transform [11].

---

11 For the Haar wavelet shown in Fig.5.3.3, there is no overlaps between each channel. The Haar wavelet is easy to be optically implemented. However, its locality in time and frequency domain is not good.

Regarding the sampling lattice for Gabor and discrete wavelet transforms (see Fig.5.3.4), it is noticed that the lattice is uniformly spaced in Gabor transform because of fixed time and frequency resolutions. Differently, the sampling lattice of a discrete wavelet (consulting Eq.(5.1.5)) is only uniformly spaced in the logarithm scale. More samples are picked up in time domain for high frequency components and in frequency domain for low frequency components. This is close to our daily applications. For those high frequency components, what we actually interested in are their variations in time domain. A selected large dilation parameter will generate a shrinked wavelet in time domain to meet the requirement. To truthfully represent all the information of signal, a smaller sampling space is necessary in time domain. For the low frequency components, the variation in frequency domain is more important than that in time domain. And therefore a smaller dilation parameter is chosen to generate a narrow bandwidth filter to analyze the signal in frequency domain.

5.4 Optical Wavelet Processor for Short 1-D Signals

Similar to the case of Gabor coefficient processor, the processing of short 1-D signals is first considered, which can be fit in the window time of 1-D input device, say a Bragg cell device.

From the definition of wavelet transform, it is obvious that the wavelet transform can be realized by filtering the signal $f(x)$ by a filter with an impulse response $\psi_a(-x)$. After the discretizing of the dilation parameter, the wavelet transform

can actually be explained as the filtering operation performed on the signal by a bank of bandpass filters. In this sense, the wavelet theory is, in fact, a tool to guide people to design appropriate filters for signal processing. The inverse wavelet transform can also be physically implemented by a convolution of the dilated wavelets with the signal's wavelet transform on variable "b" followed by an integration on variable "a".

Various algorithms have be developed for their realization in electronic computer [5.5],[5.10]. An optical system, which performs both forward and inverse wavelet transform on short 1-D signals which lengths are limited by the aperture time of the input device, was recently proposed [5.14],[5.15] and experimentally tested. They are described as follows.

5.4.1 System Architecture

Based on Eq.(5.1.8), an opto-electronic system architecture to perform both the wavelet transform and inverse wavelet transform is principally depicted in Fig.5.4.1.

For the part performing wavelet transform on 1D signal (shown in Fig.5.4.1), the laser beam from a pulsed laser is first spatially filtered and expanded. After that, it is one-dimensionally focused by a cylindrical lens CL1 to form a horizontal narrow bar onto the window of an acousto-optic modulator. The input signal, which is going to be wavelet transformed, is first modulated by

a RF driver of the A-O modulator and then sent into the above A-O modulator. Therefore, the output beam of the A-O modulator carries one frame of input signal with the frame width of the aperture time of the used A-O modulator. Spherical lens SL2 behind the A-O cell causes the modulated light beam to be expanded along the vertical direction and Fourier transformed along the horizontal direction. An optical pattern, which is uniform in vertical direction and carries the Fourier transform of the input signal in horizontal direction, is thus obtained at the back focal plane of the lens SL2. An intensity modulated mask [12], which is schematically shown in Fig.5.4.2 and technically realized either by a fixed transparency or by a spatial light modulator (SLM) to represent a bank of lowpass and bandpass filters corresponding to the Fourier transforms of functions $\phi_{2^{-}}(-\nu)$ and $\psi_{2^{-}}(-\nu)$ is located at the above plane. The filtered pattern is then imaged in vertical direction and Fourier transformed in horizontal direction onto the back focal plane of the cylindrical lens CL3 by the cylindrical lens combination CL2-CL3-CL4, where the focal lengths of CL2 and CL4 are half of the focal length of CL4. The signal's wavelet transform together with signal's coarse information is thus obtained at the back focal plane of CL3.

In order to further process the obtained wavelet transform, a beam splitter BS is inserted. In one branch, the output pattern is detected by a 2D CCD detector for electronic processing and/or displaying purposes. In another branch,

12 The Mallat's wavelet is used in the experiment. The linear phase term in Eq.(4.3.1) is omitted. The effect of this is the space shift of the output pattern in each channel.

the optical pattern at the back focal plane of CL3 is used as the input pattern of the consecutive optical processing system, such as an optical matched filter, an optical correlator, etc.

To perform the inverse wavelet transform described by Eq.(5.1.8), the system architecture shown in Fig.5.4.3 is used. Its input plane matches with the output plane of the proceeding optical processing system, which performs certain processing operations on the output of the above explained system of Fig.5.4.1. Cylindrical lens combination CL5-CL6-CL7, which is same as cylindrical lens combination CL2-CL3-CL4, is used to image the input pattern in vertical direction and Fourier transform it in horizontal direction onto the back focal plane of CL6 where the same intensity modulated mask as above is located. At the other side of this mask, spherical lens SL3 performs Fourier transform in horizontal direction and focuses the pattern in vertical direction. The operations in Eq.(5.4.8), i.e. a convolution along the "b" and an integration along the "a" directions, are thus realized. The summations and integrals are realized by the time integrating effect of a 1D CCD detector. Apparently, to guarantee a successful recovery operation, the working environment of the system should be mechanically stable.

To assure that the system works properly, a matching of the modulations of the pulsed laser and of the used A-O modulator must be established. For an A-O modulator with an aperture time of τ_a, the pulsed laser firing interval

should be the same τ_u. And in order to freeze the traveling of the acoustic wave in the A-O modulator during a laser strobe, the duration of the laser pulse must also be substantially short. The synchronization diagram is give in Fig.5.4.3

5.4.2 Preliminary Experimental Results

To test the above proposed wavelet processor for 1-D signal, two different 1-D signals, i.e. a step function and a linearly chirpped step function, were used. Slight modifications were made to the proposed system similar to the optical Gabor coefficient processor. The pulsed laser was replaced by a HeNe laser and the signal is coupled into the processor by a pre-made transmittance mask rather than an acousto-optic device.

The basic wavelet chosen in the following experiment is the Mallat's wavelet given by Eqs.(5.2.1) and (5.2.2). The number of N was chosen to be 4 in the experiment, so that the function $\Sigma_N(\omega)$ in Eq.(5.2.2) is now [5.5]

$$\Sigma_4(\omega)=\frac{5+30\cos^2\frac{\omega}{2}+30\sin^2\frac{\omega}{2}\cos^2\frac{\omega}{2}+2\sin^4\frac{\omega}{2}\cos^2\frac{\omega}{2}+70\cos^4\frac{\omega}{2}+\sin^4\frac{\omega}{2}}{105\sin^8\frac{\omega}{2}} \tag{5.4.1}$$

A bank of six filter representing $\Phi_{2^j}(\omega)$ and $\Psi_{2^j}(\omega)$ (j=-4,...,-1,0) together with a full pass filter was generated by computer and photographed to make the mask. However, by this method, only the intensity of Eq.(5.2.1) was preserved on the film. Without the phase term, the resulted patterns at the wavelet transform plane are shifted to different positions referring to resolution levels,

but the corresponding intensity distributions of the results are maintained. When the inverse transform is performed, the phase term in Eq.(5.2.1) is cancelled. The result thus obtained will be identical to that of using the phase term.

A transmittance mask for the step function was first made and inserted into the experimental setup at the input plane. The wavelet transform of this input signal was detected by the SONY CCD camera with its detector array located at the output plane with is the back focal plane of CL6. It is shown in Fig.5.4.5. In the output pattern, the first row is the original step function signal pattern for the purpose of comparison. The second row is the low-pass filtering result corresponding to Eq.(5.1.9), which is the blurred signal containing the coarse information. All the other rows are the wavelet transforms at different resolution levels, which contain the detail information of the signal. The forward wavelet transform results for the chirped setup function are given in Fig.5.4.6.

The inverse wavelet transform was also tried on the chirped step function. Based the inverse wavelet transform of Eq.(5.1.8), the reconstructed signal of the linearly chirpped periodic gate function is also shown in Fig.5.4.7. Because of the quality of the optical setup, some distortions appear on the resulted waveform. However, it does show the capability of synthesizing the signal's wavelet representation optically.

5.5 Optical Wavelet Processor for Long 1-D Signals

For the applications where the input signal is too long to fit in the aperture time of the input device, new schemes need to be developed to adopt the long input signals. As it is already known that the wavelet transform on a signal is, in fact, the correlation of the signal with the dilated wavelet. Therefore, it is possible to use the schemes for performing convolution / correlation of long data stream described in Chapter 3.

Specifically, consider the system schematically shown in Fig.5.5.1. In this system, a basic wavelet and the dilated wavelets are first generated. To perform the wavelet transform, the long input signal and a dilated wavelet are shuffled by one of the data permutation schemes described in Section 3.5. A followed optical 2-D correlator then delivers the wavelet transform of the input signal for current dilation parameter in its 2-D shuffled format. Shuffling the 2-D pattern back to 1-D by the similar permutation method as for input shuffling gives the wavelet transform of current dilation parameter in natural sequence. To proceed to next dilation parameter, it is only necessary to download the dilated wavelet of the dilation parameter to the optical processor. A series of wavelet transform of different dilation parameters is finally resulted. This operation delivers the wavelet transform sequentially rather than a single shot. In some applications, only limited numbers of dilation parameters are desired. Therefore, only those dilated wavelets corresponding to the required dilation parameters are prepared and used to calculate the wavelet transform of the input signals. Processing time becomes shorter.

The other scheme discussed in Section 3.4 could also be used. There, the input long signal and the dilated wavelet are shuffled to a group of matrices and vectors, respectively. The followed optical vector-matrix multiplier then delivers the required wavelet transform for different dilation parameters when the reference is updated each time by a dilated wavelet of new dilation parameter.

5.6 Optical Wavelet Processor for 2-D Signals

To extend the above discussed 1-D wavelet transform to 2-D, there are two possibilities. First, the dilations and translations are used independently to the two dimensions. This causes the transform domain a Four-Dimensional (4-D) space. In the second case, the translation is used for the two dimensions while a single dilation is shared. A 3-D transform domain is thus resulted, which may be considered as a degenerated wavelet representation. In the following discussions, only the second case is considered.

5.6.1 Proposed System Architecture

To optically implement the degenerated wavelet transform of a 2-D image, the system shown in Fig.5.6.1 is suggested. In the system, the input image is fed into optical path through SLM A, the light beam which carries the image is then separated into certain number [13] of branches. In each branch, the image

13 This number depends on the number of dilated wavelets selected to describe the image.

is subject to a corresponding frequency filtering that is determined by the corresponding dilation parameter. A parallel reading of the output patterns in each channel delivers the degenerated wavelet transform of image. The system shares the same architecture of DOG or Lapacian pyramid but with an entirely different filter design. However, because of the limitation of the space-bandwidth product [5.26] of optical processing system, the number of dilation parameters is limited and also the spatial resolutions in two dimensions. To get more dilation parameters and higher spatial resolutions, a simplified but not real-time system could be used (see Fig.5.6.2). This system in the sense of architecture is nothing more than a conventional optical matched filter. An SLM which carries the spectra of the dilated wavelets (degenerated) is located at the Fourier plane of the image to be processed. A wavelet transform of current dilation parameter is then detected by a 2-D CCD at the back focal plane of lens L2.

5.6.2 Computer Simulation Results

A 256x256 image of an oscilloscope is selected to perform the simulation of degenerate 2-D wavelet transform. With one lowpass filter selected as the scale function, five bandpass filters were thus generated as the spectra of dilated wavelets in the simulation. These filters are all symmetric to the origin and chosen to be ideal lowpass or bandpass filters. As discussed before, although

the selected wavelet does not have good localization because of its slow decay in time domain, it is simple to be optically implemented. Their specifications are given in Table 5.1.

The forward wavelet transform were simulated on the image (Fig.5.6.3(a)) through each of the frequency band. The resulted wavelet transforms of different dilation parameters are presented in Fig.5.6.3. To recover the image, the coherent process in the optical system was also simulated. The recovered image is very close to its original (see Fig.5.6.4). The error of the recovered image, to our knowledge, is due to the computation accuracy of the calculation process.

5.7 Technical Problems

Serious error source in implementing an optical signal processing system is the component misalignment. To predict its effect on optical wavelet transform, computer simulations are carried out on 2-D wavelet transform.

In the first experiment, the lowpass filter was shifted away from its correct position for different values varying from 1 to 5. The results in Fig.5.7.1 indicates that the recovery results are sensitive to the misalignment. However, they are tolerable up to 3 pixel misalignment. When the shift values was changed from 3 to 4, a dramatic deterioration of the reconstructed image occurred, which was caused by the lost of DC component at the moment. This result indicates that the

minimum bandwidth of lowpass filter is also limited by the resolution of the positioners. For example, when a positioner with resolution of 20 microns is employed to adjust the position of the filter, the minimum bandwidth of the lowpass filter can not be less than 40 microns.

In the second experiment, each of the bandpass filters is shifted by 4 pixels. As shown in Fig.5.7.2, the shift of the bandpass filter of low central frequencies does cause poor image quality, however it is still much better than the case in Fig.5.7.1(d). As the frequency band goes higher and higher, the quality of the recovered image becomes less sensitive to the misalignment. For the bandpass filter corresponding to the highest center frequency, four pixel misalignment seems have no effect on the recovered image. And this shows that, more careful adjustment should be made to those filters corresponding to low frequencies.

5.8 Applications

In the following sub-sections, applications of optical wavelet transform to system failure prediction, signal processing in dense target environment, image coding and nonlinear system analysis are briefly described.

5.8.1 System Failure Prediction

Failure prediction is an important topic for high performance maintenance of complex mechanical systems. Appropriately mounted sensors may provide

signals which contain informations of abnormal system behaviors which act as precursors to failure. Methods of signal processing are thus necessary to extract the information from the available signals and to trigger the alarm when a failure precursors is detected. The speed of such processing is crucial for various applications.

Because of the above mentioned properties, a wavelet transform can be used in the signal processing part of a failure predictor. A system diagram of failure predictor using wavelet processor as its kernel unit is proposed and shown schematically in Fig.5.8.1. Sensors mounted on appropriate parts of a complex mechanical system generate signals related to the system operation conditions. Any substantial variation of these signals from their normal patterns may indicate precursors to failure. Processing of these signals is performed by the wavelet processor, which can deliver the wavelet transform corresponding to a carefully selected basic wavelet in real-time. Obviously, any pattern change of the detected signals will cause pattern to change in their wavelet transforms. Observation of these changes and a comparison of the obtained wavelet pattern with patterns under normal operation conditions may indicate abnormal changes of system operation conditions. Furthermore, to predict the type of failure to occur, the pattern correlator correlates the obtained wavelet patterns with the pre-fabricated wavelet patterns corresponding to certain system failures .

Now, the principles of two kernel units of the proposed failure detector, a wavelet processor and a pattern correlator, are described in detail.

i) Wavelet Processor

The function of this unit is to perform the above defined wavelet transform in real-time for their further usage. To construct this processor, the selection of basic wavelet function is very important. A best selected wavelet may maximize the failure detectability and minimize false alarm. Two factors must be considered in the selection of a basic wavelet. One is the time and frequency resolution. Although wavelet transform, in general, has better time and frequency resolution than other conventional time-frequency representations, a well selected basic wavelet may further improve its time and frequency resolution. Mallat's wavelet described in section 5.3 is a good candidate. Other functions with good localization in both time and frequency domains can also be used. Another factor is based on the fact that the wavelet transform can also be interpreted as the correlation of a signal with a group of dilated wavelets. The basic wavelet selected in terms of the characteristics of the detected signal corresponding to abnormal system behavior, which might be a precursor of system failure, will supply benefits to both manual failure determination and the subsequent pattern correlation. It is thus necessary to perform a thorough study of signal waveforms and the corresponding wavelet patterns when some system failures are to occur.

ii) Pattern Correlator

This unit, in fact, performs a correlation operation between the above

obtained wavelet pattern and the pattern corresponding to certain system failures. Many available schemes to realize such a correlation electronically or optically are available. Based on the same principles as for the use of an optical wavelet processor, it is suggested to use an optical correlator. Since the introduction of the optical correlator by VanderLugt, matched spatial filters have become more and more popular in optical pattern recognition. Although it gives the highest possible signal to noise ratio when detecting a known signal or image corrupted by additive white noise, the correlation peak of this traditional form of optical correlator is not sharp enough for a better observation. Several methods have been suggested to solve the problem. Among them are a phase-only matched filter, a binary phase-only matched filter, a two-bit correlator and a joint transform correlator [4.16]-[4.22]. Since a phase only matched filter might achieve a much higher optical efficiency than a classical matched filter, it is proposed to the build the pattern correlator based on a phase only matched filter.

To practically design the phase only filter used in the proposed failure predictor, the wavelet patterns corresponding to certain system failures need to be investigated. And the filters should be calculated based on them. After a real time wavelet pattern from the proceeding wavelet processor enters the phase only correlator, any appearance of correlation peak at the output may indicate the appearance of a possible system failure.

Not only has the advantages of high optical efficiency and very sharp correlation peak, the phase only filter is also proved to be robust [4.18] which is very important in the usage of the filter under practical noisy condition. To construct this unit of the proposed failure predictor, other pattern recognition methods can also be used.

5.8.2 Dense Target Signal Processing

Signal processing in a dense target environment has been found useful in applications such as medical diagnosis and weather forecast. It was proved that the echo from the assemblage of targets is described by

$$e(t) = \int_{0}^{\infty} \int_{-\infty}^{\infty} D(x, y)\sqrt{y}\, s(y(t - x))\, dx\, dy \quad (4.7.1)$$

where $D(x, y)$ is the target density, $s(t)$ is the radar signal, x and y are the distance and velocity, respectively. A closer look at this equation reveals that $D(x, y)$ is in fact related to the wavelet transform of the echo function $e(t)$. An optical setup to obtain the above target information is therefore, in principle, no more than an optical wavelet processor for 1-D signal described in section 4.5. Instead of a discrete bank of filters, on the filtering mask, the pattern is continuous in both dilation and translation directions. Specifically, the transmittance is determined by the 2-D function of

$$t(x_m, y_m) \propto \frac{1}{\sqrt{y_m}} S\left(\frac{x_m}{y_m}\right) \quad (4.7.2)$$

where $S(\cdot)$ is the Fourier transform of signal $s(\cdot)$

In the system, the echo signal from the radar receiver is first fed into a 1-D input device such as a Bragg cell and then optically wavelet transformed through the optical wavelet processor. The resulted wavelet pattern at the output plane is then detected by a 2-D CCD array and delivers to either an electronic post processing system or a monitor for manual determination. Similar to the failure prediction system, the selection of the wavelet should based on both the requirement of radar system and high resolutions in both time and frequency domain.

5.8.3 Image Coding

To efficiently encode an image various techniques such as predictive coding and transform coding were developed to decorrelate the image pixels [4.23],[4.24]. A method based on pyramidal multiresolution decomposition of image was suggested by Burt and Adelson [4.25]. However, as analyzed by Mallat, in a Laplacian pyramid, the detail signals of resolution levels are partially correlated with each other. To extract and represent only the difference of signal in different resolution levels, wavelet transform is proposed as a new tool to encode an image.

Generally speaking, both pyramid encoding and wavelet encoding are subject to a same processing system except the methods of choosing the corresponding

bandpass filters. However, because of the orthogonality of wavelet set, there is no redundant information encoded by wavelet scheme. Higher compression ratio is thus promised. Now, the sampling and quantization process in wavelet encoding method is considered. Since the bandwidth of the bandpass filters becomes smaller and smaller as they approach low frequencies, it is said that the sampling rate is proportional to the dilation parameter. At the same time, it is known that human eyes are sensitive to the intensity variation in low frequency band while insensitive in high frequency range. Therefore, variable quantization levels are assigned to different resolution levels, which are inversely proportional to the dilation parameters. A constant sampling rate and quantization level product is thus resulted.

5.8.4 Other Applications

Other applications of wavelet transform can be found widely in fields like speech signal processing, seismic signal analysis, speech synthesizing, turbulence analysis and nonlinear system analysis.

5.9 Summary

In summary, this chapter described the study of the wavelet transform. Optical implementation of the wavelet transform for short 1-D signal was described in detail. Using the designed system, real-time (at least video rate) processing of wavelet transform is expected. Test results for step function and chirped signal

were shown. The recovered signal demonstrate the recovery capability of the proposed system. Long 1-D wavelet transform and 2-D wavelet transform were also discussed in the chapter. Computer simulation results were presented. Problem of component misalignment was considered and simulated. The conclusion is that the recovery quality highly depends on the alignment accuracy in lower frequency band while it is insensitive to the higher frequency band. Applications to system failure prediction, signal processing in dense target environment, image coding and nonlinear system analysis were also briefly discussed.

5.10 References

[5.1] H. Wechsler, *Computational Vision*, Academic Press, San Diego, 1990.

[5.2] I. Daubechies, "The Wavelet Transform, Time-Frequency Localization and Signal Analysis," *IEEE Trans. Info. Theo.*, vol.36, no.5, pp.961-1005, September 1990.

[5.3] A. Grossman and J. Morlet, "Decomposition of Hardy Functions into Square Integrable Wavelets of Constant Shape," *SIAM J. MATH.*, vol.15, no.4, pp.723-736, July 1984.

[5.4] S. G. Mallat, "Multifrequency Channel Decompositions of Images and Wavelet Models," *IEEE Trans. Acoust. Speech and Sig. Proc.*, vol.37, no.12, pp.2091-2110, December 1989.

[5.5] S. G. Mallat, "A Theory for Multiresolution Signal Decomposition: The Wavelet Representation," *IEEE Trans. Pattern Anal. Mach. Intell.*, vol.11, no.7, pp.674-693, 1989.

[5.6] P. G. Lemarie (Ed.), *Les Ondelettes en 1989*, Lect. Notes in Math., vol.1438, Springer-Verlag, 1990.

[5.7] S. Mallat and W. L. Hwang, "Singularity Detection and Processing with Wavelets," *IEEE Trans. on Info. Theo.*, vol.38, no.2, pp.617-643, March 1992.

[5.8] R. Wilson, A. D. Calway and E. R. S. Pearson, "A Generalized Wavelet Transform for Fourier Analysis: The Multiresolution Fourier Transform and its Application to Image and Audio Signal Analysis," *IEEE Trans. on Info. Theo.*, vol.38, no.2, pp.674-690, March 1992.

[5.9] G. W. Wornell and A. V. Oppenheim, "Estimation of Fractal Signals from Noisy Measurements Using Wavelets," *IEEE Trans. on Sig. Proc.*, vol.40, no.3, March 1992.

[5.10] O. Rioul and P. Duhamel, "Fast Algorithms for Discrete and Continuous Wavelet Transforms," *IEEE Trans. Info. Theo.*, vol.38, no.2, pp.569-586, March 1992.

[5.11] R. Kronland-Martinet, J. Morlet and A. Grossman, "Analysis of Sound Patterns through Wavelet Transform," Int. J. Pattern Recogn. Artificial Intell., vol.1, no.2, pp.273-302, 1987.

[5.12] J. W. Nilsson, *Electric Circuits*, 3rd Ed., Addison-Wesley, Mass., 1990.

[5.13] K. Grochenig and W. R. Madych, "Multiresolution Analysis, Haar Bases, and Self-Similar Tilings of R^n," *IEEE Trans. Info. Theo.*, vol.38, no.2, pp.556-568, March 1992.

[5.14] Y. Zhang, Y. Li, E. G. Kenterakis, A. Katz, X. J. Lu, R. Tolimieri and N. P. Caviris, "Optical Realization of Wavelet Transform for a One-Dimensional Signal," *Opt. Lett.*, vol.17, no.3, 1 February 1992.

[5.15] Y. Li and Y. Zhang, "Optical Implementation of Gabor and Wavelet Expansions of 1- and 2-D Signals," *Proc. SPIE*, vol.1702, 1992.

[5.16] C. S. Weaver and J. W. Goodman, "A Technique for Optically Convolving Two Functions," *Applied Optics*, vol.5, no.7, pp.1248-1249, July 1966.

[5.17] S. Jutamulia, K. Comany and D. A. Gregory, "Intensity-Invariant Joint Transform Correlator," *Optics & Photonics News*, p.13, December 1991.

[5.18] J. L. Horner and P. D. Gianino, "Phase-Only Matched Filtering," *Appl. Opt.*, vol.23, no.6, pp.812-816, 15 March 1984.

[5.19] P. G. Gianino and J. L. Horner, "Additional Properties of the Phase-Only Correlation Filter," *Opt. Eng.*, vol.23, p.695, 1984.

[5.20] C. S. Anderson and R. C. Anderson, "Comparison of Phase-Only and Classical Matched Filter Scal Sensitivity," *Opt. Eng.*, vol.26, p.276, 1987.

[5.21] D. L. Flannery, J. S. Loomis and M. E. Milkovich, "Design Elements of Binary Phase-Only Filters," *Appl. Opt.*, vol.27, no.20, pp.4231-4235, 15 October 1988.

[5.22] D. M. Cottrell, R. A. Lilly, J. A. Davis and T. Day, "Optical Correlator Performance of Binary Phase-Only Filters Using Fourier and Hartley Transforms," *Appl. Opt.*, vol.26, no.18, pp.3755-3761, 15 September 1987.

[5.23] A. N. Netravali and J. O. Limb, "Picture Coding: A Review," *Proc. IEEE*, vol.68, pp.336-406, 1980.

[5.24] W. K. Pratt, Ed., *Image Transmission Techniques*, New York: Academic, 1979.

[5.25] P. J. Burt and E. H. Adelson, "The Laplacian Pyramid as a Compact Image Code," *IEEE Trans. Comm.*, vol.COM-31, no.4, pp.532-540, April 1983.

[5.26] Y. Li and Y. Zhang, "Optical Gabor and Wavelet Expansions of One and Two Dimensional Signals," in preparation.

[5.27] I. Daubechies, "Orthonormal Bases of Compactly Supported Wavelets," *Comm. on Pure and Appl. Math.*, vol.XLI, pp.909-996, 1988.

(a) (b)

Fig.5.0.1. Two pulses for analyzing Gabor and wavelet transforms. (a) Pulse with short duration and (b) pulse with long duration.

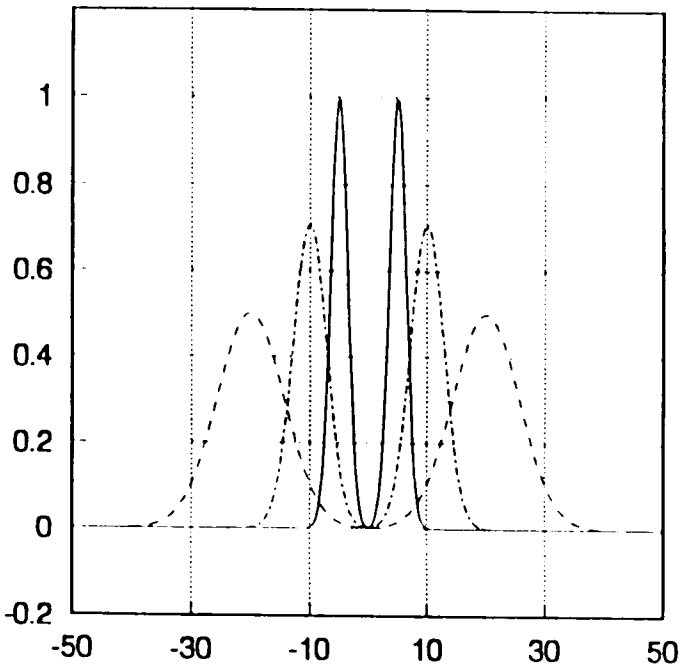

Fig.5.1.1. Gaussian wavelet in frequency domain.

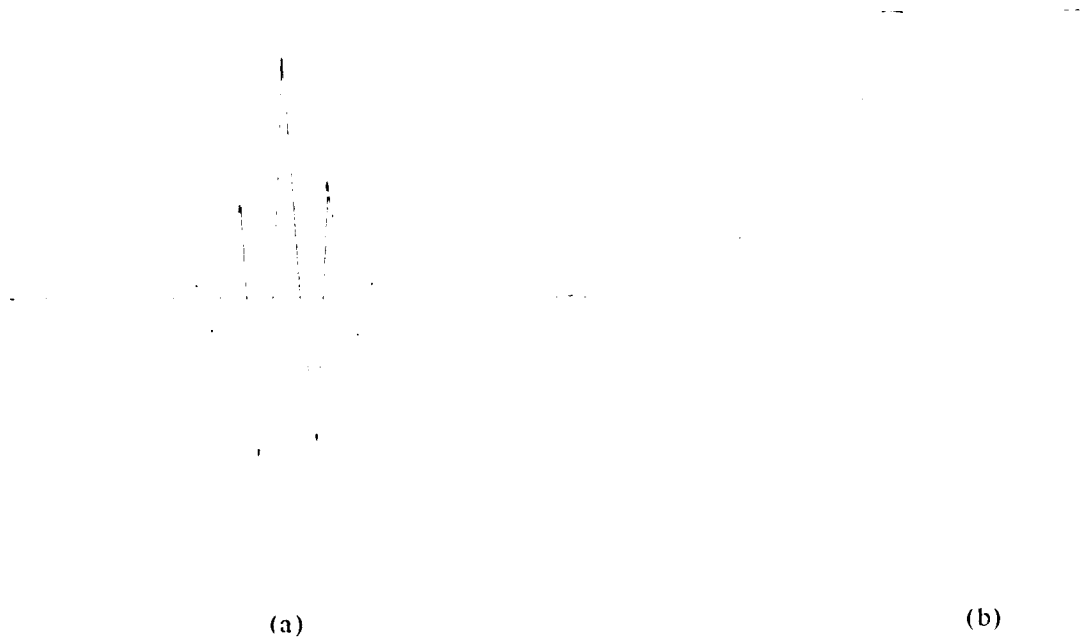

(a) (b)

Fig.5.2.1. Analytic wavelet suggested by Mallat. (a) Its waveform in time domain and (b) its spectrum.

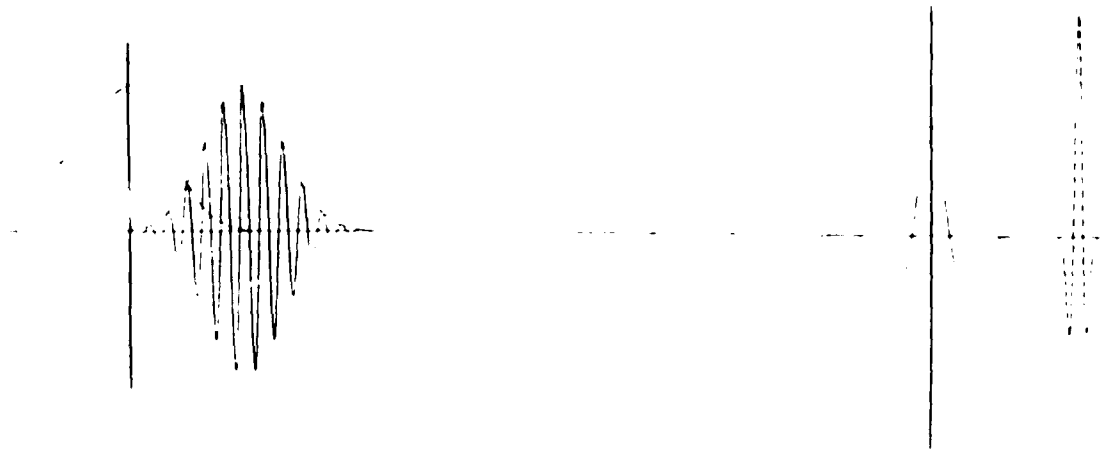

Fig.5.3.1. Comparison of Gabor window and wavelet function in time domain. (a) Time-shifted and frequency-modulated Gabor windows. (b) Translated and dilated wavelets.

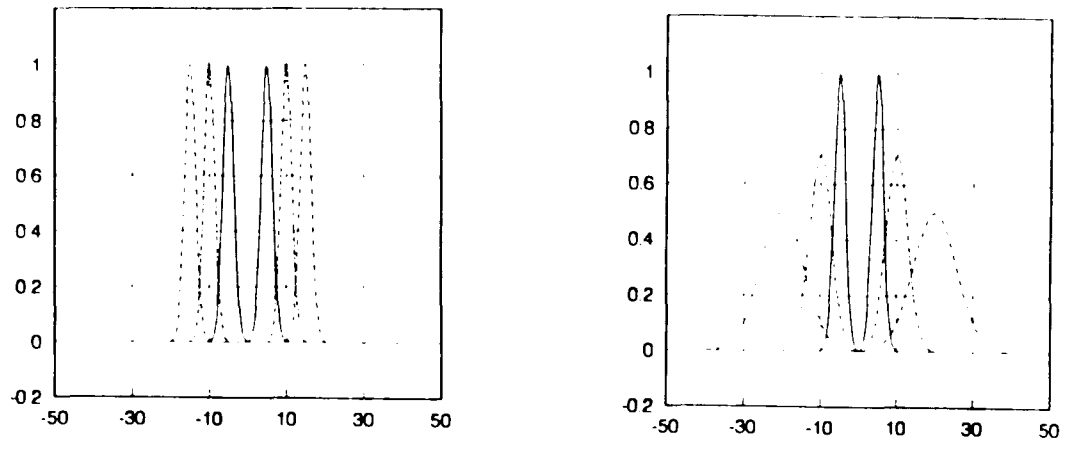

(a) (b)

Fig.5.3.2. Comparison of Gabor window and wavelet function in frequency domain. (a) Gabor windows and (b) wavelets.

Fig.5.3.3. (a) Gabor filters and (b) wavelet filters generated by ideal lowpass and bandpass filters.

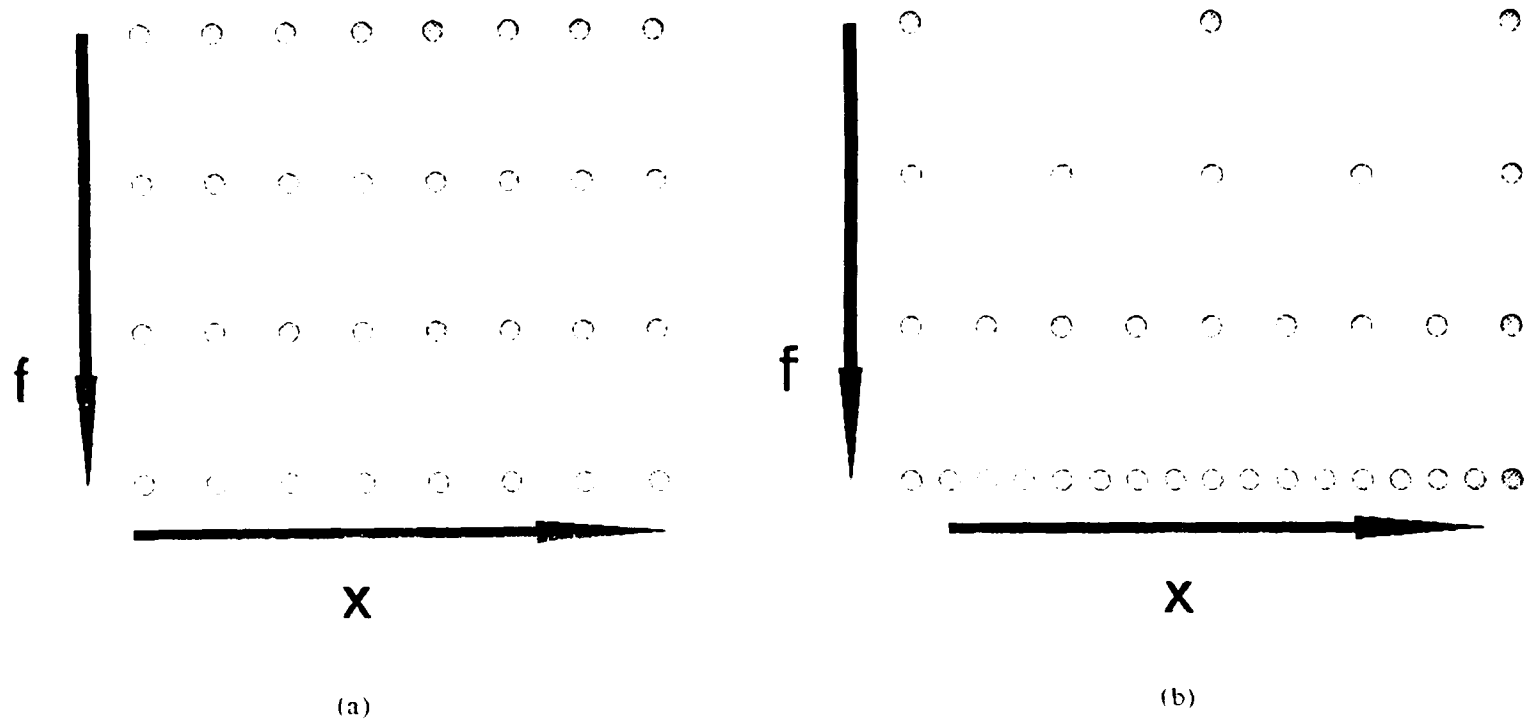

Fig.5.3.4. Sampling grids of Gabor and wavelet transforms. (a) Equally spaced sampling grid of Gabor transform. (b) Unequally spaced sampling grid of wavelet transform which is equally spaced in logarithm scale.

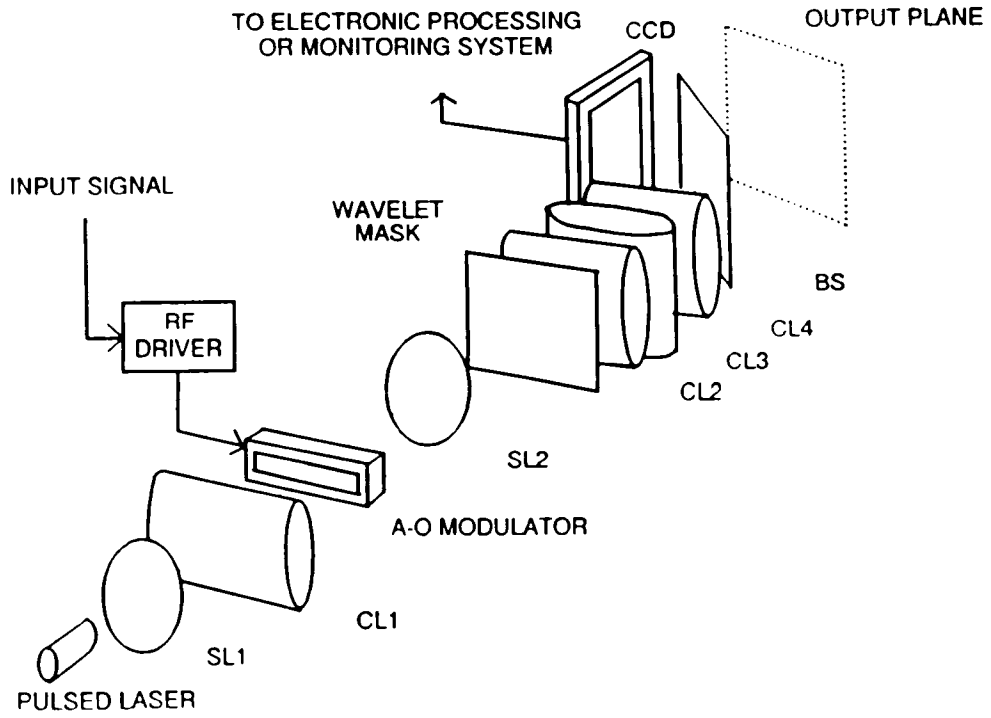

Fig.5.4.1. Optical wavelet processor for short 1-D signals.

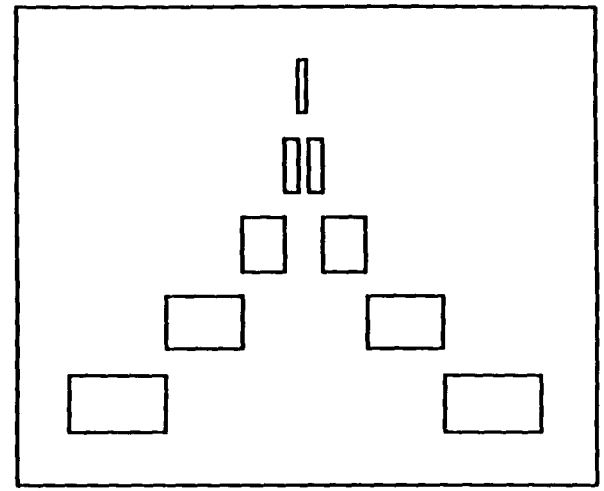

Fig.5.4.2. Mask pattern for optical 1-D wavelet transform, which contains one lowpass filter and four bandpass filters.

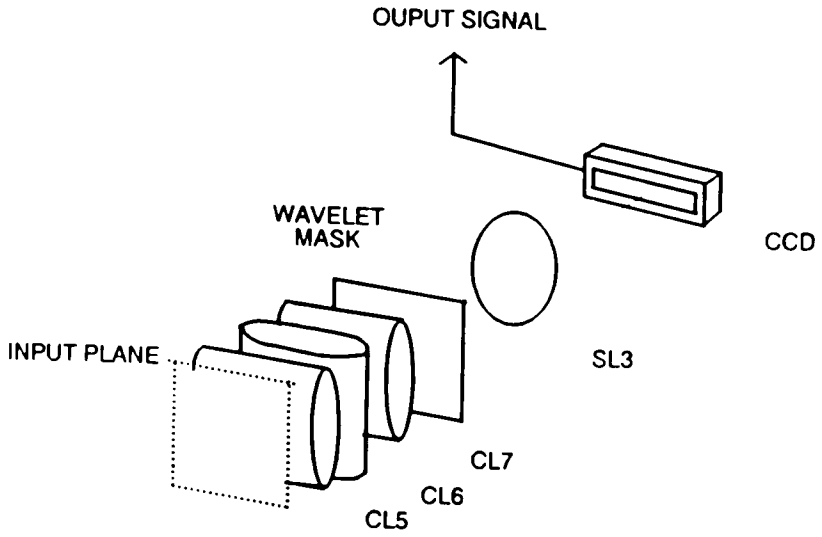

Fig.5.4.3. Optical wavelet synthesizer to perform inverse wavelet transform.

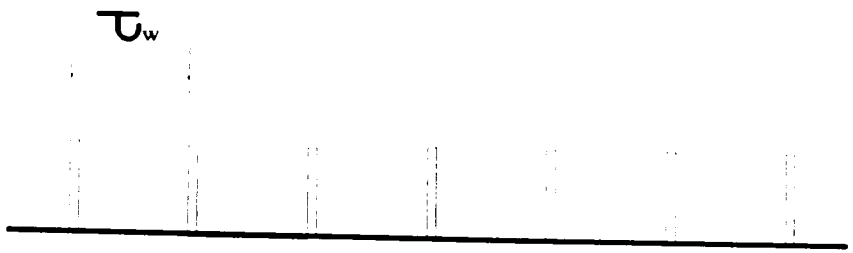

Fig.5.4.4. Firing pulses for pulsed laser, where τ_w is the aperture time of A-O modulator.

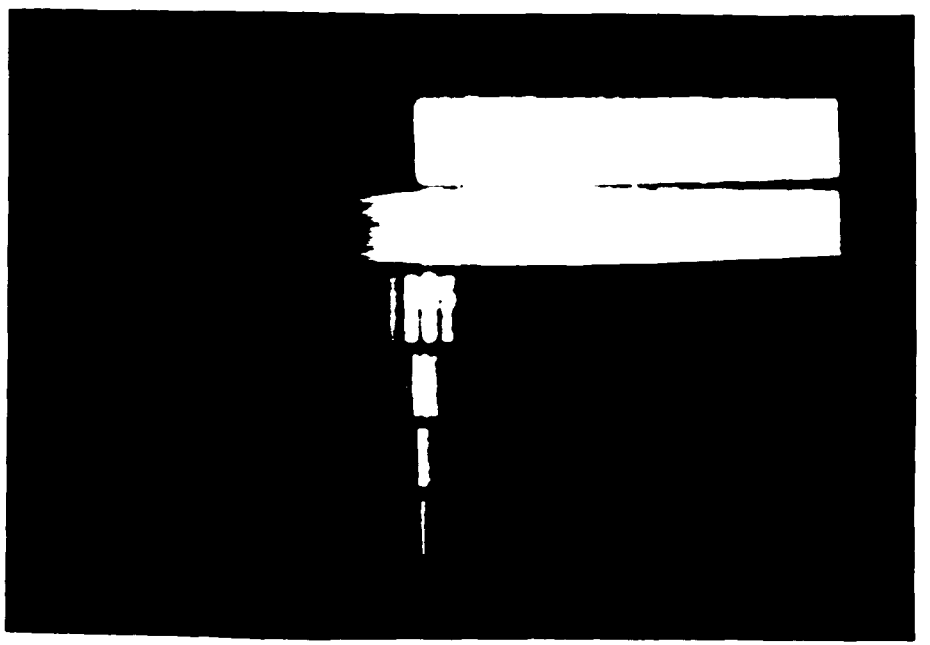

Fig.5.4.5. Experimental results of the wavelet transform of a step function.

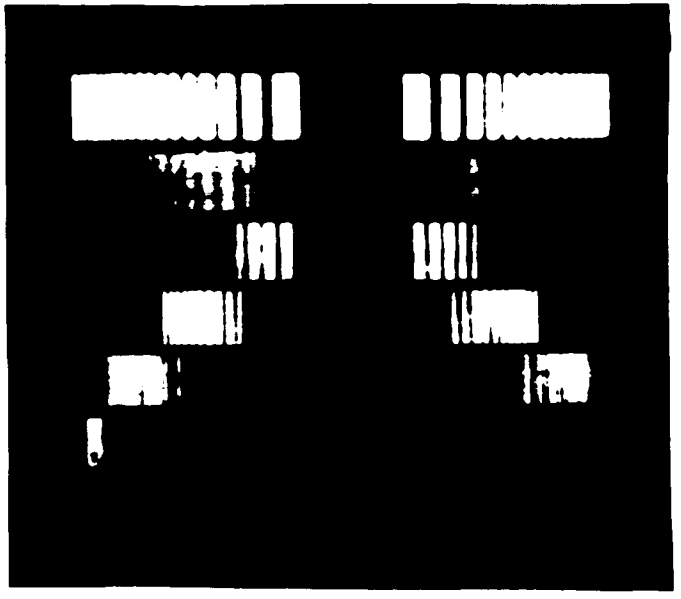

Fig.5.4.6. Experimental results of the wavelet transform of a chirped signal.

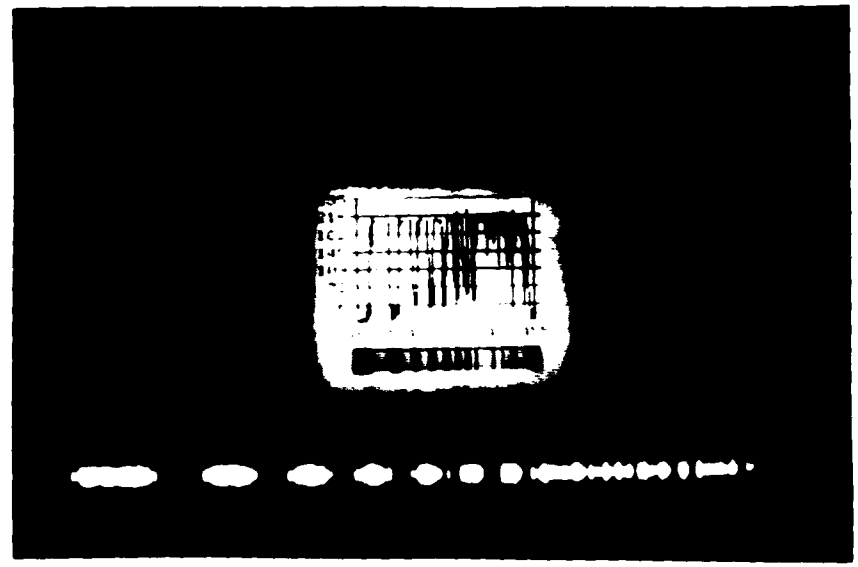

Fig.5.4.7. Recovered chirped signal.

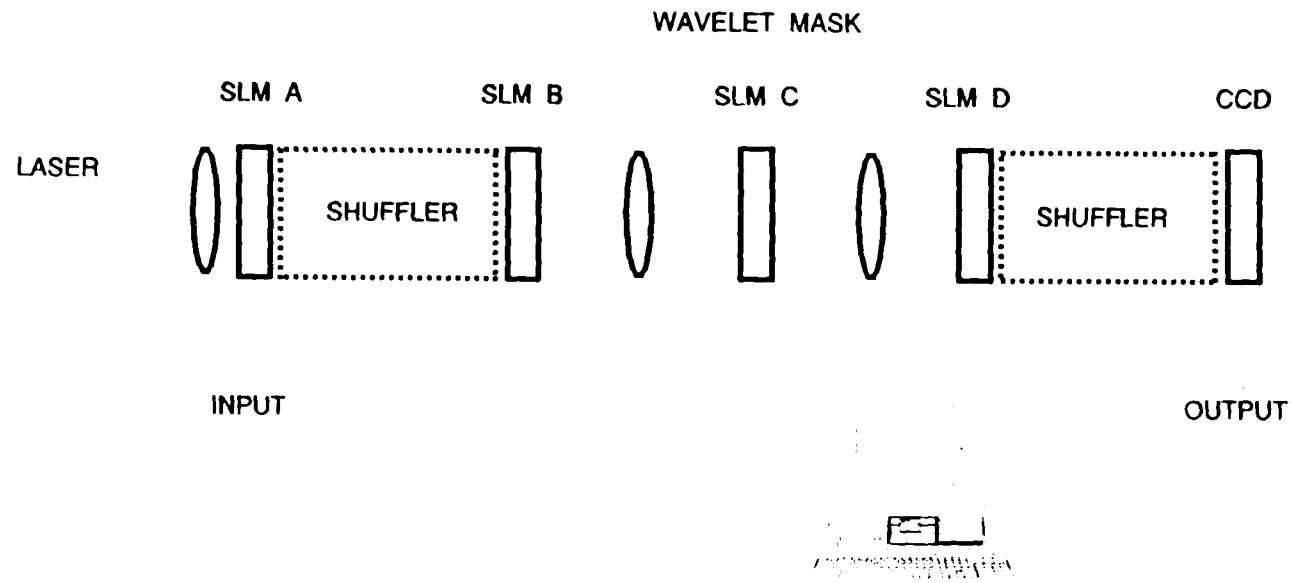

Fig.5.5.1. Optical wavelet processor for long 1-D signals, where shuffler is one of the schemes described in Section 3.5.3.

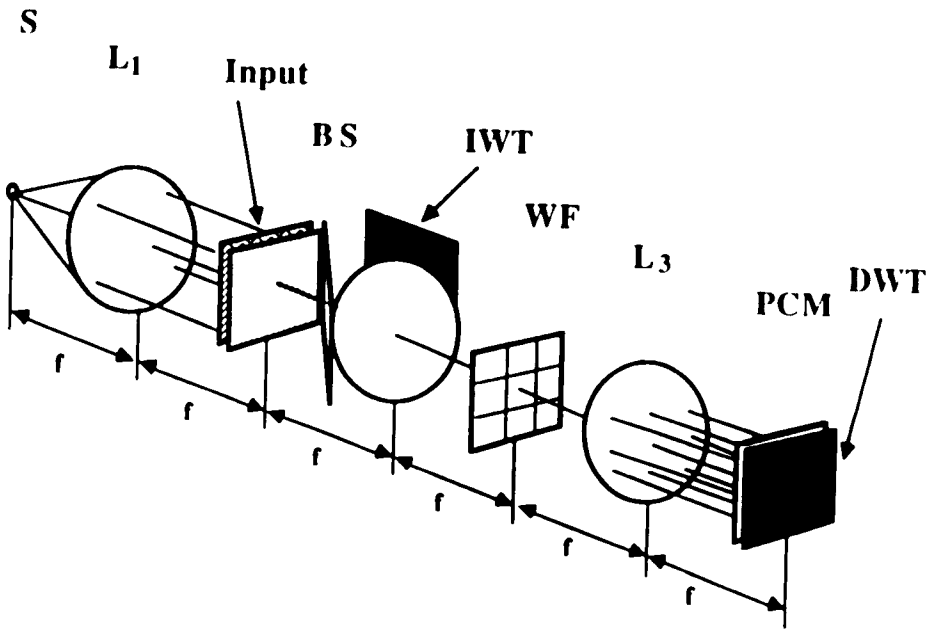

Fig.5.6.1. Parallel 2-D wavelet processor based on lenslet array or hologram.

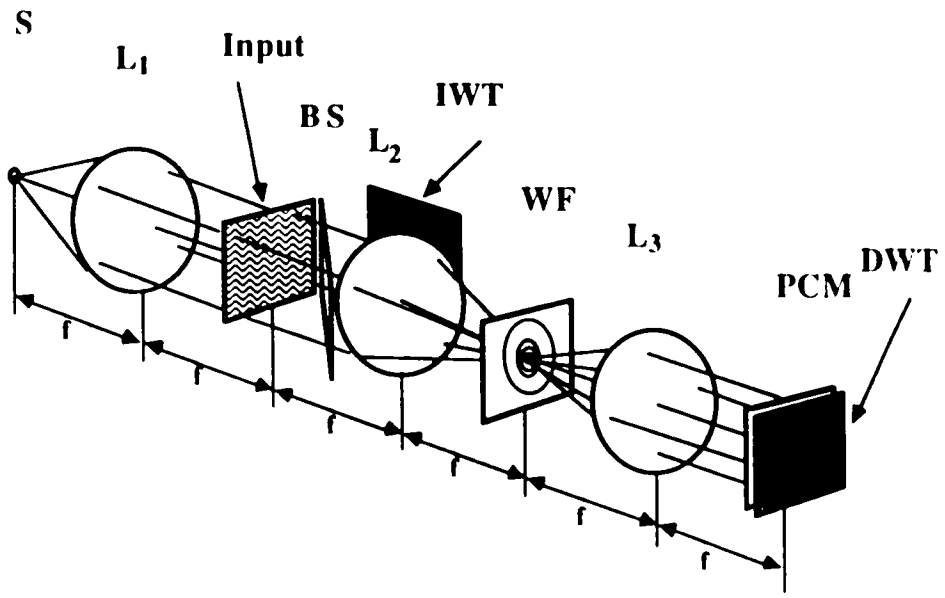

Fig.5.6.2. 2-D wavelet processor based on sequential display of the dilated wavelets.

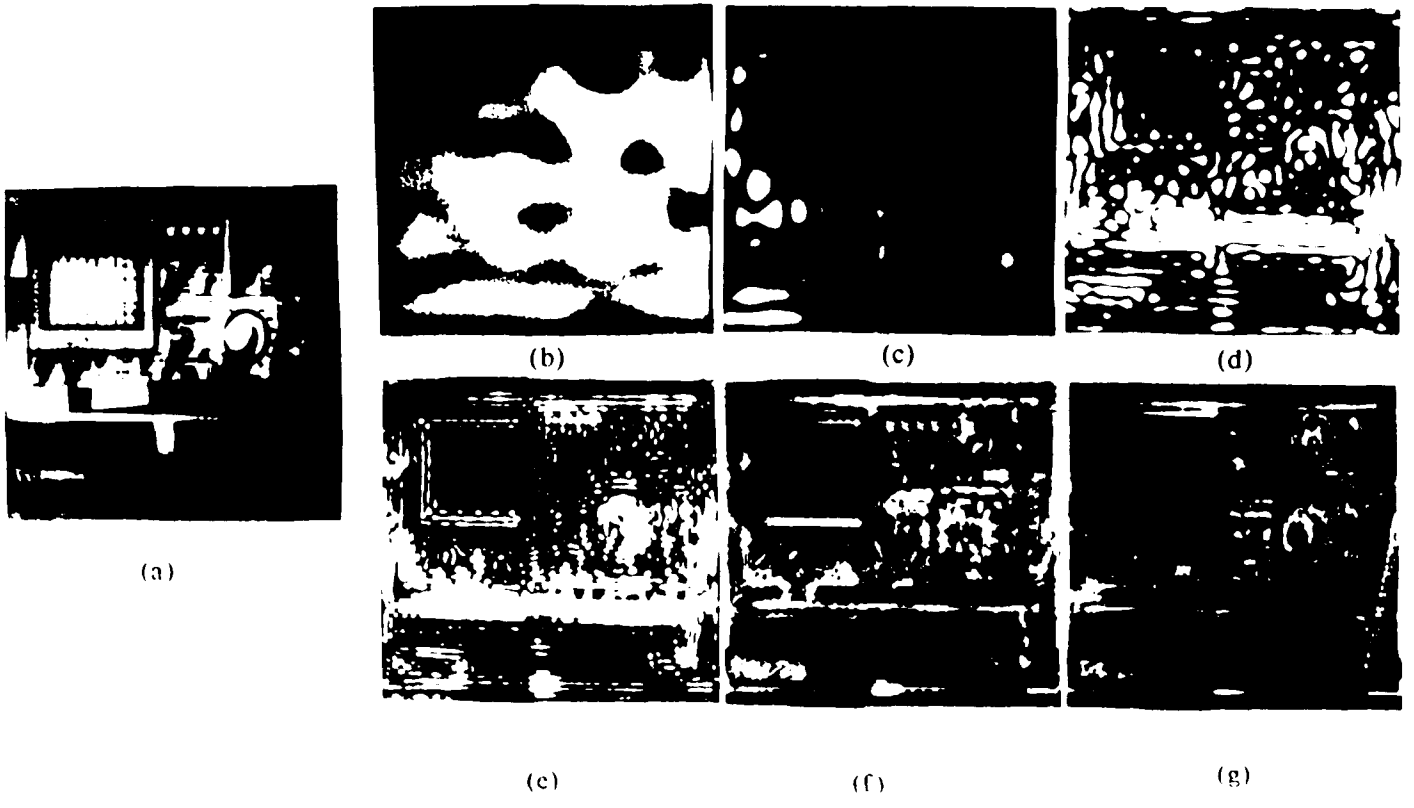

Fig 5.6.3. 2-D Wavelet transform on (a) input image. (b) Coarse information of the image. (c) band 1, (d) band 2, (e) band 3, (f) band 4 and (g) and band 5 of wavelet transform.

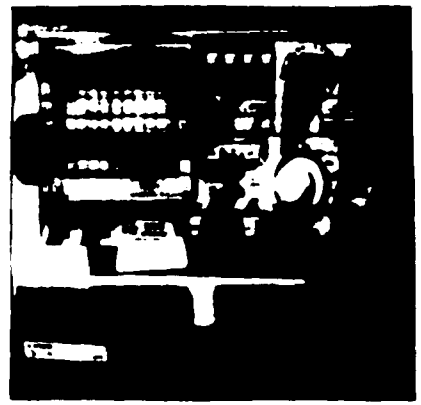

Fig 5.6.4. Recovered image

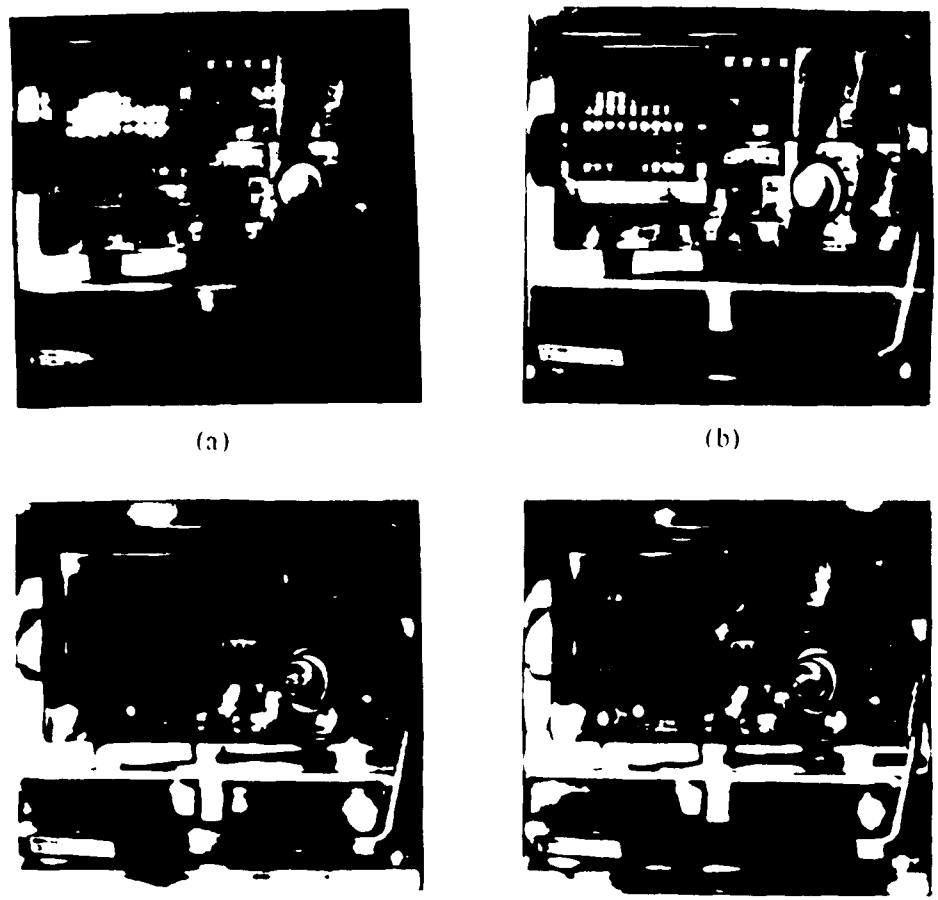

Fig.5.7.1. Effects of misalignment of lowpass filter. (a) one pixel, (b) three pixels, (c) four pixels and (d) five pixels

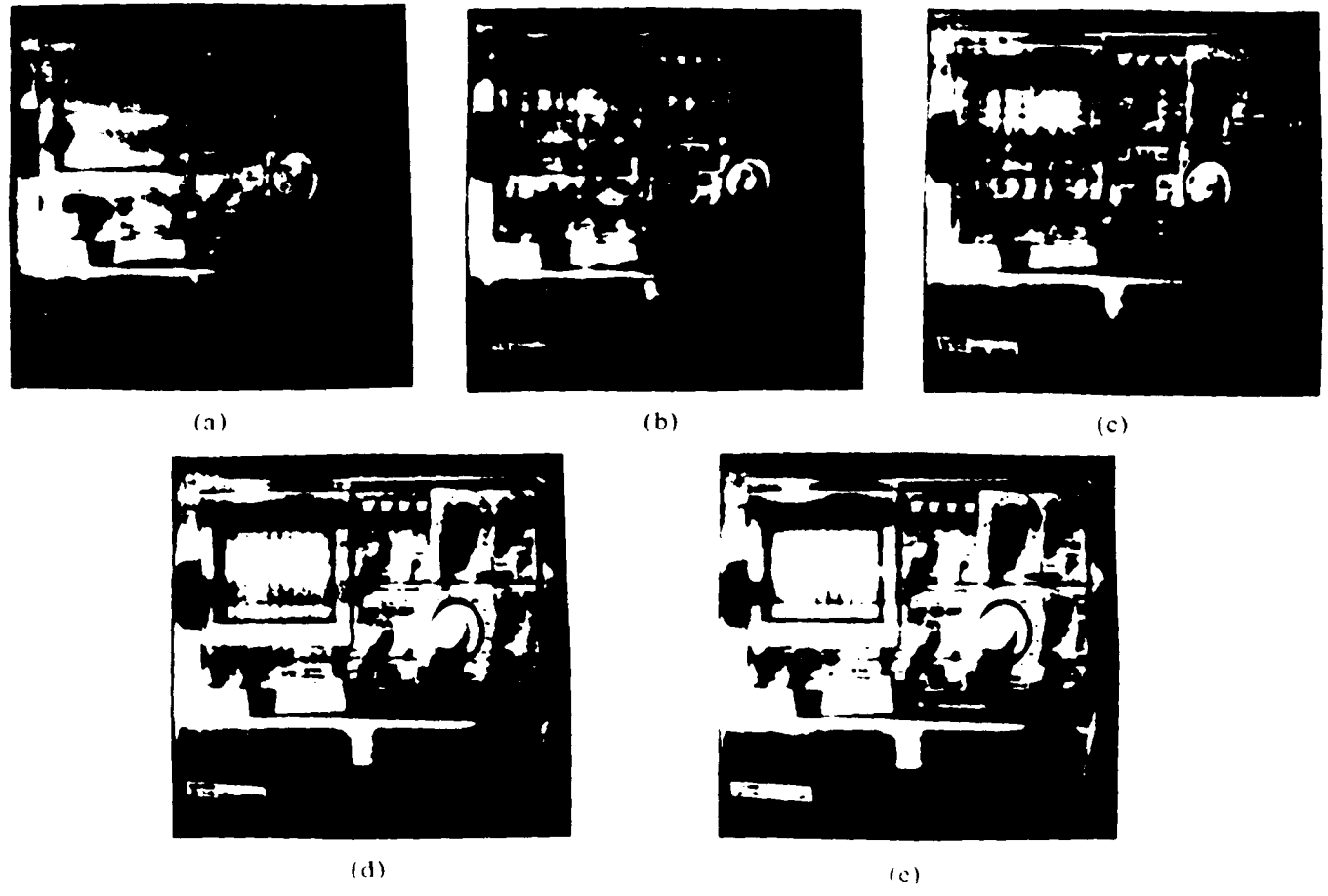

Fig.5.7.2. Effects of misalignment of bandpass filters by four pixels. (a) Band 1, (b) band 2, (c) band 3, (d) band 4 and (e) band 5. In the experiment only one band is misaligned each time.

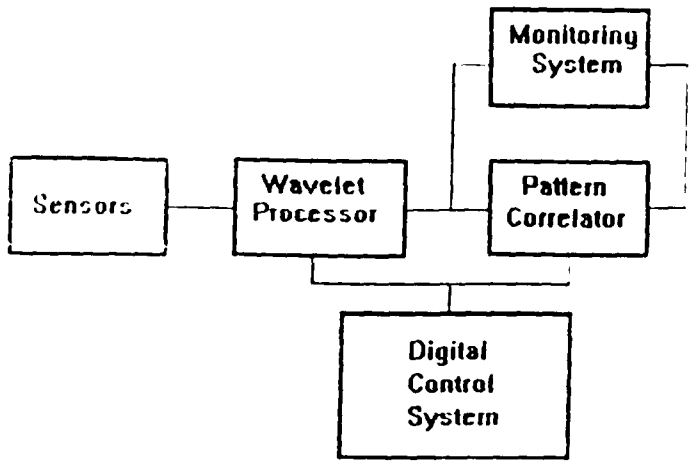

Fig.5.8.1. Principle diagram of wavelet transform based system failure predict-r.

Filters	Pixel Range
Lowpass	0 - 4
Bandpass 1	5 - 9
Bandpass 2	10 - 19
Bandpass 3	20 - 39
Bandpass 4	40 - 79
Bandpass 5	80 - 159

Table 5.1 Specifications of wavelet filters used in experiments in Sections 5.6 and 5.7.

6 IMAGE PROCESSING BASED ON THE CONCEPT OF GABOR AND WAVELET TRANSFORMS

The above discussed Gabor and wavelet transforms can be found various applications in image processing. However, for those schemes discussed in the last two chapter, their processing capability is seriously limited by the spatial-bandwidth product of optical system [6.1]. In the following, an opto-electronic system architecture which can be used to process motion pictures based on either Gabor transform or wavelet transform is described.

6.1 System Architecture

Principally, this system consists of two 1-D Gabor coefficient or wavelet transform processors described above and performs 1-D Gabor transforms or wavelet transforms on horizontal and vertical lines, respectively, at one instant. It is schematically shown in Fig.6.1.1. The condition for the system to deliver correct results is that the selected Gabor window function or basic wavelet should be separable, which means

$$w(x_1, x_2) = w_1(x_1)w_1(x_2) \qquad (6.1.1)$$

For most of the applications, this condition is reasonable.

In the system, each frame of the motion pictures is duplicately fed into to two similar optical branches A and B by SLM's, such as liquid crystal TV's (LCTV).

Two acousto-optic (A-O) modulators are employed to generate scanning bars in horizontal and vertical directions on the images in the two branches, respectively. And therefore, only two 1-D signals corresponding to two mutually orthogonal lines of one frame of image are obtained at one instant. They are subject to the following 1-D Gabor transforms or 1-D wavelet transforms, respectively. From the obtained Gabor coefficients or wavelet transform of the 1-D signals, important informations of certain spatial or temporal targets [14] and their textures may be detected.

Specifically, consider Branch A of the system. The coherent light from the laser source is first spatially filtered and shaped to a narrow horizontal bar. A following A-O deflector discretely deflects the light bar in vertical direction. Therefore the frame of motion pictures currently displayed on the SLM is illuminated and discretized to numbers of lines. Only one horizontal lines of image is fed into the cascaded 1-D Gabor coefficient or wavelet transform processor at one instant. At the output plane, the Gabor coefficients or the wavelet transform of this lines of signal is obtained. As the scanning lines go from the top of the frame to the bottom of the frame, the Gabor coefficients or the wavelet transform of each scanning line are obtained sequentially. Each of these obtained 2-D Gabor coefficient or the wavelet transform pattern is called a field of Gabor coefficient or wavelet transform. Therefore, N fields of Gabor coefficients or wavelet transform are generated if the image is discretized to N lines. For the Branch B,

---

14 By name of spatial target, an interested object in one frame of motion pictures is described. The name of temporal targets regards the time variation of an interested object between frames.

the A-O deflector is placed vertically and it scans the image in horizontal direction by a vertical bar. The following Gabor coefficient or wavelet transform processor for 1-D signals then delivers the Gabor coefficients or the wavelet transform of each vertical scanning lines sequentially as the scanning line runs from left to right.

6.2 Application to Target Detection

From the preliminary experiment in Section 4.4, it is known that Gabor transform with a one-sided exponential function can be used to allocate the position of jump in 1-D signal. Also, as analyzed by Friedlander and Porat [6.2], the detection based on Gabor coefficients has good performance even under strong noise environment. Therefore, the here proposed 2-D target detector based on 1-D Gabor coefficient processor is also insensitive to noise. To analyze it, consider the motion pictures shown in Fig.6.2.1. Because of the similarity between Branches A and B, only Branch A is described in detail.

First of all, the information given by the system for one frame of the motion pictures is discussed. For the scanning line H1 in Frame 2, since there is no object covered by this line, the Gabor coefficient at the output plane should be zeros except the fluctuations generated by noise. For line H4 in Frame 2, however, there are six intensity jumps caused by the edges of three object. Because of there different textures, the Gabor coefficients of this line of image referring to each edge are located at different positions (see Fig.6.2.2), where some small-valued

Gabo: coefficients are omitted for simplicity. The coefficients clearly demonstrate the locations of the each edge and the spatial frequency contents of the object with certain texture on this line of image. The obtained information in this branch describes all the vertical edges, the vertical components of tilted edges and the spatial frequencies of textures in horizontal direction. Similarly, the information delivered by branch B contains all the horizontal edges, the horizontal components of tilted edges and the spatial frequencies textures in vertical direction.

Secondly, as the scanning line runs from the top to the bottom of Frame 2, all the Gabor coefficients corresponding to line H2, which is the line just at the top of objects, are zeros. When line H3 is illuminated, because of the presence of the objects, non-zero Gabor coefficients start to appear. They maintain their appearance until line H5 except an intensity variation caused by the non-uniform intensity of objects in vertical direction. Fig.6.2.3 principally shows the changing of Gabor coefficient corresponding to the left edge of the shaded rectangular.

Finally, consider the case that an object shows at one instance and disappear at another instance. The triangle object with lower texture frequency is an example. This appears first time in Frame 2, stays in Frame 3 and then disappears in Frame 3. Therefore, for the Gabor coefficient (at point a) corresponding to the left edge of the object on line 4. It is zero in Frame 1, jumps to certain value in Frame 2, stay at this value in Frame 3 and jumps back to zero in Frame 4 (see Fig.6.2.4). The arrival time of the object is given by this diagram. On the other hand, by

determining the gate width in Fig.6.2.4, the staying time of this object can also be obtained. The variation of the intensity of the interested object will cause the intensity fluctuation of the diagram in Fig.6.2.4 proportionally.

6.3 Summary

A novel electro-optic system architecture for image processing based on Gabor and wavelet transform was proposed, which can be used to detect the existence of both spatial and temporal targets. Because of its using of time-frequency representation of 2-D signal, better performance than conventional schemes is expected when the signal is contaminated by noise.

6.4 References

[6.1] Y. Li and Y. Zhang, "Optical Gabor and Wavelet Expansions of One and Two Dimensional Signals," in preparation.

[6.2] B. Friedlander and B. Porat, "Detection of Transient Signals by the Gabor Representation," *IEEE Trans. on Acoust., Speech and Sig. Proc.*,vol.37, no.2, pp.169-180, February 1989.

6.5 Figures

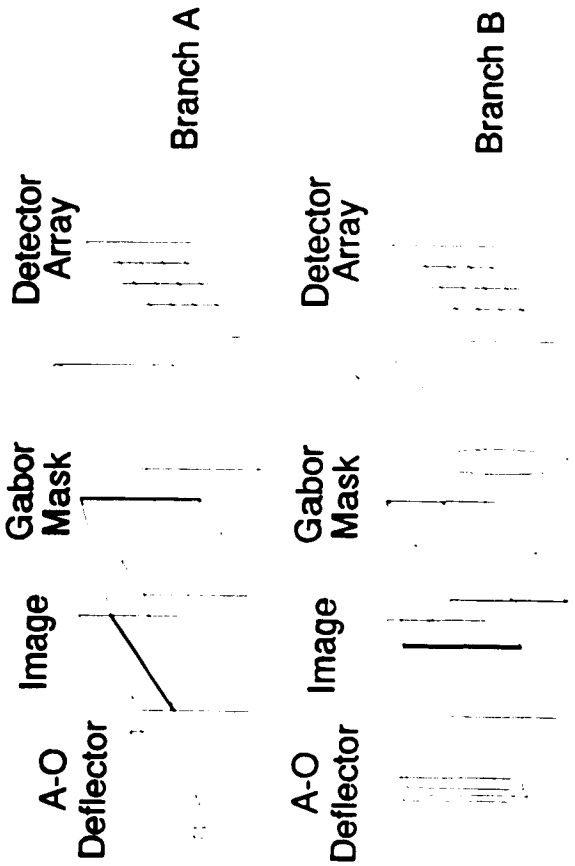

Fig.6.1.1. Optical image processor based on the concept of Gabor and wavelet transform.

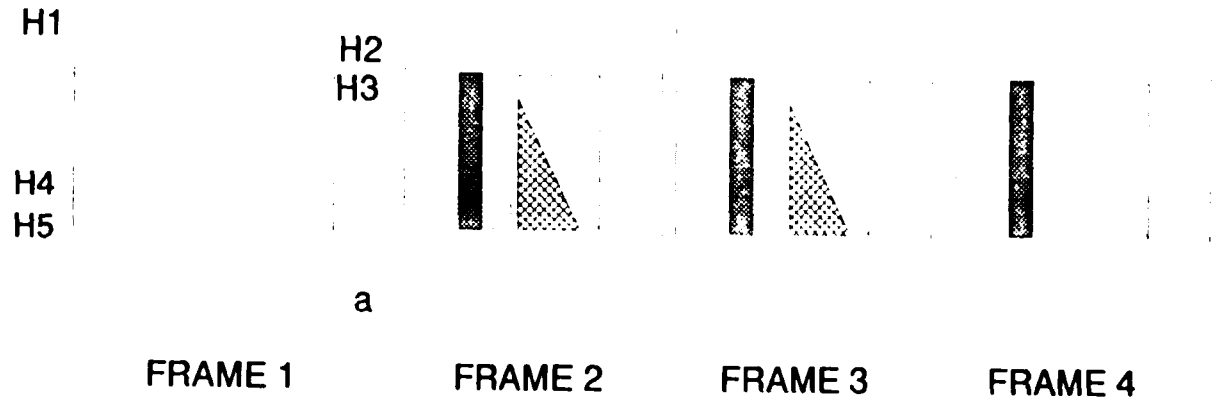

Fig.6.2.1. Four frames of a motion picture.

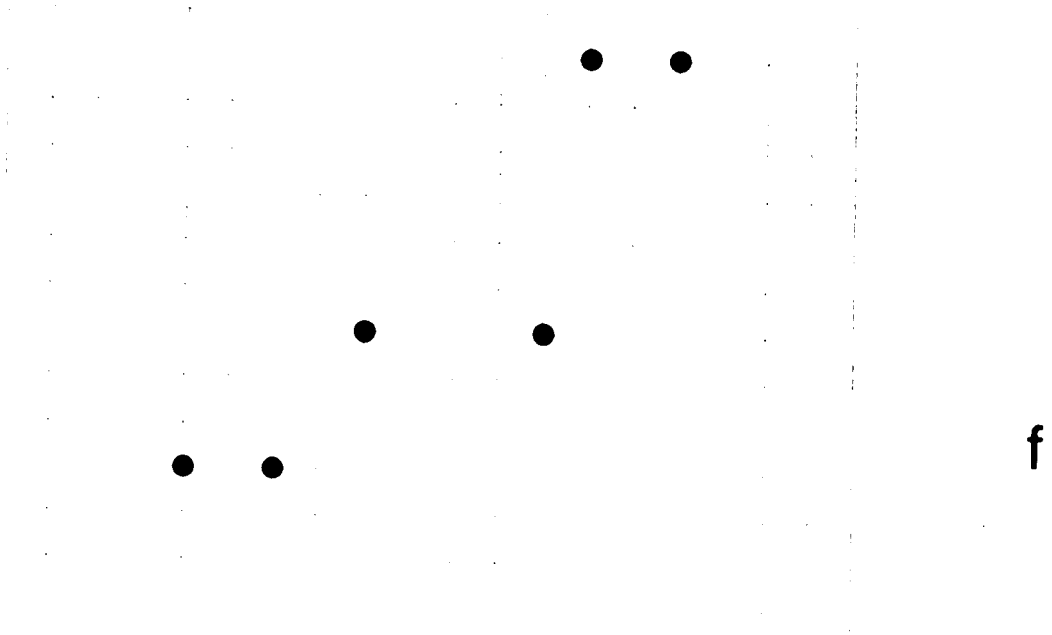

Fig.6.2.2. Gabor coefficients of the line H4 in Fig.6.2.1.

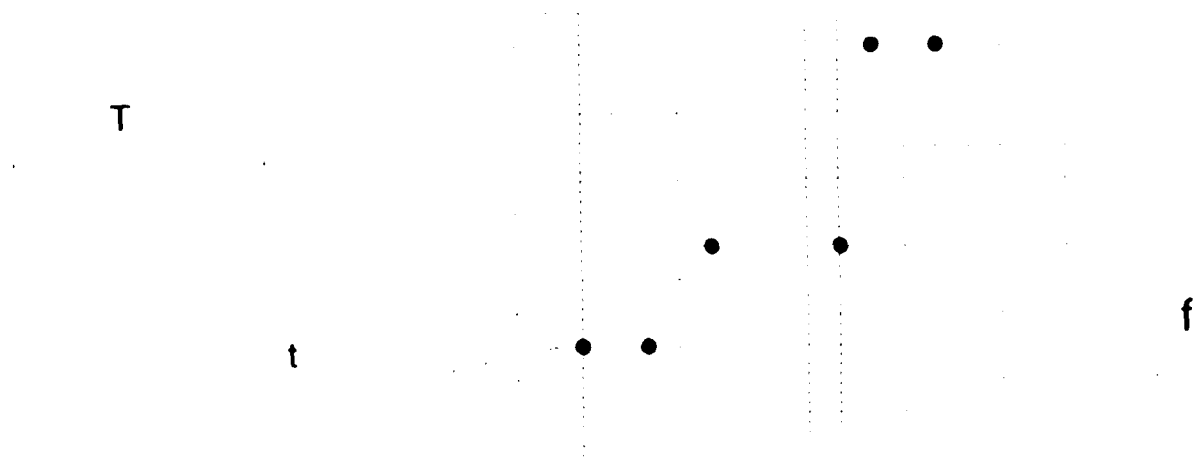

Fig.6.2.3. Variation of Gabor coefficient corresponding to the left edge of the shaded rectangular in Frame 2 of Fig.6.2.1.

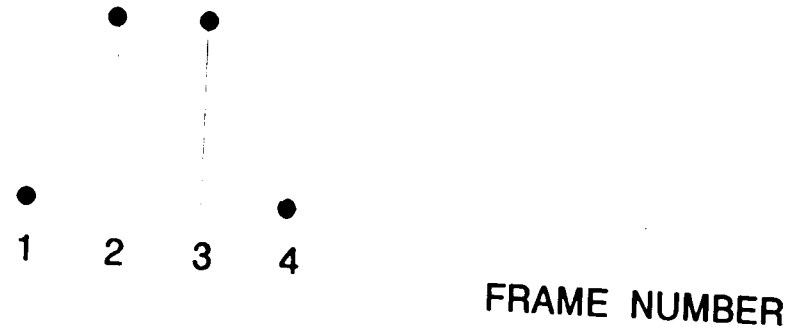

Fig.6.2.4. Variation of Gabor coefficient corresponding to point a for different frames.

7 SUMMARY

To summarize this doctoral dissertation, new methods of optical long data stream convolution/correlation, optical Gabor and wavelet transform implementations and their applications to image coding, system failure prediction, signal processing in dense target environment and nonlinear dynamic system analysis were studied.

Some background materials about optical signal processing was briefly discussed in the first chapter. In the second chapter, the state-of-the-art optical signal processing techniques were reviewed. Beginning at the third chapter, new methods of optical implementation of the long data stream convolution/correlation, the Gabor transform and the wavelet transform were presented.

In Chapter Three, an optically implementable algorithm, which separates a long data stream into several shorter sequences based on the Chinese remainder theorem, was first described. Using this algorithm, the convolution/correlation of long data streams are performed by small scale vector-matrix multiplications, which can be realized using the state-of-the-art optical algebraic processing technologies. Computer simulation results of this algorithm were presented. A suitable optical processing architecture was also proposed. As an alternative to the above algorithm, the convolution/correlation of the two 1-D data sequences was converted into a convolution/correlation of the two corresponding 2-D arrays. An opto-electronic scheme using the algorithm to solve the problem of real-time convolution/correlation of long data

streams was thus described. Three video rate optical and opto-electronic data permutation schemes were presented and compared. Computer simulations for the entire three-stage algorithm and their results were presented. Technical problems, fundamental limitations of the described schemes were studied.

An opto-electronic Gabor coefficient processor for one-dimensional (1-D) signals was presented in Chapter Four. Using an acousto-optic modulator as an input device, a liquid crystal SLM as a reconfigurable window and a two-dimensional (2-D) CCD detector array as an output device, a real-time opto-electronic Gabor coefficient processing architecture for short 1-D signals was established and experimentally tested. Technical considerations and some preliminary experimental results were also shown there. As an application of that processor, a Gabor transform based transient signal detection scheme was proposed. Schemes for implementing Gabor coefficient processors for long 1-D signals and 2-D signals were also discussed.

In the following chapter, wavelet transform was discussed in detail. A scheme for optical realization of wavelet transform for short 1-D signal was thus designed. Using commercially available components, the constructed system can perform wavelet transform for 1-D signals in real-time. Some experimental results were demonstrated. As an extension of this scheme, 2-D optical wavelet transformer with different translation parameters and a single dilation parameter for the two dimensions was proposed and computer simulated. Technical problems of optical implementation were studied. Applications of the wavelet transforms to system failure prediction, signal processing in dense target environment, image coding and nonlinear system analysis

were briefly described. Optical implementations of long data stream wavelet transform were also proposed in the chapter by using the long data stream convolution/correlation schemes given in Chapter Three.

Finally, as an application of Gabor and wavelet transform, a novel system architecture was designed for detection of spatial and temporal target in motion pictures, which was based on 1-D Gabor and wavelet transform. Although this system does not perform processing in real-time, it is expected less sensitive to spatial noise than conventional detectors because of its utilization of time-frequency representation.

APPENDIX A

A List of Abbreviations

1-D	One-dimensional
2-D	Two-dimensional
CCD	Charge Coupled Device
CRT	Cathode Ray Tube
DFT	Discrete Fourier Transform
FFT	Fast Fourier Transform
FIR	Finite Impulse Response
HDTV	High Definition Television
IIR	Infinite Impulse Response
JTC	Joint Transform Correlator
LCLV	Liquid Crystal Light Valve
LCTV	Liquid Crystal Television
N-D	N-dimensional
NTT	Number Theory Transform
SLM	Spatial Light Modulator
TFT	Thin Film Transistor
VLSI	Very Large Scale Integrated Circuit

APPENDIX B

Zak Transform

Related to the practical situations where time-continuous signals are sampled at a certain uniform rate and at an unknown or uncontrolled sampling phase, the Zak transform of a complex-valued and time-continuous signal $f(t)$ is defined by [B.1]

$$F(z,\omega) = \sum_{k=-\infty}^{+\infty} f(z+k)e^{-j2\pi k\omega} \qquad (B.1)$$

where $-\infty < z, \omega < +\infty$.

Now, the basic properties of the Zak transform without mathematical derivations are listed. In the following descriptions, symbol $Zak\{\cdot\}$ represents Zak transform, symbol $D_\gamma f$ is defined by $\gamma^{\frac{1}{2}} f(\gamma t)$ $(\gamma > 0)$ as dilation operation, symbols $T_a f$ and $R_b f$ means $f(t+a)$ and $e^{-2\pi jbt} f(t)$, respectively.

Property 1:

$$Zak\{f\}(t,\omega) = e^{2\pi jz\omega} Zak\{F\}(\omega,-z) \qquad (B.2)$$

where F represents the Fourier transform of the input function

Property 2:

$$Zak\{f\}(z+z',\omega) = e^{j2\pi z'\omega} Zak\{f\}(z,\omega) \quad (B.3)$$

and

$$Zak\{f\}(z,\omega+\omega') = Zak\{f\}(z,\omega) \qquad (B.4)$$

where z' and ω' are integers.

Property 3:

$$Zak\{T_a f\}(z,\omega) = Zak\{f\}(z+a,\omega) \qquad (B.5)$$

and

$$Zak\{R_b f\}(z,\omega) = e^{-i2\pi bz} Zak\{f\}(z,\omega+b) \qquad (B.6)$$

Property 4:

$$Zak\{D_\gamma f\}(z,\omega) = (Zak\{f\})_\gamma\left(\gamma z, \frac{\omega}{\gamma}\right) \qquad (B.7)$$

Property 5:

$$Zak\{f_-\}(z,\omega) = Zak\{f\}(-z,-\omega) \qquad (B.8)$$

and

$$Zak\{f^*\}(z,\omega) = (Zak\{f\})^*(z,-\omega) \qquad (B.9)$$

Property 6:

$$f(z) = \int_0^1 Zak\{f\}(z,\omega)d\omega \qquad (B.10)$$

For details of Zak transform, please consult reference [B.1].

References

[B.1] A. J. E. M. Janssen, "The Zak Transform: A Signal Transform for Sampled Time-Continuous Signals," *Philips J. Res.*, vol.43, pp.23-69, 1988.

A LIST OF THE THESIS RELATED PUBLICATIONS

Journal and Proceeding Papers:

[1] "Optical Implementation of Gabor and Wavelet Expansions of 1- and 2-D Signals" (with Y. Li), *SPIE Proc.*, vol. 1702, April 1992.

[2] "Massively Parallel Optical Interconnects for Long Sequence Data Convolution" (with Y. Li), *SPIE Proc.*, vol. 1704, April 1992.

[3] "Image Analysis via Optical Wavelet Transform" (with X. J. Xu, A. Katz, E. G. Kenterakis, Yao Li and N. P. Caviris), accepted by *Optics Communication* for publication in 1992.

[4] "Optical Realization of Wavelet Transform for a One-Dimensional Signal" (with Y. Li, E. G. Kanterikis, A. Katz, X. J. Lu, R. Tolimieri and N. P. Caviris), *Optics Letters*, vol.17, no.3, pp.210-212, February 1, 1992.

[5] "Optical Analog-to-Digital Conversion using Acousto-optic Theta Modulation and Table Look-up" (with Yao Li), *Applied Optics*, vol.30, no.30, pp.4368-4371, October 20, 1991.

[6] "An Optically Implementable Algorithm for Convolution/Correlation of Long Data Streams" (with Yao Li), *Optics Communications*, vol.85, no.5,6, pp.473-480, October 1, 1991.

[7] "Six-port Optical Reflectometer," (with G. Colef, Y. Li and G. Eichmann), *IEEE Transaction on Instrumentation and Measurement*, vol.40, no.5, pp.869-871, October, 1991.

[8] "Optical Determination of Gabor Coefficients of Transient Signals" (with Yao Li), *Optics Letters*, vol.16, no.13, pp.1031-1033, July 1, 1991.

[9] "Opto-electronic Gabor Detector for Transient Signals" (with Yao Li), *SPIE Proc.*, vol.1981, pp.23-31, 1991.

[10] "Optically Implementable Algorithm for Convolution/Correlation of Long Data Streams" (with Yao Li), *SPIE Proc.*, vol.1974, pp.188-198, 1991.

[11] "Optical Analog-to-Digital Conversion using Acousto-optic Theta Modulation" (with Yao Li), *SPIE Proc.*, vol.1974, pp.167-173, 1991.

Conference Papers:

[12] "Optical Signal Processing Based on Wavelet Transform" (with X. J. Lu, A. Katz, E. G. Kanterakis, Y. Li and N. P. Caviris), *OSA 1991 Annual Meeting Technical Digest*, p.11, 1991, San Jose.

[13] "Real-Time Optoelectronic Gabor Detection of Transient Signals" (with A. Katz, X. J. Lu, E. G. Kanterikis, Y. Li and N. P. Caviris), *OSA 1991 Annual Meeting Technical Digest*, p.12, 1991, San Jose.

[14] "Optical 2-D Permutation for Convolution of 1-D Long Data Streams" (with Y. Li, E. G. Kanterikis, A. Katz and X. J. Lu), *OSA 1991 Annual Meeting Technical Digest*, p.126-127, 1991, San Jose.

[15] "Optical Analog-to-Digital Conversion using Acousto-optic Theta Modulation and Table Look-up" (with Yao Li), *OSA 1990 Annual Meeting Technical Digest*, pp.124-125, 1990, Boston.

[16] "Six-Port Optical Reflectometer" (with G. Colef, Y. Li and F. Eichmann), *OSA 1990 Annual Meeting Technical Digest*, 1990, Boston.

[17] "Opto-Electronic 3D Solid Model Relational Data Base Machine" (with G. Eichmann and Y. Li), *OSA 1990 Annual Meeting Technical Digest*, p.73, 1990, Boston.

[18] "Opto-Electronic 3D Solid Model Relational Data Base Machine" (with G. Eichmann and Y. Li), accepted by 1990 Syracuse University Minnowbrook Workshop on Data Base Machines.

[19] "A New Method of Determining the Volterra Kernels of Smooth Dynamic Nonlinear Systems in Frequency Domain" (with Z. G. Shen), presented at the First Meeting on Nonlinear Circuits and Systems of Electronic Society of China, 1988.

[20] "Canonical Piecewise-Linear Time Series Model of Smooth Dynamic Nonlinear Systems" (with Z. G. Shen), presented at the Seventh Annual Meeting of the Circuit and System Branch of Electronic Society of China, 1987.

Papers in preparation:

[21] "Optical Implementation of Long Data Stream Convolution" (with Y. Li and H. J. Caulfield), to be submitted to *Optical Engineering*.

[22] "Optical Gabor and Wavelet Expansions of One and Two Dimensional Signals" (with Y. Li), in preparation.

BIBLIOGRAPHY

Agarwal, R. C. and C. S. Burrus, "Fast One-Dimensional Digital Convolution by Multidimensional Techniques," *IEEE Trans. on Acoust., Speech and Sig. Proc.*, vol.ASSP-22, pp.1-10, February 1974.

Agarwal, R. C. and C. S. Burrus, "Fast Convolution using Fermat Number Transforms with Applications to Digital Filtering," *IEEE Trans. on Acoust., Speech and Sig. Proc.*, vol.ASSP-22, pp.87-99, April 1974.

Agarwal, R. C. and C. S. Burrus, "Number Theoretic Transforms to Implement Fast Digital Convolution," *Proc. IEEE*, vol.63, pp.550-560, April 1975.

Agarwal, R. and J. W. Cooley, "New Algorithms for Digital Convolution," *IEEE Trans. on Acoust., Speech and Sig. Proc.*, vol.ASSP-25, no.5, pp.392-410, October 1977.

Anderson, C. S. and R. C. Anderson, "Comparison of Phase-Only and Classical Matched Filter Scale Sensitivity," *Opt. Eng.*, vol.26, p.276, 1987.

Bastiaans, M. J., "Gabor's Expansion of a Signal into Gaussian Elementary Signals," *Proc. IEEE*, vol.68, no.4, pp.538-539, April 1980.

Bastiaans, M. J., "A Sampling Theorem for the Complex Spectrogram, and Gabor's Expansion of a Signal in Gaussian Elementary Signals," *Opt. Eng.*, vol.20, no.4, pp.594-598, July/August 1981.

Bastiaans, M. J., "Gabor's Signal Expansion and Degrees of freedom of a Signal," *OPTICA ACTA*, vol.29, no.9, pp.1223-1229, 1982.

Berg, N. J. and J. N. Lee, *Acousto-Optic Signal Processing: Theory and Implementation*, Marcel Dekker, New York, 1983.

Bergmans, J. W. M. and A. J. E. M. Janssen, "Robust Data Equalization, Fractional Tap Spacing and the Zak Transform," *Philips J. Res.*, vol.42, pp.351-398, 1987.

Blahut, R. E., *Fast Algorithm for Digital Signal Processing*, Addison-Wesley, Reading, 1985.

Blouke, M. M., "Charge-Coupled Devices Reach Maturity," *Laser Focus World*, pp.A17-A19, March 1991.

Brenner, K. H. and A. W. Lohmann, *Opt. Com.*, vol.42, p.310, 1982.

Burt, P. J. and E. H. Adelson, "The Laplacian Pyramid as a Compact Image Code," *IEEE Trans. Comm.*, vol.COM-31, no.4, pp.532-540, April 1983.

Casasent, D. and B. V. K. V. Kumar, "Optical Image Plane Correlator for Ambiguity Surface Computation," *Applied Optics*, vol.18, no.10, pp.1673-1678, 15 May 1979.

Caufield, H. J., *Optical Computing*, Editor SPIE Milestones Series, vol.1142, 1989.

Caulfield, H. J. and H. H. Szu, "Optical Wavelet Transform in Higher Dimensions," Proc. SPIE, vol.1705, April 1992.

Cottrell, D. M., R. A. Lilly, J. A. Davis and T. Day, "Optical Correlator Performance of Binary Phase-Only Filters Using Fourier and Hartley Transforms," *Appl. Opt.*, vol.26, no.18, pp.3755-3761, 15 September 1987.

Daubechies, I., "Orthonormal Bases of Compactly Supported Wavelets," *Comm. on Pure and Appl. Math.*, vol.XLI, pp.909-996, 1988.

Daubechies, I., "The Wavelet Transform, Time-Frequency Localization and Signal Analysis," *IEEE Trans. Info. Theory*, vol.36, no.5, pp.961-1005, 1990.

Daugman, J., "Complete Discrete 2-D Gabor Transforms by Neural Networks for Image Analysis and Compression," *IEEE Trans. Acoust., Speech and Sig. Proc.*, vol.36, no.7, pp.1169-1179, July 1988.

Eichmann, G., C. Lu, M. Jankowski and R. Tolimieri, "Shape Representation by Gabor Expansion," *Technical Note*.

Flannery, D. L., J. S. Loomis and M. E. Milkovich, "Design Elements of Binary Phase-Only Filters," *Appl. Opt.*, vol.27, no.20, pp.4231-4235, 15 October 1988.

Florence, J. M., "Design Consideration for Phase-Only Correlation Filters," *SPIE Proc.*, vol.1151, pp.195-202, 1989

Friedlander, B. and B. Porat, "Detection of Transient Signals by the Gabor Representation," *IEEE Trans. on Acoust., Speech and Sig. Proc.*,vol.37, no.2, pp.169-180, February 1989.

Gabor, D., "Theory of Communication," *J.I.E.E.*, vol.93, pp.429-459, 1946.

Gianino, P. G. and J. L. Horner, "Additional Properties of the Phase-Only Correlation Filter," *Opt. Eng.*, vol.23, p.695, 1984.

Gibbs, H. M., G. Khitrova and N. Peyghambarian, *Nonlinear Photonics*, Springer-Verlag, Berlin, 1990.

Goodman, J. W., *Introduction to Fourier Optics*, McGraw-Hill, New York, 1968.

Goto, N., Y. Yanayama and Y. Miyazaki, "Integrated Optic Matrix-Vector Multiplier using Multifrequency Acoustooptic Bragg Diffraction," *Appl. Opt.*, vol.30, no.5, pp.523-530, 1991.

Grochenig, K. and W. R. Madych, "Multiresolution Analysis, Haar Bases, and Self-Similar Tilings of R^n," *IEEE Trans. Info. Theo.*, vol.38, no.2, pp.556-568, March 1992.

Grossman, A. and J. Morlet, "Decomposition of Hardy Functions into Square Integrable Wavelets of Constant Shape," *SIAM J. MATH.*, vol.15, no.4, pp.723-736, July 1984.

Ha, B. and Y. Li, "Real-Time Self-Pumped Optical Phase Conjugate Based Wigner Distribution Processor for Complex Signals," *Applied Optics*, vol.30, pp.174-176, 1991.

Horner, J. L. and H. O. Bartelt, "Two-Bit Correlation," *Applied Optics*, vol.24, no.18, pp.2889-2893, 1985

Horner, J. L. and P. D. Gianino, "Phase-Only Matched Filtering," *Applied Optics*, vol.23, no.6, pp.812-816, 1984

Horner, J. L. and J. R. Leger, "Pattern Recognition with Binary Phase-Only Filters," *Applied Optics*, vol.24, no.5, pp.609-611, 1985

Janssen, A. J. E. M., "The Zak Transform: A Signal Transform for Sampled Time-Continuous Signals," *Philips J. Res.*, vol.43, pp.23-69, 1988.

Javidi, B. and C. J. Kuo, "Joint Transform Image Correlation Using a Binary Spatial Light Modulator at the Fourier Plane," *Applied Optics*, vol.27, no.4, pp.663-665, 1988

Jutamulia, S., K. Company and D. A. Gregory, "Intensity-Invariant Joint Transform Correlator," *Optics & Photonics News*, p.13, December 1991.

Katz, A., X. J. Lu, E. G. Kanterakis, Y. Li, Y. Zhang and N. P. Carivis, "Real-Time Optoelectronic Gabor Detection of Transient Signals," *OSA 1991 Annual Meeting Technical Digest*, p.12, 1991, San Jose.

Kellman, P., "Time Integration Optical Signal Processing," *Ph.D. Dissertation*, Stanford University, Stanford, CA, June 1979.

Kostrzeswki, A., "Optical Arithmetic-Logic Processors Based on Location, Content Addressable and Associative Memories," *Ph.D Dissertation*, City University of New York, New York, 1990.

Krattenthaler, W. and F. Hlawatsch, "Improved Signal Synthesis from Pseudo-Wigner Distribution," *IEEE Trans. Signal Processing*, vol. SP-39, pp. 506-509, February 1991.

Kronland-Martinet, R., J. Morlet and A. Grossman, "Analysis of Sound Patterns through Wavelet Transform," Int. J. Pattern Recogn. Artificial Intell., vol.1, no.2, pp.273-302, 1987.

Lemarie, P. G. (Ed.), *Les Ondelettes en 1989*, Lect. Notes in Math., vol.1438, Springer-Verlag, 1990.

Li, Y. and Y. Zhang, "Optical Implementation of Gabor and Wavelet Expansions of 1- and 2-D Signals," *Proc. SPIE*, vol.1702, 1992.

Li, Y. and Y. Zhang, "Optical Gabor and Wavelet Expansions of One and Two Dimensional Signals," in preparation.

Lohmann, A. W. and N. Streibl, "Map Transformations by Optical Anamorphic Processing," *Appl. Opt.*, vol. 22, no. 6, pp. 780-783, 15 March 1983

Mallat. S. G., "A Theory for Multiresolution Signal Decomposition: The Wavelet Representation," *IEEE Trans. Pattern Anal. Mach. Intell.*, vol.11, no.7, pp.674-693, 1989.

Mallat, S. G., "Multifrequency Channel Decompositions of Images and Wavelet Models," *IEEE Trans. Acoust. Speech and Sig. Proc.*, vol.37, no.12, pp.2091-2110, December 1989.

Mallat, S. G. and W. L. Hwang, "Singularity Detection and Processing with Wavelets," *IEEE Trans. on Info. Theo.*, vol.38, no.2, pp.617-643, March 1992.

Marks II, R. J., J. F. Walkup and T. F. Krile, "Ambiguity Function Display: An Improved Coherent Processor," *Applied Optics*, vol.16, no.3, March 1977.

Morozumi, S., "Application to the Pocket Color T.V.-TFT Array," *Electron. Mag.*, vol. 30, p. 39, 1985

Mosca, E. P., R. D. Griffin, F. P. Pursel and J. N. Lee, "Acoustooptical Matrix-Vector Product Processor: Implementation Issues," *Applied Optics*, vol.28, no.18, pp.3843-3851, 15 September 1989.

Nakano, H. and K. Hotate, "Operational Error in the Optical Real-Time Multiple Matrix Multiplier and its Compensation," *Applied Optics*, vol.25, no.18, pp.3132-3136,15 September 1986.

Nakano, H. and K. Hotate, "Optical System for Real-Time Multiplication of the Multiple Matrix with a 2-D Light Source Array," *Applied Optics*, vol.26, no.5, pp.917-923, 1 March 1987.

Neff, J. A., R. A. Athale and S. H. Lee, "Two-Dimensional Spatial Light Modulator: A Tutorial," *Proc. IEEE*, vol.78, no.5, pp.826-855, 1990.

Netravali, A. N. and J. O. Limb, "Picture Coding: A Review," *Proc. IEEE*, vol.68, pp.336-406, 1980.

Nilsson, J. W., *Electric Circuits*, 3rd Ed., Addison-Wesley, Mass., 1990.

Oppenheim, A. V. and R. W. Schafer, *Digital Signal Processing*, Prentice-Hall, New Jersey, 1975.

Pratt, W. K., Ed., *Image Transmission Techniques*, New York: Academic, 1979.

Psaltis, D. and R. A. Athale, "High Accuracy Computation with Linear Analog Optical Systems: a Critical Study," *Appl. Opt.*, vol.25, no.18, pp.3071-3077, 15 September 1986.

Rader, C. M., "Discrete Convolution via Mersenne Transforms," *IEEE Trans. on Comput.*, vol.C-21, pp.1269-1273, December 1972.

Rhodes, W. T., "One-Dimensional to Two-Dimensional and Two-Dimensional to One-Dimensional Mappings in Optical Signal Processing," *SPIE Proc.*, vol.128, pp.322-331, 1977.

Rhodes, W. T., "Acousto-Optic Signal Processing: Convolution and Correlation," *Proc. IEEE*, vol.69, no.1, pp.65-79, January 1981.

Rhodes, W. T. and P. S. Guilfoyle, "Acoustooptic Algebraic Processing Architectures," *Proc. IEEE*, vol.72, no.7, pp.820-830, July 1984.

Rioul, O. and P. Duhamel, "Fast Algorithms for Discrete and Continuous Wavelet Transforms," *IEEE Trans. Info. Theo.*, vol.38, no.2, pp.569-586, March 1992.

Stoner, W., "Review of 1-D Signal Processing Using the Optical Transfer Function," *SPIE Proc.*, vol.634, pp.64-79, 1986.

Tamura, P. N., J. J. Rebholz and T. C. Lee, *J. Opt. Soc. Am.*, vol.69, p.1451, 1979.

Texas Instruments Incorporated, *First-Generation TMS320: User's Guide*, Houston, 1989

Turpin, T. M., "Spectrum Analysis Using Optical Processing," *IEEE Proc.*, vol.68, no.1, pp.79-92, January 1981.

Vander Lugt, A. B., *Signal Detection by Complex Spatial Filtering*, Radar Lab., Rept. No. 4594-22-T, Institute of Science and Technology, The University of Michigan, Ann Arbor, 1963.

Vander Lugt, A. B., "Signal Detection by Complex Spatial Filtering," *IEEE Trans. Infor. Theo.*, vol.IT-10, no.2, 1964.

Weaver, C. S. and J. W. Goodman, "A Technique for Optically Convolving Two Function," *Appl. Opt.*, vol. 5, no. 7, pp. 1248-1249, July 1966

Wechsler, H., *Computational Vision*, Academic Press, San Diego, 1990.

Wilson, R., A. D. Calway and E. R. S. Pearson, "A Generalized Wavelet Transform for Fourier Analysis: The Multiresolution Fourier Transform and its Application to Image and Audio Signal Analysis," *IEEE Trans. on Info. Theo.*, vol.38, no.2, pp.674-690, March 1992.

Winograd, S., "On Computing of Discrete Fourier Transform," *Math. of Comp.*, vol.32, no.141, pp.175-199, January 1978.

Wornell, G. W. and A. V. Oppenheim, "Estimation of Fractal Signals from Noisy Measurements Using Wavelets," *IEEE Trans. on Sig. Proc.*, vol.40, no.3, March 1992.

Yariv, A., *Quantum Electronics*, 3rd Edition, John Wiley & Sons, New York, 1989.

Zhang, Y., Y. Li, R. Tolimieri, E. G. Kanterakis, A. Katz, X. J. Lu and N. P. Caviris, " Opto-Electronic Gabor Detector for Transient Signals," *Proc. SPIE*, vol.1981, pp.23-31, April 1991.

Zhang, Y. and Y. Li, "Optical Determination of Gabor Coefficients of Transient Signals," *Opt. Lett.*, vol.16, no.13, pp.1031-1033, 1 July 1991.

Zhang, Y., Y. Li, E. G. Kenterakis, A. Katz, X. J. Lu, R. Tolimieri and N. P. Caviris, "Optical Realization of Wavelet Transform for a One-Dimensional Signal," *Opt. Lett.*, vol.17, no.3, 1 February 1992.

Zhu, Z. Y., "Neuron-Like Textural Processing Based on Gabor Representation and Neural Networks," *Doctoral Thesis Proposal*, City University of New York, New York, 1991.